# Development and Characterization of Poly(lactic acid)/Acetylated Starch Blends

by

Rasool Nasseri Pourtakalo

A thesis

presented to the University of Waterloo

in fulfillment of the

thesis requirement for the degree

Doctor of Philosophy

in

Chemical Engineering

Waterloo, Ontario, Canada, 2018

## Examining Committee Membership

The following served on the Examining Committee for this thesis. The decision of the Examining Committee is by majority vote.

| | |
|---|---|
| External Examiner | NAME: Marie-Claude Heuzey<br>Title: Full Professor |
| Supervisor(s) | NAME: Christine Moresoli<br>Title: Full Professor<br>NAME: Aiping Yu<br>Title: Associate Professor |
| Internal Member | NAME: Michael Pope<br>Title: Assistant Professor |
| Internal Member | NAME: Yuning Li<br>Title: Full Professor |
| Internal-external Member | NAME: Jean Duhamel<br>Title: Full Professor |

## Author's Declaration

I hereby declare that I am the sole author of this thesis. This is a true copy of the thesis, including any required final revisions, as accepted by my examiners.

I understand that my thesis may be made electronically available to the public.

## Abstract

In this study, the acetylation of starch was investigated as a means to improve its thermal processability and compatibility with poly(lactic acid) (PLA) and ultimately widen the range of potential applications for PLA/acetylated starch (AS) blends. The work was divided in two parts: (1) the characterization of AS according to degree of substitution (DS) and (2) the preparation and characterization of PLA/AS blends.

The crystalline structure of AS, examined by X-ray diffraction, was destroyed upon acetylation. Differential scanning calorimetry (DSC) revealed that the removal of the crystalline structure during acetylation facilitated molecular movement and glass transition which should facilitate the thermal processability of AS. Decreased molecular weight of AS upon acetylation, which leads to the improvement of thermal processability, was confirmed by dilute solution viscometry. Thermogravimetric analysis (TGA) showed improved thermal stability upon acetylation which widens the processing temperature window of AS. Lower hydrophilicity of AS was revealed by contact angle analysis which is expected to generate more effective interactions with conventional polymers. Enhancement of the thermal expansion (measured by thermomechanical analysis (TMA)) and the lower density (measured by suspension) should improve the compatibility of AS with conventional polymers.

The molecular mobility of AS with degree of substitution (DS) 1.5 and 3 was investigated by temperature-modulated DSC (TMDSC) and solid-state $^{13}$C NMR (SS-NMR). The relaxation time of hole formation, estimated from TMDSC data, was proposed as the representative of $\alpha$-relaxation time near $T_g$. The $T_g$ estimated from the VFT model was similar to the $T_g$ measured by DSC and by heat-cool mode TMDSC supporting the analogy between the relaxation time of hole formation and the $\alpha$-relaxation time. The cooperative rearranging region (CRR) size, investigated by heat-cool mode TMDSC, was smaller for DS3 compared to DS1.5 which was attributed to the disruption of hydrogen bonds. TMDSC experimental data at moderate temperature, predictions at ambient temperature and SS-NMR results at ambient temperature suggest different mobility of acetylated starch according to DS.

The acetylation of starch generated PLA/AS blends with distinct properties. A biphasic morphology was predicted by the compressible regular solution (CRS) model and confirmed by

scanning electron microscopy (SEM) observations for all PLA/AS blends, except the PLA/DS3 blend. The thickness of the interphase of the biphasic PLA/AS blends, estimated theoretically from the properties of the pure component and experimentally by small angle X-ray scattering (SAXS), increased with increasing DS of AS. The estimated interphase was generally related to the length scale of the dynamic heterogeneity of the PLA matrix. Slowdown of the PLA chain dynamics at the interphase region was estimated for PLA/DS0 and PLA/DS1.5 blends and related to the hydrogen bonding between the PLA chains and AS observed by FTIR.

The properties of PLA/AS blends were affected by the DS of AS. The thermal stability of PLA/AS blends, obtained by TGA, was improved compared to neat PLA. DSC results indicated that AS had a plasticization and nucleation effect in the PLA/AS blends. The highest tensile strength, toughness, and impact strength was achieved when DS2.5 was added to PLA which may reflect the biphasic structure and the thick diffused interphase of this blend. The water diffusion coefficient and the water vapor permeability (WVP) of PLA/AS blends were influenced by the presence of AS. The water diffusion coefficient decreased while the WVP increased for PLA/AS blends by incorporation of AS.

The rate of crystallization of neat PLA and PLA/AS blends with different DS were investigated. The PLA/DS0.5 and PLA/DS1.5 blends showed the highest and the lowest rate of crystallization in isothermal crystallization conditions, respectively. The highest rate of crystallization in isothermal crystallization conditions for the PLA/DS0.5 blend may reflect the highest nucleation activity of DS0.5 along with the faster dynamics of the PLA chains. In the context of the PLA/DS1.5 blend, the highest initial degree of crystallinity may seem contrary with the lowest crystallization rate of this blend in isothermal crystallization conditions. The non-isothermal crystallization investigation, however, revealed similar rates of crystallization for the PLA/DS1.5 blend compared to the other PLA/AS blends at the lowest cooling rate ($2°C$/min) while having the fastest rate of crystallization at the highest cooling rate ($5°C$/min). The positive activation energy for the crystallization of the PLA/DS1.5 blend may reflect an endothermic process in the crystallization of this blend as a result of interfacial interactions. The largest amorphous phase thickness observed by SAXS for the PLA/DS1.5 blend could explain the significance of the interfacial interactions in this blend.

Finally, the results of this study showed that the acetylation of starch is a promising avenue for PLA/starch blends. Increasing the processability of starch and its compatibility with PLA through acetylation, provides the opportunity of making a wide range of materials with different applications. Various mechanical, thermal, and water transport properties, transparency and crystallization behavior can be achieved by incorporating AS with different DS into PLA.

For final applications, the effect of AS concentration on the properties of the PLA/AS blend should be investigated. The concentration of the AS dispersed phase in PLA/AS blends should lead to differences in morphology, interfacial characteristics and ultimately properties of the blend. Transparency, visual appearance and degradation rate of the blends are also very important factors in final applications that need to be studied in the future.

## Acknowledgement

I would like to express my sincerest gratitude to my supervisor Prof. Moresoli for her support, mentorship, and giving me the freedom and opportunity to explore the areas of polymer science that I always wanted to explore. I also would like to gratefully thank my co-supervisor Dr. Aiping Yu for her constructive advice along the way.

I am very grateful to my thesis committee members, Dr. Michael Pope, Dr. Yuning Li, Dr. Jean Duhamel, and Dr. Marie-Claude Heuzey for their time to review my thesis.

I would like to gratefully acknowledge OMAFRA New Directions Program (2013-2016) for funding this study.

Dr. Duhamel and Dr. Gauthier are also thankfully acknowledged for providing some chemicals.

Thanks to Dr. Peldszus (contact angle measurements), Dr. Ghavami, and Ms. Jenn Coggan (compression molding and mechanical testing) for providing the access to some instruments.

I would like to thank Janet Venne (SSNMR), Dr. Rivers (TMA), and Dr. Rahman (SAXS) for some technical assistance.

I am grateful to Dr. Power for some valuable discussions on SSNMR experiment.

Many thanks to my fellow lab members Katharina Hassel, Huayu Niu, Joseph Khouri, Nikole Lyn, Omar Mustafa Al-Kubaisi, and Chu Yin Huang, for their advice, valuable discussions, and friendship.

Last but not least, I would like to thank my family from the bottom of my heart for their unending love and support.

## Table of Contents

## List of Figures

## List of Tables

## List of Nomenclatures

| | |
|---|---|
| $a_I$ | Interphase thickness |
| $b$ | Kuhn segment length |
| $C_p$ | Heat capacity |
| $C"$ | Out-of-phase component of heat capacity |
| $C'$ | In-phase component of heat capacity |
| $D$ | Diffusion coefficient |
| $d$ | thickness |
| $E_a$ | Activation energy of crystallization |
| $G$ | Crystallization rate |
| $I(q)$ | Scattered intensity |
| $K_c$ | Kinetic crystallization constant |
| $K$ | Crystallization rate constant |
| $k_B$ | Boltzmann constant |
| $L$ | Long period |
| $l_a$ | Amorphous phase thickness |
| $l_c$ | Lamellar thickness |
| $M_n$ | Number average molecular weight |
| $M_t$ | Water uptake |
| $M_w$ | Weight average molecular weight |
| $M$ | Magnetization |
| $m_I$ | Weight fraction of matrix with slower dynamics |
| $N_a$ | Cooperativity degree |
| $N_{av}$ | Avogadro's number |
| $N_i$ | Degree of polymerization |
| $N$ | Number of equal-size hole |
| $n$ | Avrami exponent |

| | |
|---|---|
| $q$ | Scattering vector |
| $R_a$ | Arithmetic average roughness |
| $R_g$ | Root mean square average roughness |
| $R$ | Universal gas constant |
| $T_{1\rho}$ | Spin-lattice relaxation time |
| $T_{5\%}$ | Temperature of onset of degradation |
| $T_c$ | Cold crystallization temperature |
| $T_{cc}$ | Temperature of $\alpha'$ to $\alpha$ crystal transformation |
| $T_g$ | Glass transition temperature |
| $T_m$ | Melting temperature |
| $T_{max}$ | Temperature at the maximum degradation rate |
| $T_p$ | Crystallization peak temperature |
| $t_{1/2}$ | Crystallization half time |
| $V_a$ | Volume of a Cooperative Rearranging Region |
| $\alpha'$ | one crystalline form of PLA |
| $\alpha$ | Volumetric expansion coefficient, one crystalline form of PLA |
| $\beta$ | Linear thermal expansion coefficient, nonexponentiality parameter, cooling rate, one crystalline form of PLA |
| $\gamma(r)$ | One dimensional correlation function |
| $\gamma$ | one crystalline form of PLA |
| $\Delta g_{mix}$ | Gibbs free energy change upon mixing |
| $\Delta T_p$ | supercooling |
| $\Delta\mu^*$ | Activation energy of relaxation |
| $\delta$ | Solubility parameter |
| $\xi_a$ | Cooperativity length |
| $[\eta]$ | Intrinsic viscosity |
| $\eta_{sp}$ | Specific viscosity |
| $\nu$ | Segmental volume |

| | |
|---|---|
| $\rho$ | Density |
| $\tau_h$ | Relaxation time of hole formation |
| $\tau_{sl}$ | Spin-lock time |
| $\phi_i$ | Volume fraction |
| $\phi_n$ | Nucleation activity |
| $\chi_{C_0}$ | Initial degree of crystallinity |
| $\chi_{C_{AS}}$ | Degree of crystallinity of acetylated starch |
| $\chi_{AB}$ | Flory-Huggins interaction parameter |
| $\chi_c$ | Degree of crystallinity |
| $\chi_t$ | Relative crystallinity |
| $\omega_i$ | Degree of incompatibility |
| $\omega$ | Frequency of sinusoidal temperature modulation |

## List of Acronyms

| | |
|---|---|
| AS | Acetylated Starch |
| CP | Cross Polarization |
| CRR | Cooperative Rearranging Region |
| CRS | Compressible Regular Solution |
| DS | Degree of Substitution |
| DSV | Dilute Solution Viscometry |
| DTG | First derivative of TGA curves with respect to temperature |
| FTIR | Fourier Transform Infrared Spectroscopy |
| $^{1}$H NMR | Proton Nuclear Magnetic Resonance spectroscopy |
| MAS | Magic Angle Spinning |
| PCL | polycaprolactone |
| PEA | polyesteramide |
| PHAs | poly(hydroxyalkanoates) |
| PLA | Poly(lactic acid) |
| PPLA | Processed poly(lactic acid) |
| SAXS | Small Angle X-ray Scattering |
| TGA | Thermogravimetrical Analysis |
| TMA | Thermomechanical Analysis |
| TMDSC | Temperature Modulated Differential Scanning Calorimetry |
| TPS | Thermoplastic Starch |
| UPLA | Unprocessed poly(lactic acid) |
| VFT | Vogel-Fulcher-Tammann |
| WAXRD | Wide Angle X-ray Diffraction |
| WVP | Water Vapor Permeability |

# 1. Motivation, Scope and Thesis Structure

## 1.1. Motivation

Growing environmental concerns due to the disposal of petroleum derived polymers and the depletion of fossil fuel resources have led to considerable research efforts on the development of alternative materials from natural resources [1-4]. Biodegradable polymers such as poly(lactic acid) (PLA), poly(hydroxyalkanoates) (PHAs), polycaprolactone (PCL) and polyesteramide (PEA) have attracted extensive attention. Among these biodegradable polymers, PLA is a promising candidate due to the renewability of its feedstock, its compostability, and good mechanical and permeability properties [5, 6]. The high cost and slow rate of degradation of PLA, however, limit its use in general applications. These shortcomings can be alleviated by blending PLA with less expensive biodegradable polymers. Starch is a promising biodegradable material due to its low price, abundance and renewability [7]. The thermal processing of starch is limited by its high degree of crystallinity and the lack of thermal transition before degradation [8] while its hydrophilic characteristics and poor compatibility limit its application in PLA blends. The processability of starch and its compatibility with PLA may be improved by chemical modifications. For example, the acetylation of starch is a relatively simple process and can produce modified starch with a wide range of hydrophobicity and crystallinity characteristics by manipulation of the degree of substitution (DS) of the hydroxyl groups with acetyl groups [9]. The acetylation of starch weakens the intermolecular hydrogen bonding and decreases crystallinity, thus facilitating the mobility of the molecules and provides an opportunity to participate in glass transition [10]. Therefore, acetylation of starch can improve its thermal processability.

The main motivation of this study was to improve the processability of starch and its compatibility with PLA. It is hypothesized that the blending of PLA with acetylated starch (AS) can create materials with improved properties and lower the cost of PLA materials. Scrutinizing the effect of the degree of substitution (DS) of AS on the properties of PLA/AS blend was the overall objective of this thesis.

## 1.2. Research Objectives

The objective of this PhD was to investigate the acetylation of starch as a means to improve thermal processability and compatibility of starch materials with PLA and ultimately widen the range of potential applications for PLA/ acetylated starch (AS) blends. The work was divided in two parts: (1) the characterization of AS according to its degree of the substitution (DS) and (2) the preparation and characterization of PLA/AS blends. More specific objectives are listed below:

1- Investigate the effect of DS on thermal processability and compatibility of AS in PLA blends.

2- Evaluate the influence of DS of AS on the chains dynamics of starch by assessing the effect of temperature on hydrogen bonding and crystallization as the most influential parameters on the dynamic behavior.

3- Investigate the effect of DS of AS on the interphase properties (thickness and chain dynamics in the interphase) of the PLA/AS blends.

4- Assess the effect of DS of AS on the morphology and the thermal, mechanical and water transform properties of PLA/AS blends.

5- Evaluate the effect of DS of AS on the isothermal and non-isothermal crystallization behavior and lamellar crystalline structure of PLA/AS blends.

## 1.3. AS and PLA Materials Used in This Study

The materials used in this study consisted of AS and PLA/AS blends with the following characteristics:

The AS was kindly provided by Professor Chunbao (Charles) Xu (Western University). The DS of AS was characterized by Professor Xu's research group. Five AS with DS of 0, 0.5, 1.5, 2.5, and 3 were investigated and coded as DS0, DS0.5, DS1.5, DS2.5, and DS3, respectively.

PLA was obtained from NatureWorks Inc. (USA) (4032D, $M_n$=58000 g/mol, D-content 1.8 %,). This PLA grade was selected due to the slow rate of crystallization of this grade that provides the opportunity to eliminate crystalline regions by fast cooling. Crystallinity interferes with the interphase investigation by changing the chain dynamics. The slow rate of crystallization of this grade is also suitable for altering the crystallization behavior with incorporation of AS.

The PLA/AS blends were prepared with 15 wt% AS. This low percentage of AS was selected to induce the formation of matrix- droplet biphasic morphology and for providing uniform distribution of the AS dispersed phase which are necessary for the investigation of the interphase in PLA/AS blends.

## 1.4. Scope and Thesis Structure

This dissertation, which focuses on the characterization of acetylated starch (AS) with different degrees of substitution (DS) and the development and characterization of PLA/AS blends, is structured in 8 chapters. In chapter 1, the motivation and scope of the work and the structure of the thesis are presented. In chapter 2, background information on PLA, starch and PLA blends is presented. In chapter 3, the influence of the acetylation of starch on its thermal processability and compatibility with PLA is presented. The thermal processability of AS was investigated from the point of view of its crystallinity, thermal transition and stability and molecular weight attributes. The compatibility of AS with PLA was assessed from its surface energy, thermal expansion, and density characteristics. Chapter 4 is dedicated to the structural dependence of the molecular dynamics in AS where the effect of acetylation and alteration of the inter and intramolecular interactions and chain packing on the chain dynamics and molecular mobility is presented for moderate temperature and ambient temperature conditions. Chapter 5 presents the interphase properties of PLA/AS blends based on a thermodynamic analysis combined with experimental characterization analysis. The effect of the DS of AS on the morphology, thermal, mechanical and water transport properties of PLA/AS blends is discussed in chapter 6. The crystallization of PLA in PLA/AS blends under isothermal and non-isothermal conditions is reported in chapter 7. The overall conclusion drawn from this work is presented in chapter 8 along with the recommendations for future work. Chapters 3 to 7 are presented in manuscript format. As a consequence of this format, some information will be repetitive, particularly in the introduction and material and methods sections.

# 2. Background Information

## 2.1. Poly(lactic acid)

Poly(lactic acid) (PLA) is an aliphatic, biodegradable and compostable polyester derived from lactic acid (2-hydroxy propionic acid). The production of PLA has numerous advantages including the renewability of its agricultural source (corn), sequestering of carbon dioxide and assisting with farm economies [11]. PLA is one of the few polymers for which its physical and mechanical properties can be manipulated by stereochemical structure [12]. PLA was developed initially for biomedical applications. More common applications of PLA have emerged after commercial introduction of bio-based PLA (bio-fragmentation for monomer synthesis) in 2003 [13]. In comparison to existing petroleum-based polymers, PLA has appropriate optical, physical, mechanical and barrier properties that are desirable for a number of applications [14].

### 2.1.1. PLA Production

Lactic acid (2-hydroxy propionic acid) is the simplest hydroxy acid with a chiral center. Two optically active configurations of lactic acid are $_{L}$(+) and $_{D}$(-) isomers, Figure 2-1. Bacterial fermentation of carbohydrates is the main route for lactic acid production. The majority of bacteria used in fermentation processes mainly produce $_{L}$-lactic acid [13].

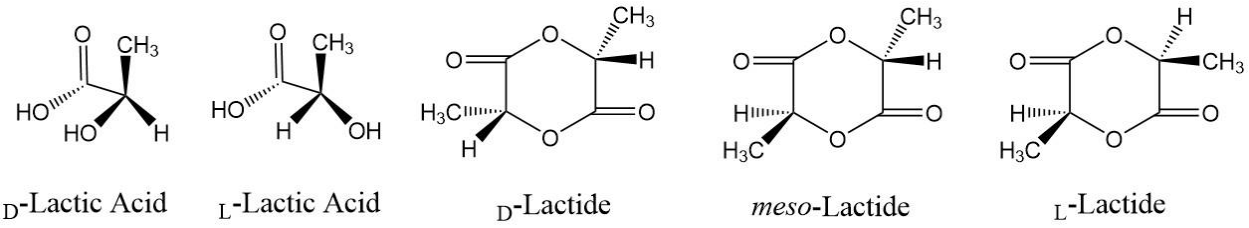


Figure 2-1. Stereochemistry of lactic acid and lactide molecules.

PLA with high molecular weight can be produced by three methods: (i) direct condensation polymerization; (ii) azeotropic dehydration and (iii) ring-opening polymerization through lactide formation, Figure 2-2. Although direct condensation is the least expensive method, obtaining a solvent-free high molecular weight PLA by this method is very difficult. Azeotropic dehydrative condensation of lactic acid can be used to produce high molecular weight PLA. In this method, the pressure for the distillation of lactic acid is reduced for 2-3 h at 130°C in the presence of a catalyst

in order to remove the condensation water. Ring-opening polymerization is the current commercial method of producing high molecular weight PLA. After the fermentation of carbohydrates, D-lactic acid, L-lactic acid or a mixture of the two are pre-polymerized to obtain an intermediate low molecular weight PLA, which is then catalytically converted into the cyclic dimer of lactic acid, lactide. Different types of lactide might be produced as follows: L-lactide (two L-lactic acid molecules), D-lactide (two D-lactic acid molecules) and *meso*-lactide (one L-lactic acid and one D-lactic acid molecule), Figure 2-1. After the distillation of lactide, high molecular weight PLA is formed by ring-opening polymerization of the lactide. PLA derived from greater than 93% L-lactic acid are crystallizable while PLA produced from 50 to 93% L-lactic acid is totally amorphous. Both *meso*- and D-lactide make twists in the otherwise very regular poly(L-lactide) molecular architecture.

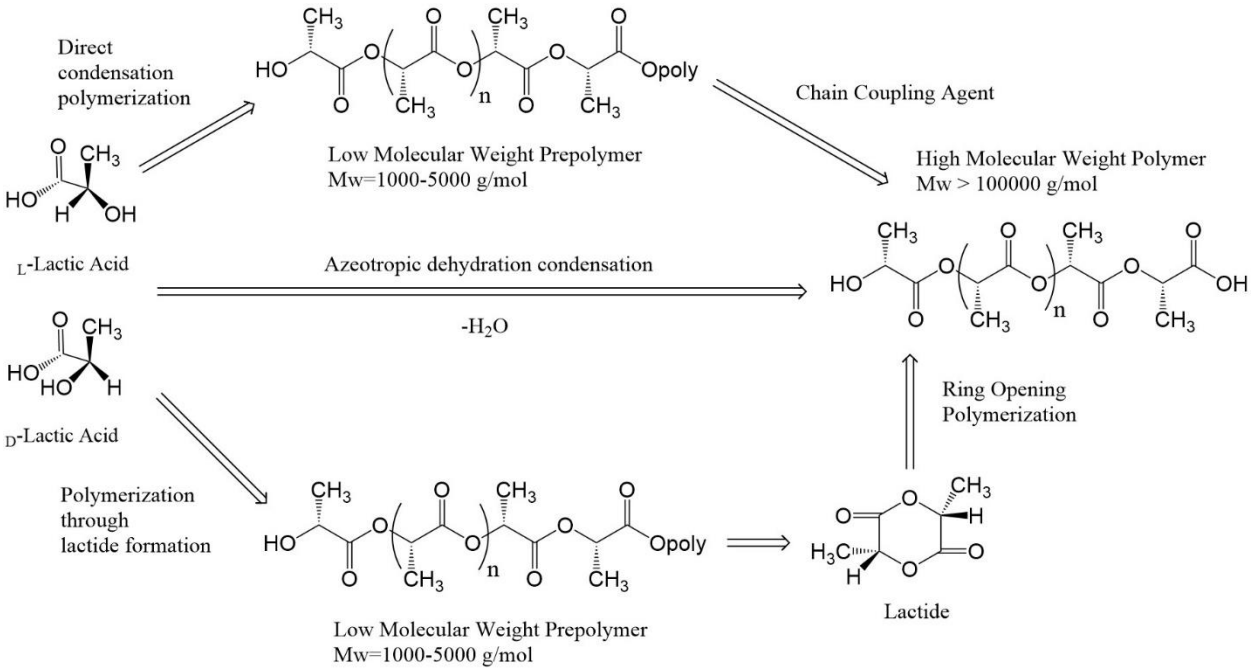


Figure 2-2. Synthesis methods for obtaining high molecular weight PLA [11].

## 2.1.2. Crystalline Forms of Poly (L-lactic Acid)

Four different crystallization forms ($\alpha$, $\beta$, $\gamma$, and $\alpha'$) have been reported for poly(L-lactic acid) (PLLA). The most common polymorph is $\alpha$ which forms by crystallization from melt or solution. The orthorhombic unit cell of the $\alpha$ form with dimensions of $a$=10.7 Å, $b$=6.45 Å, and $c$=27.8 Å is made of two chains with helical conformation. By applying high temperature under high drawing

conditions, the $\beta$ form is obtained. The $\beta$ form has a frustrated structure, containing three chains in a trigonal unit cell with $a$=$b$=10.52 Å and $c$=8.8 Å. The $\gamma$ form has two antiparallel helices packed in an orthorhombic unit cell with $a$=9.95 Å, $b$=6.25 Å, and $c$=8.8Å and is obtained from epitaxial crystallization on hexamethylbenzene substrate. When PLLA is crystallized below 120°C ($T_c$=90°C), the $\alpha'$ form can be obtained. It is a disordered crystal that has the same configuration as the $\alpha$ from but with a looser packing [15].

### 2.1.3. Thermal Properties of PLA

Like many other semicrystalline polymers, PLA shows a glass transition temperature ($T_g$) and melting temperature ($T_m$). The $T_g$ of PLA is about 58°C and its $T_m$ is about 170°C. The $\beta$ transition (localized motions that involve whole side chain and localized group movements) temperature of PLA is about -45°C below which it behaves as a brittle polymer [14].

## 2.2. Starch

Starch is produced by most green plants as energy source. Starch is the most common carbohydrate in human diets and animal foods [16]. Native starch is biosynthesized in the form of semi-crystalline granules with crystallinity in the range of 15 to 45% and its density is about 1.5 g/cm$^3$ [17]. Starch granules are found mainly in seeds, roots and tubers, as well as in stems, leaves, fruits and even pollen. Starch granules can be isolated easily by gravity, sedimentation, centrifugation and filtration [18].

At the molecular level, starch is a heterogeneous material with two major constituents: amylose, a linear structure of α-1,4 linked glucose units and amylopectin, a highly branched structure of short α-1,4 chains linked by α-1,6 bonds [19]. Highly branched nature of amylopectin causes a huge amount of complexity in investigation of its properties. The amylose content of conventional starch is in the range of 18 to 33% [17]. In addition to these two major constituents, starch granules contain very small amounts of proteins, lipids and phosphorus [18]. Generally the amylose fraction of starch has a relatively broad molecular weight distribution, with weight-average values much higher than number-average molecular weight. The different values reported in the literature for $M_n$ (4.6–10.3×10$^5$ g/mol) and $M_w$ (7–8.7×10$^6$ g/mol) of potato amylose illustrate these variations [17]. The amylopectin is considered as a much larger macromolecule than amylose. For example,

reported values of the weight average molecular weight of amylopectin for potatoes range between $14\times10^6$ to $195\times10^6$ g/mol [17].

## 2.3. Starch Modification and PLA/Starch Derivatives Blends

PLA/starch blends cannot be developed directly from native starch since native starch will degrade during its thermal processing [8] and the poor hydrophilic characteristics and compatibility of native starch with PLA.

### 2.3.1. Starch Plasticization and PLA/Plasticized Starch Blends

During the plasticization of starch, gelatinization occurs. In the gelatinization process or the heating of starch in the presence of a plasticizer, the crystalline structure of starch is first disrupted then followed by partial phase separation of the amylose and amylopectin components and finally gel ball formation which occurs in the amylopectin short branches. By cooling the gelatinized amylopectin, the double-helical crystalline structures reform from its dissociated short-branches which is called retrogradation. Plasticization can be used to alter the starch which can improve its thermal processability by reducing the glass transition temperature [8].

Plasticized starch also referred to as thermoplastic starch (TPS) has been used in order to improve PLA properties in PLA blends. A few key examples are presented below. Huneault and Li [20] reported the blending of water-free glycerol-plasticized TPS with PLA in the absence and presence of interfacial modification. In the absence of interfacial modification, the PLA/TPS blend morphology observed through scanning electron microscopy was very coarse. After modification of PLA by maleic anhydride, the PLA/TPS blends showed much finer dispersed phase and dramatic improvement in ductility. Li and Huneault [21] compared sorbitol and glycerol as plasticizers for TPS in PLA/TPS blends. They found that glycerol/sorbitol ratio has an important effect on the blend properties. Finer blend dispersed phase, higher tensile strength and modulus were observed but lower crystallization rate was measured for blends containing TPS plasticized with sorbitol. An alternative approach based on the addition of polymeric chain extender, a molecule with functional properties to reconnect polymer chains that have broken due to the different degradation mechanisms (thermal, oxidative, hydrolytic degradation), was investigated by Zhang et al. [22].. The addition of the polymeric chain extender Joncryl demonstrated smoother film edge and surface and improved mechanical properties for PLA/TPS plasticized by glycerol

and triethyl citrate. The effect of glycerol, formamide, and water as plasticizers of TPS on the properties of PLA/TPS blends was studied by Wang et al. [23]. Results of this study showed that water and formamide can improve the interaction and compatibility between TPS and PLA which lead to higher mechanical properties in the PLA/TPS blends.

### 2.3.2. Compatibilization Methods of PLA/Starch Derivatives Blends

The need for plasticization of starch has several drawbacks such as starch retrogradation and embrittling as well as phase separation which creates materials with heterogeneous characteristics. Furthermore, the poor interfacial interactions between starch and PLA remain a problem. The interfacial interactions between starch and PLA can be improved by using nonreactive compatibilizers such as amphiphilic molecules [24] and reactive compatibilizers such as maleic anhydride (MA) [25], epoxidized soybean oil [26] and tung oil anhydride [27]. Alternatively, the compatibility of starch with PLA can be improved by chemical modifications of starch which will also improve the starch processability. It has been reported that butyl-etherification and silane modification of starch [28, 29] improved interfacial interactions and blend properties of PLA/starch blends. Table 2-1 presents a summary of the literature data of the different approaches of improving compatibilization of PLA/starch blends and their effectiveness.

Table 2-1. Summary of the literature data of the different approaches of improving compatibilization of PLA/starch blends and their effectiveness

| PLA type | Starch type | Modification method | Processing conditions | Concentration | Mechanical properties* | | | | reference |
|---|---|---|---|---|---|---|---|---|---|
| | | | | | Tensile strength | | Elongation at break | | |
| | | | | | PLA/neat starch | Increase (%) | PLA/neat starch (%) | Increase (%) | |
| 4032D Natureworks (58kDa) (USA) | Corn starch local Ontario Market (Canada) | Acetylation | Twin-screw extruder 180°C 30 rpm 7 min | 85% PLA 15% Acetylated Starch, DS3 | 36.2 MPa | +26 | 2.4 | +10 | This work |
| Shimadzu (120kDa) (Japan) | Wheat starch Midwest Grain Products (USA) | maleic anhydride (MA) as a reactive compatibilizer | Twin-screw extruder 185°C | 55% PLA 45% starch 1phr (MA) | 30 MPa | +75 | 2.7 | +52 | [25] |
| 4032D Natureworks (USA) | Corn starch Zhuchang stimulation trdae (China) | Epoxidized soybean oil and maleic anhydride (MA) as reactive compatibilizers | Twin-screw extruder 175°C 10 min 40 rpm | 80% PLA 10% MA-graft-starch 10% (ESO) | 38 MPa | +13 | 64 | +127 | [26] |
| 4032D Natureworks (USA) | Corn starch Zhuchang stimulation trdae (China) | Tung oil anhydride (TOA) as a reactive compatibilizer and plasticizer | Twin-screw extruder 175°C 5 min 40 rpm | 65% PLA 30% starch 5% (TOA) | 40 MPa | -27 | 6.5 | +161 | [27] |
| 2002D Natureworks (USA) | Cassava starch, ETC international trading (Thailand) | Silane coupling agent as a reactive compatibilizer | Twin-screw extruder 165°C 40 rpm | 90% PLA 10% silane modified starch | 23.9 MPa | (-18 to 64.5) with different silane coupling agent | 2 | (-35 to 22) with different silane coupling agent | [28] |
| 2002D Natureworks (USA) | Waxy maize starch (S9679), Sigma Aldrich | Butyl-etherification | Internal mixer 165°C 80 rpm 10 min | 80% PLA 20% Butyl-etherified starch | 22 MPa | +104 | 1.5 | +200 | [29] |
| Natureworks, extrusion grade (87.5kDa) (USA) | Acron starch Dragon Flying Acron Development (China) | Dimer fatty acid polyamide (DFAPA) as plasticizer and nonreactive compatibilizer | Twin-screw extruder 175°C 400 rpm | 60% PLA 40% starch 8phr (DFAPA) | 49.5 MPa | +11 | 16.32 | +42 | [30] |

* Reported percentage of increase is calculated as: $\frac{property\ of\ PLA/modified\ starch\ blend - property\ of PLA/neat\ strach\ blend}{property\ of\ PLA/neat\ strach\ blend} \times 100$

## 2.3.3. Acetylation of Starch

Acetylation of starch is a relatively simple process and provides a wide range of hydrophobicity by manipulating the degree of substitution of hydroxyl groups with acetyl groups [9]. In a typical acetylation reaction starch and acetic anhydride (amount defined by the molar ratio between starch and acetic anhydride and desired DS) would react in the presence of a catalyst to produce acetylated starch, Figure 2-3. Acetylation of starch weakens the intermolecular hydrogen bonding and decreases crystallinity, thus facilitating the mobility of the molecules and provides an opportunity to participate in glass transition [10]. Therefore, acetylation of starch can improve its thermal processability.

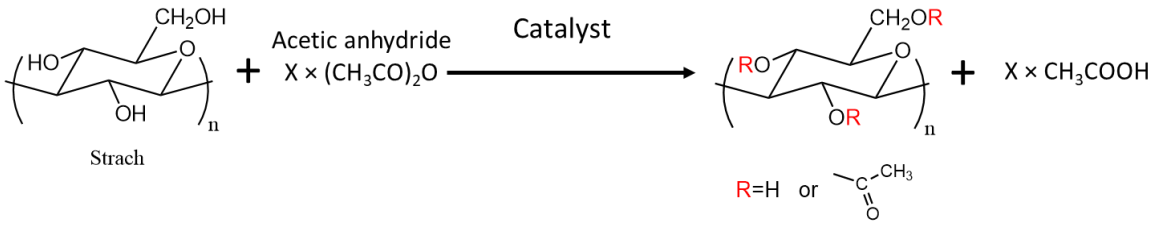


Figure 2-3. Typical acetylation reaction of starch.

The degree of substitution determines the number of hydroxyl groups that are replaced by acetyl groups in a repeating unit of starch molecules. Since each glucose unit has three hydroxyl groups, DS can vary from 0 to 3. Acetylation is a random process and not all glucose repeating units may be acetylated to the same level. Because of the random acetylation of the hydroxyl groups of the glucose units, the DS of AS gives a measure of the overall acetylation level (the number of replaced acetyl groups divided by the number of repeating units) which may lead to fractional values.

Starch acetylation is influenced by several factors such as source of starch, concentration of reactants, catalyst type, concentration, reaction time and pH of reaction medium [31]. In the reaction of acetic anhydride with starch, C-3 and C-6 esters (esterification from carbon number 3 and 6) are more likely to form, however, it may change in the presence of different catalysts [32]. The catalysts that are commonly used in starch acetylation include NaOH and $H_2SO_4$. Activation of starch with base occurs through formation of starch alcoxide ($ST\text{-}O^-$), which reacts with acetic anhydride to build a starch acetate and NaOAc [32]. Weak acid or alkaline salts result in exclusive formation of C-2 esters, and alkaline catalysts promote the formation of C-2 (with limited amount of C-6 and C-3 esters), while acids are not site-selective catalysts [33].

## 2.4. Polymer Blend Interphase

In the context of a polymer blend, the interface can be described as the boundary between two phases of different chemistry. Due to the interdiffusion of the two phases and interactions at the interface, there is not a sharp boundary between the two phases while there is a gradual concentration change from the pure component of one phase to the pure component of the other phase along a region called interphase.

Due to thermodynamic considerations, most polymer blends are immiscible [34]. Therefore, the properties and performance of polymer blends reflect the properties of the pure components and

their interphase characteristics (thickness, dynamics, and interfacial interactions) [35]. While the morphology of polymer blends has been extensively studied, there is limited information available on the polymer-polymer interphase due to the limited number and complexity of the techniques suitable for the direct investigation of the interphase [36]. Generally the role of the interphase in a blend will be specific to the given property. For example, the influence of the interphase is generally much more pronounced for mechanical properties measured at large deformation [37]. It is agreed that a thick and soft interphase (no vitrification of the chains of the matrix exists in the interfacial region) is generally necessary to achieve high strength [37]. The contributions of the interfacial interactions to the crystallization kinetics remain unclear. The interfacial interactions might restrict the movement of the polymer chains for conformational ordering required for nucleation. Alternatively, interfacial interactions might be beneficial for the adsorption of polymer chains [38].

Theoretical efforts to investigate the interphase have focused on the development of models to estimate its thickness and composition profile since early 1970s. Helfand et al. [39-43] have developed a quantitative theoretical framework in which enthalpic penalty of interdiffusion of immiscible components balances out with the entropic gain for widening the interphase. The best energetic balance finally defines the composition and thickness of the interphase.

The experimental investigation of the interphase has generally relied on sophisticated techniques of the mutual diffusion of immiscible polymers [44-48]. Many of these techniques need careful sample preparation or labeling and typically measure the thickness of the interphase in a stacked bilayer of polymer films [49]. In contrast, the small angle X-ray scattering (SAXS) [50] and temperature modulated differential scanning calorimetry (TMDSC) [51] methods can be used for a pre-processed polymer blend without any special sample preparation.

In the SAXS method a two-phase model system is considered with the diffused interface boundary (interphase). By fitting the scattering intensity profile into this model, interphase thickness can be estimated [52].

The existence of potential relationships between the minimum thickness of the interphase and the characteristic length scale $\xi_a$ of the dynamic heterogeneities or cooperative rearranging regions (CRR) has been proposed for the matrix of biphasic structures [36]. The CRR size can be estimated from the temperature fluctuation of the amorphous regions based on Donth's approach. In this

approach, the cooperativity length scale $\xi_a$ is associated with the volume of a CRR [53] and is calculated using in-phase and out-of-phase components of heat capacity which are measured by TMDSC.

# 3. Acetylation of Starch to Improve its Processability and Compatibility for Blending Applications

Rasool Nasseri[a], Robert Ngunjiri[b], Christine Moresoli[c], Aiping Yu[d], Zhongshun Yuan[e] and Chunbao (Charles) Xu[f]

Description of contributions:

[a]: performing most of the experimentations and writing the manuscript.

[b]: performing dilute viscometry for measuring molecular weights.

[c] and [d]: main and co-supervisors.

[e] and [f]: providing the acetylated starch samples.

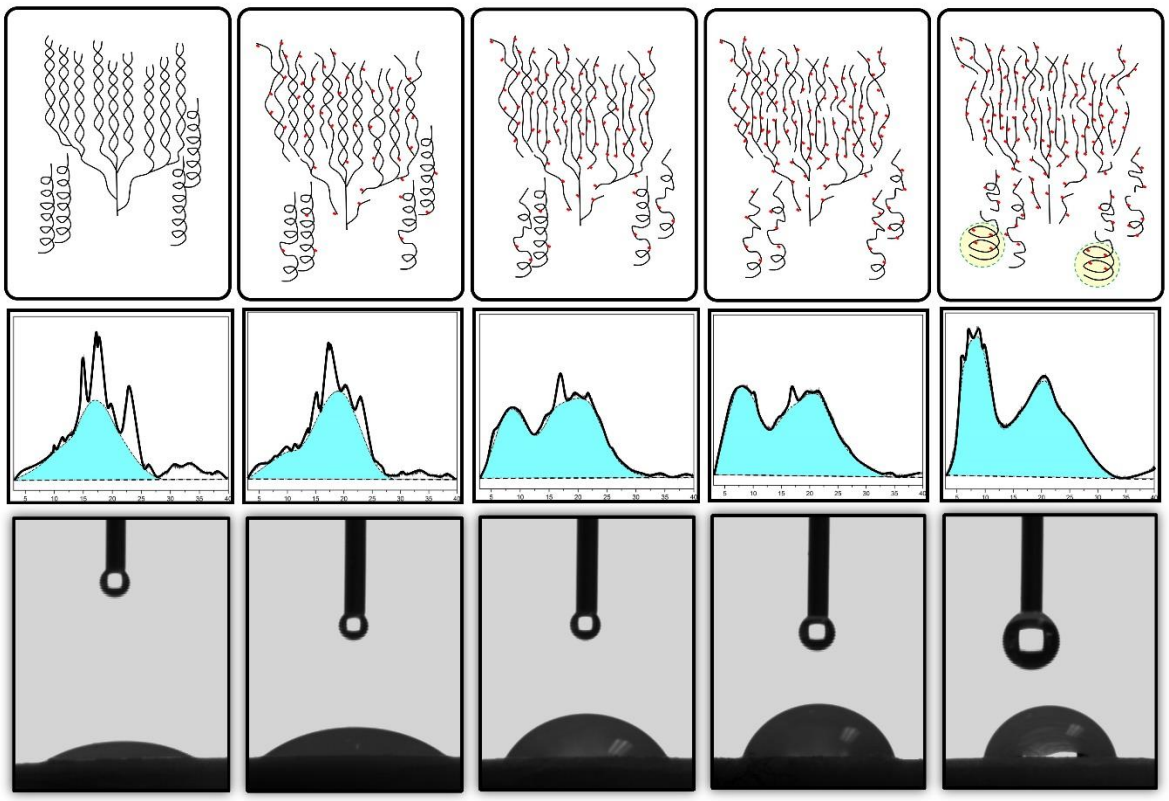

## 3.1. Synopsys

Synthesis of acetylated starch with different degrees of substitution from corn starch is reported in this chapter. The processability and compatibility of acetylated starch for blending applications are investigated. The crystalline structure of starch, examined by X-ray diffraction, was destroyed upon acetylation. Differential scanning calorimetry (DSC) revealed that the removal of the crystalline structure facilitated molecular movement and glass transition in the favor of thermal processability. Decreased molecular weight upon acetylation, which leads to the improvement of thermal processability, was confirmed with dilute solution viscometry. Thermogravimetric analysis (TGA) showed improved thermal stability upon acetylation which widens the processing temperature window. Contact angle measurements revealed lower hydrophilicity after acetylation which is expected to generate more effective interactions with conventional polymers. Enhancement of thermal expansion (measured by thermomechanical analysis (TMA)) and reduction of density (measured by suspension) should make acetylated starch more compatible with conventional polymers.

## 3.2. Introduction

Increasing consumption of polymers creates significant concerns for their waste disposal. Long-term retention of polymer materials in nature increases their environmental impact [1-4]. Blending conventional polymers with biodegradable natural polymers could partially address the waste problem. It has been postulated that the introduction of biodegradable elements in polymeric composite materials will favor their microbial degradation which would increase their porosity and produce a residual synthetic polymer skeleton with increased surface area. This residue can be degraded by natural factors such as thermal oxidation and ultraviolet photo-degradation [54, 55]. Starch has attracted a tremendous level of attention as a promising biodegradable material due to its low price, abundance and renewability [7]. Native starch is biosynthesized in the form of semi-crystalline granules with crystallinity in the range of 15 to 45% and density of about 1.5 g/cm$^3$ [17]. High degree of crystallinity of starch is the main obstacle in thermal processing due to the lack of thermal transition before degradation [8] while its hydrophilic characteristics and poor compatibility with polymers limit its application in blends. Plasticization of starch can improve its thermal processability by reducing the glass transition temperature [8] and can considerably

improve its blend properties [27, 56]. However, the use of a plasticizer has drawbacks such as retrogradation and embrittling of starch after processing and phase separation which creates materials with heterogeneous characteristics. Alternatively, the compatibility of starch with conventional polymers can be improved by chemical modifications which will also improve the mechanical properties [57, 58] and thermal stability [58] of the material. Chemical modification is generally achieved through derivatization, such as acetylation, cationization, oxidation, acid hydrolysis, and cross-linking [9]. Acetylation of starch is a relatively simple process and provides a wide range of hydrophobicity by manipulating the degree of substitution of hydroxyl groups with acetyl groups [9]. Acetylation of starch weakens the intermolecular hydrogen bonding and decreases crystallinity, thus facilitating the mobility of the molecules and provides them with an opportunity to participate in glass transition [10]. Therefore, acetylation of starch can improve its thermal processability.

The main purpose of this chapter was to evaluate the effectiveness of acetylation as a means of improving the suitability of starch for blending applications, namely the thermal processability and compatibility of starch with conventional polymers. The thermal processability of acetylated starch was investigated from the degree of crystallinity, the thermal transition and stability and molecular weight attributes. The compatibility of acetylated starch with conventional polymers was assessed from its surface energy, thermal expansion, and density characteristics.

## 3.3. Materials and Methods

### 3.3.1. Materials

Corn starch was purchased from local Ontario market (BulkBarn®, product code: 000260). The amylose content of starch was estimated to be 25.4±1.6 wt % (Mahmood *et al*'s method [59], details in Appendix I). Acetic anhydride (≥ 97.0%) and acetic acid (≥ 99.7%) were obtained from CALEDON laboratory chemicals (Canada). Potassium hydroxide (≥ 85%) was acquired from Merck (USA). Acetone (HPLC grade, ≥ 99.9%), chloroform (HPLC grade, ≥ 99.8%), dimethyl sulfoxide (HPLC grade, ≥ 99.9%), hexadecane (anhydrous, ≥ 99%) and hexane (HPLC grade, ≥ 95%) were purchased from Sigma-Aldrich (Canada). Tetrachloroethylene (≥ 99.8%) was obtained from J. T. Baker Chemicals (USA). All materials were used as received without further purification.

## 3.4. Methods

### 3.4.1. Acetylation of Starch

Corn starch was vacuum-dried at 55℃ for 24 hours prior to acetylation. Acetylated starch with degrees of substitution (DS) equal to 0.5, 1.5, 2.5 and 3 was produced. In a typical acetylation reaction, 15 g of vacuum-dried corn starch and acetic anhydride (amount defined by the molar ratio between starch and acetic anhydride and desired DS) were fed into a 250 mL three neck glass reactor. A mass of 0.375 g of a novel catalyst was firstly mixed with acetic acid. Then the mixture was added into the 250 mL three neck glass reactor equipped with a nitrogen stream. The reactor was heated at 135℃ in an oil bath with magnetic stirring. After 180 min, the reaction was stopped by placing the reactor in water. The cooled mixture was transferred into a 500 mL beaker and was precipitated with a non-solvent. The residual viscous product was rinsed with non-solvent and recovered into a 500 mL beaker. The precipitated acetylated starch was filtered and rinsed with an extra 200 mL of non-solvent in a 500 mL beaker. The mixture was filtered again and the final acetylated starch was vacuum-dried at 45℃.

### 3.4.2. Determination of degree of substitution (DS)

The degree of substitution (DS) was estimated from analyzing of proton nuclear magnetic resonance ($^1$H NMR) spectra as the ratio between the area of acetyl $CH_3$ at 2.15 ppm to the area of the starch CH at 3.5-5.5 ppm [60]. All spectra were obtained with a Varian Inova 600 NMR spectrometer equipped with a Varian 5 mm triple-resonance indirect-detection HCX probe at 25°C using DMSO as the solvent. A sample of $^1$H NMR spectra of acetylated starch (DS3) is presented in Appendix I (Figure 1).

### 3.4.3. Wide Angle X-ray Diffraction (WAXRD)

The crystalline structure of acetylated starch was characterized by wide angle X-ray diffraction (WAXRD) (D8 focus, Bruker) with CuK$\alpha_1$ radiation and 1.5406 Å wavelength operated at 40 kV and 30 mA. The X-ray diffraction patterns were recorded in a $2\theta$ angle range of 3-40 with step of 0.02° and speed of 1 sec/step.

The degree of crystallinity was estimated with the method of Nara and Komiya [61]. The area under the diffractogram was assigned to crystalline and amorphous domains by creating a smooth curve that connected the baseline of the peaks using OriginPro 8.5 software (Appendix I Figure 2). The area above the smooth curve was considered the crystalline domain and the area between the smooth curve and the linear baseline was considered as the amorphous domain. The degree of crystallinity was calculated from the area of the peak for the crystalline domain and the total area of the diffractogram:

$$\chi_{c_{AS}}\,(\%) = \frac{A_c}{A_c + A_a} \times 100 \tag{3.1}$$

where $\chi_{c_{AS}}$ is the degree of crystallinity, $A_c$ the area of the peak assigned to the crystalline domain and $A_a$ the area of the peak assigned to the amorphous domain.

### 3.4.4. Differential Scanning Calorimetry (DSC)

The thermal transitions of acetylated starch were investigated with a Q2000 TA instrument (USA). The acetylated starch (15-20 mg) was placed in an aluminum pan. A hole was poked in the lid of each pan to allow evaporation of any residual solvent or adsorbed water. The sample was initially heated from 25°C to 200°C at 10°C/min heating rate to eliminate any residual solvent, adsorbed water or thermal history. Next, the samples were cooled to -50°$C$ and then heated again to 300°$C$ (10°$C$/min heating rate). An empty pan was employed as a reference. Glass transition temperature and melting enthalpy were calculated using TA Universal Analysis version v5.5.20 software.

### 3.4.5. Dilute Solution Viscometry

Dilute solution viscometry of acetylated starch solutions subjected to saponification was conducted with No. 75 Cannon-Ubbelohde. The time for the flow of the solutions was measured at 25°$C$ in triplicates. Since the Mark-Houwink parameters are only available for neat starch, saponification in necessary for converting the acetylated starches back to neat starch. The saponification conditions were adjusted according to DS. For acetylated starch with DS=0, 1.5, 2.5 and 3, a mass of 0.25 g was used. The saponification was conducted for 3 days in 25 mL of 1 M potassium hydroxide solution at 5°$C$ with occasional stirring and then diluted to 50 mL with additional 1 M potassium hydroxide solution. For DS3, the saponification was not complete after 3 days and was

conducted for 6 days at room temperature. For DS0.5, an amount of 1 g was used and saponified at first in 25 mL of a 1 M potassium hydroxide solution for 3 days at $5°C$ and then diluted to 50 mL with an additional 1 M potassium hydroxide solution.

The viscometry experiments were conducted as follows. For neat starch (DS = 0), a volume of 15 mL of solvent (1 M potassium hydroxide solution) was transferred to the viscometer. Increasing amounts of neat starch solution were added to the solvent to make mixtures with different concentrations. For acetylated starch (DS=0.5, 1.5, 2.5 and 3), the flow time was measured for 15 mL of the undiluted solution and for diluted solutions obtained by sequential dilutions with the solvent (1 M potassium hydroxide solution). Each flow time was measured three times.

The method of Kozicki and Kuang [62] based on L'Hôpital's rule for the definition of intrinsic viscosity was used for the estimation of $[\eta]$. This method does not involve extrapolation to zero concentration and, therefore, is more accurate than the conventional Huggins's and Kraemer's equations for calculating intrinsic viscosity.

$$[\eta] = \lim_{c \to 0}\left(\frac{\eta_{sp}}{c}\right) \xrightarrow{\text{L'Hôpital's rule}} \left(\frac{d\eta_{sp}}{dc}\right)_{c=0} \tag{3.2}$$

where $\eta_{sp} = \frac{t}{t_0} - 1$ and $t$ and $t_0$ is the flow time for the solution and for the solvent, respectively. A second order polynomial was used to fit $\eta_{sp}$ versus time data and calculate the intrinsic viscosity. Accuracy measures of fits are presented in Appendix I (Figure 3 and Table 1).

The intrinsic viscosity was used to estimate the molecular weight of acetylated starch together with the Mark-Houwink parameters of partially hydrolyzed corn amylopectin in dimethyl sulfoxide (DMSO) reported by Salemis and Rinaudo [63].

$$[\eta] = 2.16 \times 10^{-3} M_w^{0.67} \quad 32\ ml\ g^{-1} < [\eta] < 160\ ml\ g^{-1} \tag{3.3}$$

$$[\eta] = 1.84 \times 10^{-1} M_w^{0.36} \quad 10\ ml\ g^{-1} < [\eta] < 32\ ml\ g^{-1} \tag{3.4}$$

Previous results reported by Cowie [64] have shown that Mark-Houwink parameters for starch in DMSO and 1 M KOH solution are quite similar.

### 3.4.6. Thermogravimetric Analysis (TGA)

Thermogravimetric analysis was performed in a Q500 TA instrument (USA). Each sample (about 20 mg) was heated from 25°$C$ to 600°$C$ at 10°$C$/min heating rate under nitrogen atmosphere (40.0 mL/min) to prevent thermo-oxidative degradation. The data were analyzed with the TA Universal Analysis version v5.5.20 software. Deconvolution of the first derivative of the TG (DTG) peak was obtained with OriginPro 8.5 software. The Lorentzian area functions were used to deconvolute the overlapping DTG peaks.

### 3.4.7. Pellet Preparation

Pellets of neat and acetylated starch were prepared with an evacuable KBr mold (International Crystal Laboratories, USA) using approximately 0.5 g of sample. The KBr mold diameter was 13 mm and the applied load was approximately 517 MPa (7 tonnes) for at least 5 min with a press Model #3925 (Carver Inc., USA). The pellets, 3-4 mm thickness were then vacuum-dried at 80°$C$ overnight and stored in a desiccator until testing.

### 3.4.8. Contact Angle Measurement

Contact angle measurements were conducted with pellets of neat starch and acetylated starch using the drop shape analyzer DSA 100 (Krüss GmbH, Germany) operated at room temperature in the static mode. Same method has been used previously in the literature for soy materials subjected to physical and chemical treatments [65]. Two reference liquids were used, water and hexadecane, with three drops of each liquid for each specimen. The shape of the drop was recorded and analyzed with DSA1 V1.9-03 9 software (Krüss GmbH, Germany). The Young-Laplace method was employed for contact angle calculation. The shape of the liquid drop was taken immediately after deposition since the drop shape was unstable. The dispersive ($\gamma^D$), polar ($\gamma^P$) and total ($\gamma^{Total}$) surface tensions are 21.8 (mJ/m$^2$), 51.0 (mJ/m$^2$), and 72.8 (mJ/m$^2$) for water and 27.5 (mJ/m$^2$), 0.0 (mJ/m$^2$), and 27.5 (mJ/m$^2$) for hexadecane, respectively [66].

The surface energy was estimated by two different methods in order to obtain more accurate estimation of surface energy. The Neumann [67] method was used to estimate the total surface energy of water according to equation (3.5).

$$\cos\theta = -1 + 2\sqrt{\frac{\gamma_s}{\gamma_l}}\, e^{-\beta(\gamma_l-\gamma_s)^2} \tag{3.5}$$

where $\gamma_l$ is the surface tension of liquid water and $\gamma_s$ is the surface energy of the solid surface and $\beta$=0.0001247 $(m^2/mJ)^2$.

The Owens-Wendt method [68] was used to estimate the dispersive and polar surface energy components of the solid surface ($\gamma_s^D$ and $\gamma_s^P$) based on the contact angle of water and hexadecane.

$$\gamma_l(1 + cos\theta) = 2\sqrt{\gamma_l^D\gamma_s^D} + 2\sqrt{\gamma_l^P\gamma_s^P} \tag{3.6}$$

where superscripts D and P refer to the dispersive and polar components, respectively.

### 3.4.9. Atomic Force Microscopy (AFM)

Atomic force microscopy (AFM) (Bruker Nano Surfaces, Santa Barbara, CA) in tapping mode was employed to measure the surface roughness of acetylated starch pellets.

### 3.4.10. Thermomechanical Analysis (TMA)

Pellets of acetylated starch (as described in the previous section) were used with a TMA equipment (Q400, TA Instruments, USA). An expansion standard quartz probe was employed and the applied modulated force was 1 mN at 0.5 Hz. All measurements were conducted with nitrogen at 50 ml/min flow rate. A similar multi-step temperature profile was used for all samples with DS ranging from 0 to 2.5, heating from ambient temperature to 120°$C$ at 10°$C$/min heating rate followed by constant temperature at 120°$C$ (15 min), heating from 120°$C$ to 150°$C$ at 1°$C$/min and constant temperature at 150°$C$ (5 min) before cooling to 120°$C$ at 1°$C$/min. The heating step from 120°$C$ to 150°$C$ and the subsequent cooling step were repeated for twice more. The multi-step temperature profile for DS3 was different where after the first heating step to 120°$C$ and constant period at 120°$C$, the sample was heated to 170°$C$ at 1°$C$/min heating rate and then cooled to 120°$C$ at 1°$C$/min heating rate. The heating step from 120°$C$ to 170°$C$ and subsequent cooling were repeated twice.

Data collection and analysis was performed with a TA Universal Analysis version v5.5.20 software. The data collected in the first slow heating step (from 120°$C$ to 150/170°$C$ at 1°$C$/min) was not reliable because of the evaporation of residual solvent but the second and third slow

heating steps were similar. The glass transition temperature and the coefficient of thermal expansion were calculated from the second and third slow heating steps and the average value was reported. The glass transition temperature was estimated from the intersection between the tangent of the expansion curve before and after the glass transition. The coefficient of thermal expansion was calculated from the initial dimension ($L_0$) and the first derivative of the dimension with respect to temperature ($\frac{\delta L}{\delta T}$) at 10°$C$ above the $T_g$ using the following equations:

$$\alpha = 3 \times \beta \tag{3.7}$$

$$\beta = \frac{1}{L_0}\frac{\delta L}{\delta T} \tag{3.8}$$

where $\alpha$ and $\beta$ are volumetric and linear thermal expansion coefficients, respectively.

### 3.4.11. Density

A sample of 2.5 g of acetylated starch (DS=0 to 3) was dissolved in a given solvent (Table 3-1) and deposited on a Teflon coated mold (6 cm diameter and 4 cm depth). After drying for 24 h at ambient temperature, films were placed in a vacuum oven at 80°$C$ over night.

Table 3-1. Solvent for the preparation of acetylated starch films according to degree of substitution

| degree of substitution | solvent |
|---|---|
| **0** | boiling water |
| **0.5** | water |
| **1.5** | dimethyl sulfoxide (DMSO) |
| **2.5** | chloroform |
| **3** | acetone |

A small piece of film (1 mm × 1 mm) cut by a razor blade was placed in 2 mL of hexane (ρ=0.659 g/mL) at room temperature in a 20 ml vial. The density of the mixture was adjusted by dropwise addition of tetrachloroethylene (ρ=1.615 g/ml) until complete suspension of the film in the middle of the liquid. When a sample remains suspended in a mixture of two liquids, the density of the sample corresponds to the density of the liquid mixture [69]. The mixture was considered ideal and its volume was taken as the summation of the volume of the two liquids, therefore:

$$\rho_{mix} = \frac{m_H + m_T}{v_H + v_T} = \frac{\rho_H v_H + m_T}{v_H + m_T/\rho_T} \quad (3.9)$$

where $m$, $v$ and $\rho$ are the mass, volume and density and subscripts $H$ and $T$ refer to hexane and tetrachloroethylene, respectively. Each experimental condition was performed in triplicates.

### 3.4.12. Statistical Analysis

Multiple-comparison Bonferroni t-test at a significance level of $\alpha$=0.1 was employed to evaluate the significance of the difference between means of properties that have replicate measurements. All reported error bars represent standard error.

## 3.5. Results and Discussion

### 3.5.1. Effect of Acetylation on the Thermal Processability of Starch

#### 3.5.1.1. Degree of Crystallinity

The high crystallinity of starch is the main obstacle during its thermal processing due to the lack of thermal transition before degradation [8]. Alteration of the crystallinity of starch is needed for successful thermal processing operations such as extrusion during blending. Acetylation of starch was investigated as a means to alter its crystallinity and improve its thermal processing. The X-ray diffraction patterns presented in Figure 3-1A indicate changes in crystallinity. By comparing the patterns of acetylated starch to those of neat starch, one observes lower intensity of the peaks characteristic of crystallinity. The intensity of these peaks decreased linearly with increasing DS up to DS1.5 and a more gradual decrease for DS2.5 and DS3 (Figure 3-1B). Similar decrease was reported previously for acetylated corn starch [70]. The reduction in crystallinity during acetylation may reflect lower inter and intramolecular hydrogen bonding due to the partial replacement of hydroxyl groups with acetyl groups resulting in some disordering of the crystalline structure [71, 72]. This disordering of the crystalline structure liberates chains and hence facilitates molecular movement and provides an opportunity for their participation in the glass transition [10]. WAXRD patterns revealed a new crystalline structure for DS3 where a new set of peaks was observed between $2\theta$=5° and 10° (Figure 3-1). As WAXRD patterns showed, the formation of this new crystalline structure initiated in DS1.5. Although, due to the randomness of substitution of hydroxyl groups by acetyl groups in DS1.5 and DS2.5, crystalline structure was not completely

formed. The emergence of a new crystalline structure was reported previously in the literature [73, 74]. Pu et al. [74] related this new set of peaks to V-type crystalline structure. The formation of a new crystalline structure was also inferred by comparison of the absorbance of acetylated starch iodine solutions measured at 620 nm and their molecular weight (see Appendix I (Figure 6) for the details). The blue-black starch-iodine solution represents the complex formed with V-amylose. The complex formation is affected by the length of the amylose chain [75-77]. As reported in Appendix I, the relationship between absorbance and molecular weight falls apart at DS3. Combining this observation with the WAXRD results (Figure 3-1A), it is inferred that this new crystalline region for DS3 is characterised by single helices which when suspended in a solvent, are capable of forming colored inclusion complexes with iodine.

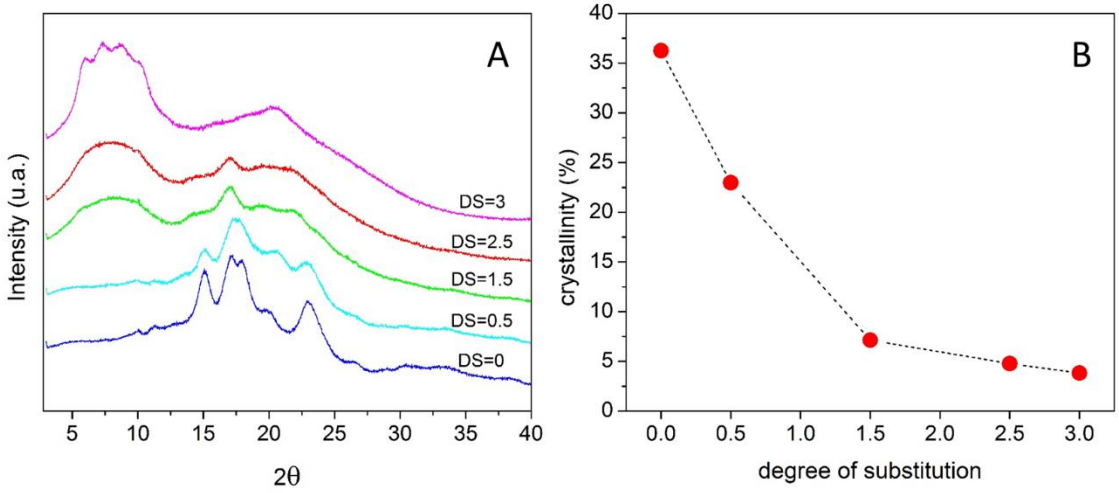


Figure 3-1. (A) WAXRD diffraction patterns of acetylated starch according to degree of substitution (DS). (B) Degree of crystallinity of acetylated starch according to DS.

### 3.5.1.2. Thermal Transition

Thermal transition profiles of acetylated starch were obtained by DSC analysis (Figure 3-2). An inflection of the baseline around 150°$C$ was seen in the heat flow pattern of DShigher than 0.5. This inflection is characteristic of glass transition for polymers. The temperature and the change in heat capacity ($\Delta C_p$) associated with this inflection are reported in Table 3-2 for DS1.5, DS2.5 and, DS3. Fringant et al. previously reported similar glass transition temperature (around 150°$C$) for pea amylose acetate (DS=2.7) and amylopectin acetate (DS=2.6) [10]. The glass transition temperature was reported to decrease with increasing DS for corn, yam and pea starch acetate [78-

80] while in the current study, the glass transition temperature remained nearly constant for DS1.5 and DS2.5 and increased by nearly 10°$C$ for DS3.

At temperature higher than 210°$C$, DS0.5-2.5 exhibited thermal decomposition (data not shown), while DS3 remained stable up to 220°$C$. An endothermic peak around 210°$C$ (Figure 3-2 inset) was observed for DS3. Such peak was previously attributed to the crystallization of amylose [10]. The presence of a new crystalline structure for DS3 was also deduced from the WAXRD patterns. The presence of crystals can act as physical junctions and reduce the molecular mobility of the polymer chains. The restricted molecular mobility could explain the higher glass transition temperature observed for DS3. This new crystalline structure could be emerging among the liberated chains explaining the increase of glass transition temperature even with lower degree of crystallinity of DS3 compared to other DS.

In the context of polymers, the heat capacity change ($\Delta C_p$) in glass transition can reflect the fraction of chains contributing to the glass transition [81]. For acetylated starch, $\Delta C_p$ near the glass transition temperature increased with increasing DS. Decreasing the intermolecular hydrogen bonding caused by partial replacement of hydroxyl groups with acetyl groups can increase the level of macromolecules with glass-rubber transition capacity which can be described by the $\Delta C_p$ increase [78-80]. For DS3, the heat capacity change is in the range of many polymers [10].

Table 3-2. Glass transition temperature ($T_g$) and heat capacity change ($\Delta C_p$) near $T_g$ estimated from DSC thermogram for acetylated starch according to DS.

| DS | $T_g$ (°$C$) (DSC) | $\Delta C_p$ (J.g$^{-1}$.K$^{-1}$) | $T_g$ (°$C$) (TMA) |
|---|---|---|---|
| **0** | - | - | - |
| **0.5** | - | - | - |
| **1.5** | 142 | 0.06 | 138.5 |
| **2.5** | 145 | 0.11 | 135 |
| **3** | 154 | 0.23 | 155 |

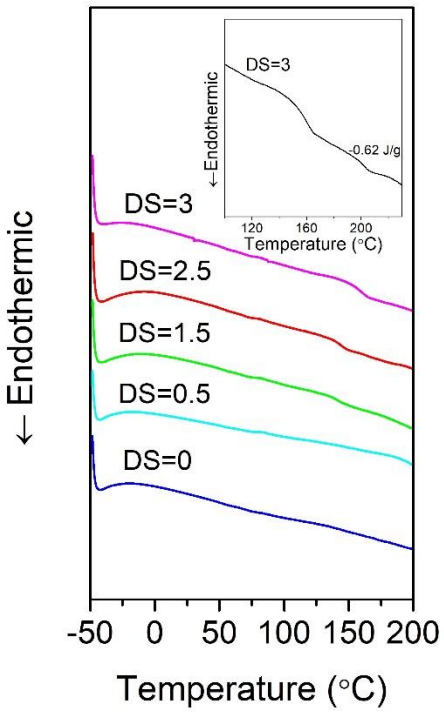


Figure 3-2. DSC profile of acetylated starch according to DS. The inset shows the thermogram of DS3 at elevated temperatures.

### 3.5.1.3. Intrinsic viscosity and molecular weight

The intrinsic viscosity, which gives a measure of the hydrodynamic radius of a sphere approximating the coil dimensions of a polymer molecule [82], was used as indication of the degradation of starch taking place during acetylation.

Intrinsic viscosity based on the Kozicki and Kuang method (Equation 3.2) and the associated molecular weight (Table 3-3) showed significant decrease due to acetylation. Volkert et al. [83] revealed that acetic acid as an activator leads to significant degradation of starch molecules reporting about 91.6% decrease of the $M_w$ (from $31.1 \times 10^6$ g/mol to $2.61 \times 10^6$ g/mol) for acetylated corn starch with DS2.5. Similar decrease was observed in this study for DS2.5 (89.7%). Bello-Pérez et al. [84] showed that high DS caused higher extent of degradation for barley starch. Lower molecular weight of starch after acetylation is expected to improve its processability.

Table 3-3. Intrinsic viscosity and molecular weight of saponified acetylated starch solution according to DS. Reported values represent 95% confidence intervals.

| DS | $[\eta]$ (Kozicki and Kuang) | $M_v$ ($10^6$ g/mol) | $[\eta]$ (Huggins) |
|---|---|---|---|
| **0** | 154.10 ± 6.60[e] | 17.50 ± 1.20[e] | 142.60 ± 3.50[e] |
| **0 (Unsaponified)** | 190.20 ± 21.60[f] | 24 ± 4.14[f] | 194.70 ± 7.60[f] |
| **0.5** | 6.41 ± 0.42[a] | 0.02 ± 0.00[a] | 6.33 ± 0.32[a] |
| **1.5** | 52.83 ± 0.93[d] | 3.50 ± 0.10[d] | 52.85 ± 0.70[d] |
| **2.5** | 33.84 ± 0.76[c] | 1.80 ± 0.08[c] | 33.88 ± 0.46[c] |
| **3** | 17.72 ± 1.93[b] | 0.32 ± 0.11[b] | 17.89 ± 1.76[b] |

Different letters denote statistically significant different samples (Bonferroni t-test at a significance level of $\alpha$=0.1)

### 3.5.1.4. Thermal Stability

Evaluation of the thermal stability of acetylated starch is an important consideration for the selection of suitable operating conditions for thermal processing [85]. Figure 3-3 summarizes TGA and DTG analysis of acetylated starch. TGA analysis of native starch (DS=0) showed two steps of mass loss which translated in to two peaks in the DTG (Figure 3-3). The first mass loss was observed in the 25-140°$C$ temperature range and was related to the release of physically adsorbed water [86]. The second mass loss observed in the 245-600°$C$ temperature range was related to starch decomposition. During starch decomposition, water is released as a result of inter and intramolecular dehydration reactions [87]. TGA analysis of acetylated starch (DS=0.5 to 3) showed three steps of mass loss which are reflected as three peaks in the DTG data, (Figure 3-3). The first step (25-140°$C$) also corresponds to the release of physically adsorbed water. The mass loss in this first step decreased with increasing DS which is in agreement with the gradual decrease of hydrophilicity resulting from the progressive replacement of hydroxyl groups with acetyl groups (Appendix I, Table 2). The second mass loss (200-300°$C$) was attributed to the condensation of the hydroxyl groups. Finally, the third mass loss (315-415°$C$) was related to the decomposition of the acetyl groups. Previous TGA-FTIR analysis identified acetic acid as the product of the decomposition of acetyl groups for this temperature range [88]. The shift of the second peak to lower temperatures for acetylated starch could reflect the degradation of starch occurring during the acetylation reaction [86]. The absence of mass loss in the 200-300°$C$ temperature range for DS3 (Figure 3-3) supports the absence of hydroxyl groups. The maximum rate of decomposition of the DS3 occurred at 367°$C$, about 50°$C$ higher than the temperature at which the highest rate of

mass loss was observed for native starch (DS=0). The TGA analysis presented in this study is in agreement with previous work showing that acetylation of starch increases its thermal stability [71, 79, 86]. The higher thermal stability of acetylated starch has been attributed to the lower hydroxyl content remaining after acetylation or the slower rate of OH condensation reaction taking place once hydroxyl groups are partially replaced by acetyl groups [71].

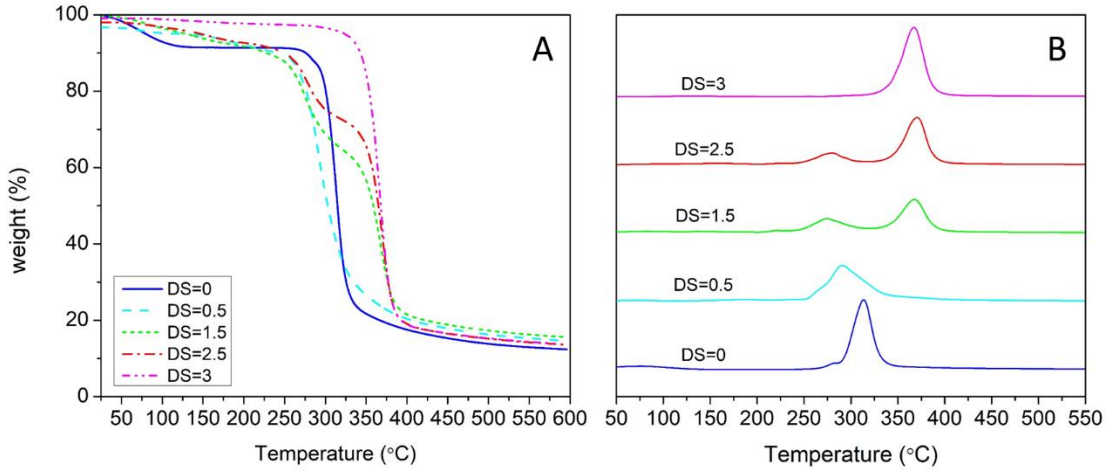


Figure 3-3. (A) TGA and (B) DTG curves of acetylated starch according to DS (10°C /min heating rate, nitrogen conditions).

The area of the second peak and third peak of the DTG for acetylated starch was obtained after deconvolution of these peaks (Figure 3-4A). The area of the second peak attributed to the condensation of hydroxyl groups (200-300°$C$) decreased with increasing DS while the area of the third peak attributed to the decomposition of acetyl groups (315-415°$C$) increased. The contribution of the thermal decomposition of the acetyl groups to the total thermal degradation of acetylated starch according to DS, presented in Figure 3-4B, shows a linear relationship according to DS. Similar linear relationship was reported previously for acetylated corn starch with DS0-1.23 [71].

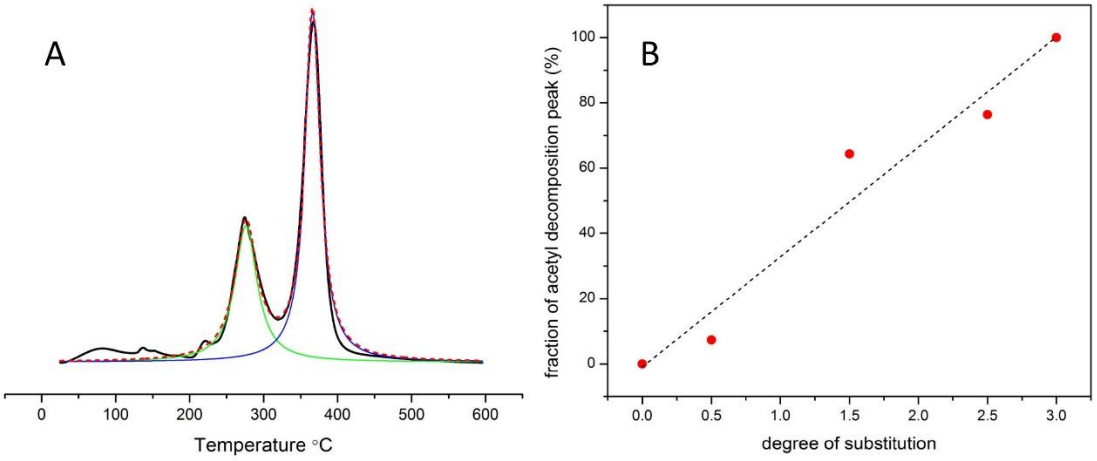


Figure 3-4. (A) Deconvolution of DTG data for DS2.5. (B) Linear relationship between the fractional area of peak for the acetyl group decomposition to the total thermal degradation according to DS, ($R^2$=0.98).

## 3.5.2. Effect of Acetylation on Critical Material Properties in Blend Applications

### 3.5.2.1. Hydrophobicity and Surface Energy

Contact angle analysis was used to evaluate the effect of acetylation on the hydrophobicity of starch. Prior to contact angle analysis, the surface roughness of acetylated starch pellets was assessed to ensure accurate measurements of the contact angle, namely the shape of the liquid drop which requires asymmetry and should be sufficiently large compared to the scale of surface roughness [89]. The surface roughness of acetylated starch pellets (~10 nm) was significantly smaller than the diameter of a typical liquid drop (few millimeters). AFM topographic images, arithmetic average roughness ($R_a$) and root mean square roughness ($R_q$) are presented in Appendix I (Figure 4 and Table 4).

Figure 3-5 shows a linear increase for the water contact angle with increasing DS, indicating decreased hydrophilicity due to the replacement of hydrophilic hydroxyl groups by hydrophobic acetyl groups. Similar effect of acetylation on the water contact angle with corn starch were reported previously by Chi et al. [70] with 43.1° for neat starch and 68.2° for acetylated starch with DS 2.89 and by Xu et al. [90] for films prepared from neat starch and acetylated starch with DS 2.45 (36.8° and 68.9°). Differences in water contact angles between our results and those reported for films prepared from acetylated starch [90] are observed for intermediate DS.

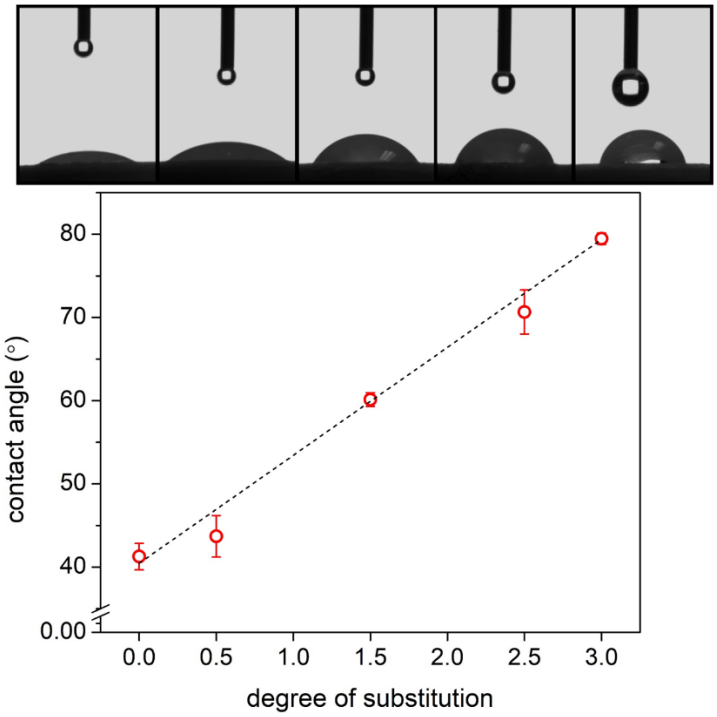


Figure 3-5. Shape and contact angle of water drop on the surface of acetylated starch pellets according to DS. Dashed line is the linear fit ($R^2$= 0.9888). Error bars represent standard error (n=3). Difference between the water contact angle of DS0 and 0.5 is not significant.

The total surface energy and its dispersive and polar components are presented in Figure 3-6 for acetylated starch. The total surface energy decreased nearly linearly with increasing DS for DS above 0.5 reflecting the decrease of the polar surface energy component and the gradual replacement of polar hydroxyl groups by less polar acetyl groups. The dispersive component of the surface energy remained relatively constant with increasing DS in agreement with the observations of Xu et al. [90] for films prepared from acetylated starch at all DS except DS 2.45. Additionally, quite similar result for total surface energies from Neumann and Owens-Wendt approaches verified the reliability of our measurements, Figure 3-6. Details of contact angle and surface energy contributions are presented in Appendix I (Table 5).

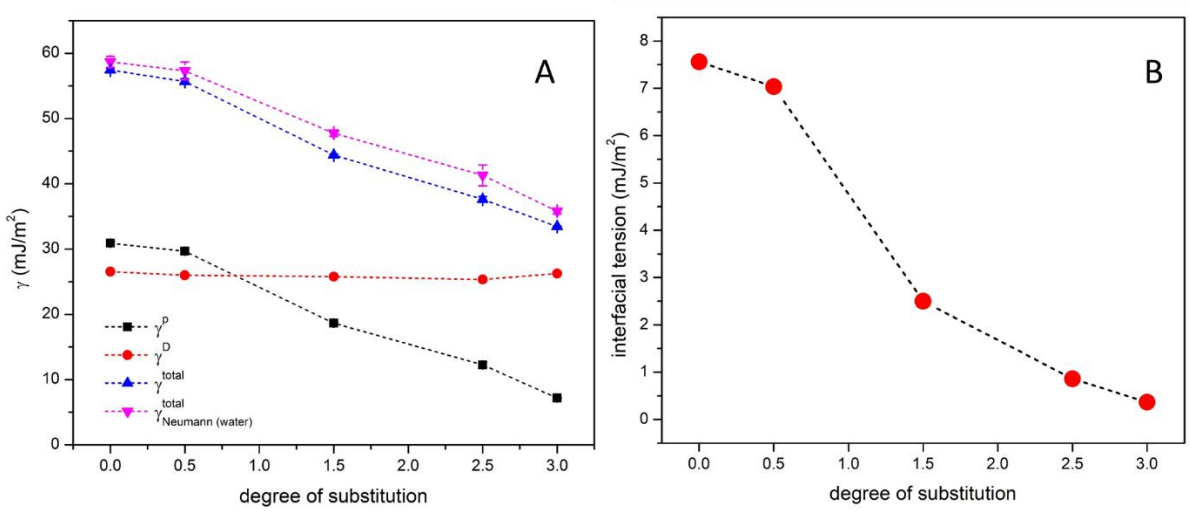


Figure 3-6. (A) Polar, dispersive and total surface energy of acetylated starch according to DS. Total surface energy was calculated using Neumann and Owens-Wendt approaches. Error bars represent standard error (n=3 for $\gamma_{Nuemann}^{Total}$; n=9 for $\gamma^P$, $\gamma^D$ and $\gamma^{Total}$). Significance of differences between values is presented in Appendix I (Table 5). (B) Estimated interfacial tension between acetylated starch and PLA according to DS.

The significant decrease of the contribution of the polar surface energy component for acetylated starch with 0.5 DS and higher suggests improved compatibility between these acetylated starch and conventional non-polar polymers. The effect of the lower polar surface energy component of acetylated starch is further evidenced by analyzing the interfacial tension between acetylated starch and PLA ($\gamma^D$, 32.5 (mJ/m$^2$), $\gamma^P$, 8.2 (mJ/m$^2$), $\gamma^{Total}$, 40.7 (mJ/m$^2$) [91]) calculated with equation 3.10 [92] and presented in Figure 3-6B.

$$\gamma_{ab} = \gamma_a + \gamma_b - 2\sqrt{\gamma_a^D \gamma_b^D} - 2\sqrt{\gamma_a^P \gamma_b^P} \quad (3.10)$$

The decreased interfacial tension suggests improved compatibilty between acetylated starch and PLA which should lead to improved mechanical performance.

### 3.5.2.2. Thermal Expansion

The thermal expansion of acetylated starch, obtained by TMA, is presented in Figure 3-7A for the third slow heating step (from 120°$C$ to 150/170°$C$ at 1°$C$/min). The starting point of all curves was transferred to zero and then different constant values were added in order to move the curves vertically (for comparison purposes). The glass transition temperature ($T_g$) was obtained from the intercept of the tangent for each region with different expansion rates (Figure 3-7A) and reported in Table 3-2. These $T_g$ estimates are slightly lower than those estimated from DSC measurements

(Table 3-2). This could be due to the lower heating rate of this method [93] or the inherent error in the $T_g$ measurement of this method. A similar trend was observed and discussed for DSC analysis. The volumetric coefficient of thermal expansion ($\alpha$), calculated from Equation 3.7 and 3.8 and presented in Figure 3-7B, increased relatively linearly with increasing DS. This increase could result from the enhancement of the molecular motion between the starch chains due to the lower hydrogen bonding when hydroxyl groups are substituted with acetyl groups during acetylation. The deterioration of the crystalline structure of starch (Figure 3-1B) could also provide opportunities for increased motion as a result of the looser packing.

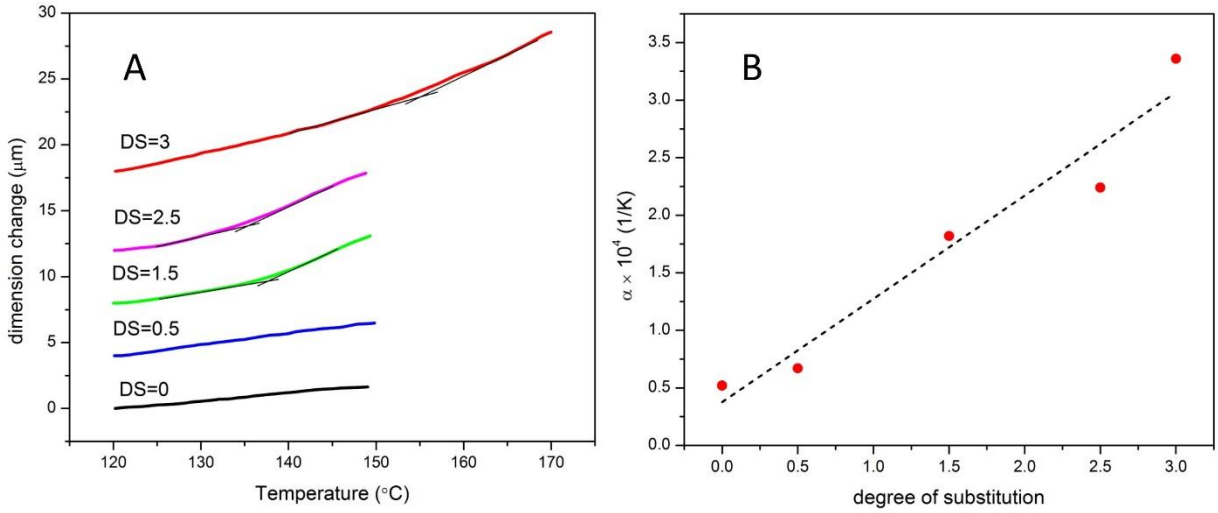


Figure 3-7. (A) TMA of acetylated starch according to DS. The starting point of all curves was moved to zero and the curves were shifted with an appropriate constant value to move the curves vertically. (B) Effect of the extent of acetylation on the volumetric thermal expansion coefficient of acetylated starch. Dashed line is the linear fit ($R^2$= 0.95).

A comparison between the estimated thermal expansion coefficients of acetylated starch with that of PLA, about 7.4 $10^{-4}$ $K^{-1}$ [94], indicates comparable magnitude. Acetylation of starch will likely improve the compatibility with conventional polymers and reduce the detachment at the interface during temperature changes.

### 3.5.2.3. Density of Acetylated Starch Films

The effect of acetylation on the molecular arrangement of starch was deduced from the changes in density for films prepared with acetylated starch. As illustrated in Figure 3-8, significant changes in density of the films were observed according to DS. The substitution of hydroxyl groups with

acetyl groups altered the packing of amylose/amylopectin molecules. Bulky acetyl groups may have increased the distance between adjacent amylose/amylopectin molecules and interfered with close packing. These changes have translated in higher volume occupied by the acetylated starch molecules and reduced the density of the films. Alternatively, destruction of the crystalline structure due to acetylation (Figure 3-1), could also explain the lower density. The crystalline domains of starch are very compact and dense. Destruction of crystalline domains, increases the amorphous content and decreases the density.

The lowering of the density caused by acetylation, also improves the similarity between acetylated starch and PLA ($\rho$=1.25 g/mL [94]).

Figure 3-8 shows a linear correlation between density and DS for all DS except DS3. The lack of correlation for DS3 may reflect the formation of the new loose packing crystalline structure described previously.

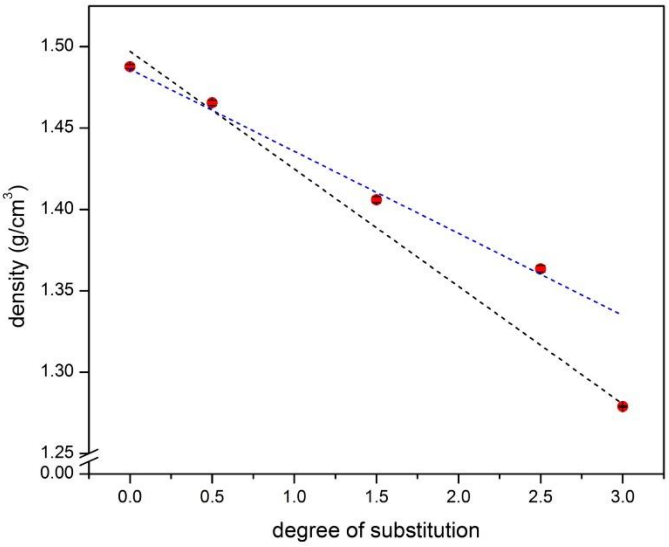


Figure 3-8. Density of acetylated starch according to DS. Error bar represent the standard error (n=3). Dashed blue lines is the linear fit ($R^2$= 0.99) with the first four DS. Dashed black lines is the linear fit ($R^2$= 0.95) with all DS. All reported values are significantly different.

### 3.5.2.4. Starch Retrogradation

After thermal processing, starch molecules will undergo recrystallization or retrogradation during cooling and storage [95]. This retrogradation or recrystallization causes embrittlement of thermoplastic starch [96]. An indication of retrogradation can be obtained from the degree of

crystallinity where lower degree of crystallinity could reflect reduced retrogradation. As illustrated in Figure 3-1B, acetylation was associated with gradual decrease of the degree of crystallinity with increasing DS. Destruction of starch crystalline structure during acetylation, decreases the crystallizable portion of starch molecules and prevents retrogradation [97] and embrittling of the thermo-processed material.

## 3.6. Conclusion

The results presented in this chapter demonstrate the potential of acetylation as a means to improve the suitability of starch for blending applications both from processing perspectives and material properties. The crystallinity was significantly reduced upon acetylation which should facilitate molecular movement and glass transition and improve thermal processability. Acetylation also decreased the crystallizable portion of starch molecules which should prevent retrogradation and embrittling of the thermo-processed starch material. Partial degradation during acetylation decreased the molecular weight and increased the thermal processability of starch. The replacement of hydroxyl groups with acetyl groups enhanced the thermal stability of starch and should widen its thermal processing temperature window. The polar surface energy component of acetylated starch decreased significantly such that the compatibility of acetylated starch with conventional polymers should be increased. The thermal expansion coefficient estimates revealed closer similarity between acetylated starch and conventional polymers. The lower density of acetylated starch in comparison to starch should enable this material to maintain the comparative advantage of polymeric materials which is their light weight.

Previous studies for synthetic polymers indicate that their processability, mechanical and barrier properties could be related to their dynamic behavior [98-101]. Therefore, in the next chapter the dependence of molecular mobility to the structure of acetylated starch will be studied. Three degrees of substitutions were selected for this study based on the DSC results. Native starch (DS0) as the reference, DS1.5 which is the middle of the DS range and is the first sample with an observable $T_g$, and DS3 that is the end of the DS range and shows a new crystalline structure. The effect of inter and intramolecular interaction and crystalline junctions will be investigated on the chain dynamics of selected acetylated starches in the next chapter.

# 4. Structural Dependence of the Molecular Mobility in Acetylated Starch

Rasool Nasseri[a], Christine Moresoli [b], Aiping Yu[c], Zhongshun Yuan[d] and Chunbao (Charles) Xu[f]

Description of contributions:

[a]: performing all the experimentations and writing the manuscript.

[b] and [c]: main and co-supervisors.

[d] and [f]: providing the acetylated starch samples.

This manuscript is prepared for submission to "Carbohydrate Polymers" journal under Elsevier publication.

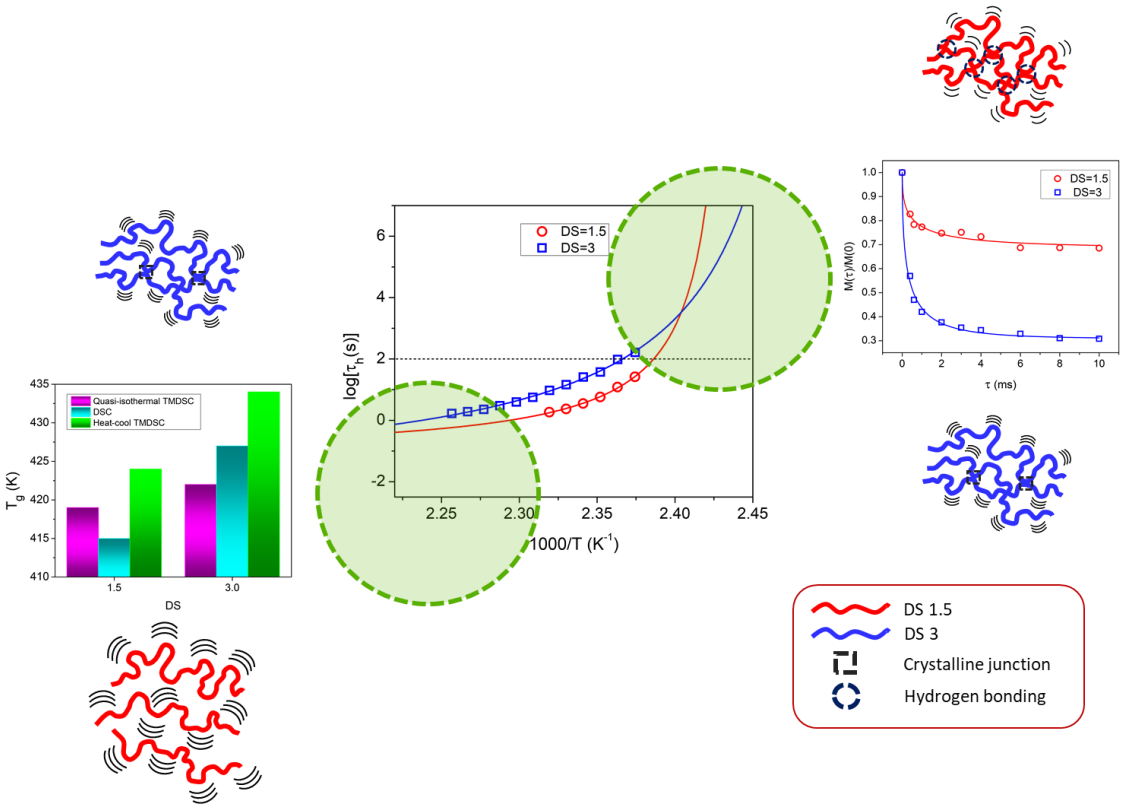

## 4.1. Synopsys

The molecular mobility of acetylated starch with a degree of substitution (DS) of 1.5 and 3 was investigated by using temperature-modulated DSC (TMDSC) and solid-state $^{13}C$ NMR (SS-NMR). The relaxation time of hole formation estimated from TMDSC data was proposed as the representative of the $\alpha$-relaxation time near $T_g$. Together with the VFT model, TMDSC data were used to estimate $T_g$ and the fragility index. The $T_g$ estimated from the VFT model was similar to the $T_g$ measured by DSC and by the heat-cool mode TMDSC supporting the analogy between the relaxation time of hole formation and the $\alpha$-relaxation time. The cooperative rearranging region (CRR) characteristics were investigated by the heat-cool mode TMDSC. The smaller size of the CRR for DS3 compared to DS1.5 was attributed to the disruption of hydrogen bonds. TMDSC experimental data at moderate temperature, predictions at ambient temperature and SS-NMR results at ambient temperature suggest different mobility of acetylated starch according to DS.

## 4.2. Introduction

Growing concerns of the environmental impact of petroleum derived polymers and the depletion of fossil fuel resources has led to considerable research efforts in the development of alternative materials from natural resources [1-4]. Starch has attracted significant attention as a promising biodegradable material due to its low cost, abundance and renewability [7]. The high degree of crystallinity of starch hinders its thermal processing due to the lack of thermal transition before degradation [8] while its hydrophilic characteristics and poor compatibility with synthetic polymers limits its application in composite materials. Chemical modifications of starch can improve its compatibility with synthetic polymers which can also increase the mechanical properties [57, 58] and thermal stability [58] of starch derived materials. The acetylation of starch, a relatively simple process, can increase its hydrophobicity by manipulating the degree of substitution of the hydroxyl groups with acetyl groups on the glucose units making up the amylose and amylopectin chains [9]. The presence of acetyl groups will alter the hydrogen bonding, the chain mobility and the packing arrangement of the amylose and amylopectin chains and crystallinity characteristics. Such structural changes lead to a semi-crystalline material that has shown improved thermal processability compared to native starch [58]. Prior studies for synthetic polymers indicate that their processability, mechanical and barrier properties could be related to

their dynamic behavior [98-101]. In this study, the molecular mobility of acetylated starch with two different degrees of substitution (DS) of 1.5 and 3, was investigated by adopting concepts and characterization techniques developed for synthetic polymers. Of particular interest was the glass transition region and the onset of long-range cooperative molecular motions and their associated α-relaxation characteristics. Since the investigation of α-relaxation characteristics of acetylated starch by dielectric spectroscopy is limited by the difficulty in producing uniform films, an alternative thermodynamic approach was adopted. This approach is based on the change of heat capacity ($\Delta C_p$) in the glass transition region measured by quasi-isothermal temperature modulated DSC (TMDSC) and analyzed with the concept of hole formation proposed by Eyring [102] and employed by Wunderlich et al. [103-108]. According to this concept, the higher expansivity and the slower temperature change in response to a thermal stimuli of polymers above the glass transition temperature ($T_g$) are due to the increased equilibrium number of equal-size holes, $N^*$. Each mole of holes adds an energy contribution $\varepsilon_h$ to the enthalpy. The total heat capacity is then expressed as [104]:

$$C_p = C_{p_0} + \varepsilon_h \frac{dN^*}{dT} \tag{4.1}$$

where $C_{p_0}$ and $C_p$ are the heat capacity of the polymer below and above $T_g$, respectively [105]. By considering first-order kinetics to describe hole formation, the hole theory can be applied to the glass transition region [104].

$$\frac{dN}{dt} = \frac{1}{\tau_h}(N^* - N) \tag{4.2}$$

where $N$ and $N^*$ are the instantaneous and equilibrium number of holes, respectively and $\tau_h$ is the relaxation time for hole formation. The relative change of heat capacity during glass transition is expressed in terms of $\tau_h$ by combining Equation 4.1 and 4.2 and considering sinusoidal temperature modulation conditions and constant $\tau_h$, as proposed by Wunderlich et al. [105]:

$$\frac{\Delta C_p}{\Delta C_{p_0}} = \frac{1/\tau_h}{\sqrt{(1/\tau_h)^2 + \omega^2}} \tag{4.3}$$

where $\Delta C_p$ is the difference between the heat capacity of the polymer below and above $T_g$, $\Delta C_{p_0}$ is the maximum change of heat capacity during the glass transition and $\omega$ is the frequency of the sinusoidal temperature modulation.

The effect of temperature on the relaxation time for hole formation ($\tau_h$) was investigated with the Vogel-Fulcher-Tammann (VFT) model developed for the $\alpha$-relaxation time since cooperative molecular motion is a prerequisite for hole formation in the glass transition region. The deviation of the temperature dependence of the $\alpha$-relaxation time from the Arrhenius behavior was quantified with the fragility index.

The effect of the degree of substitution on the dynamics of acetylated starch was also investigated by considering the concept of cooperative rearranging region (CRR) developed for synthetic polymers. Cooperative rearranging regions (CRR) represent the smallest amorphous domain where a conformational rearrangement may occur independently from its environment. The length scale of CRR (cooperativity length) can be investigated by heat-cool mode TMDSC.

Since TMDSC is limited by the operating temperature conditions, an alternative technique, solid-state NMR (SS-NMR) spectroscopy, used extensively to study the dynamics of synthetic polymers [109-112] and possesses sensitivity to intermolecular and intramolecular interactions [113], was selected. Calucci et al. [114] investigated the effect of accelerated aging (incubation at high temperature and relative humidity) of wheat grains on the dynamics of flour constituents. In their study, higher dynamics of all flour constituents including starch are observed after grain aging which may be related to the deterioration of the flour constituents. Tang et al. [115] employed SS-NMR techniques to distinguish the dynamics of the three (A-, B-, and C-) types of starch with different crystalline structures having different water content. Substantial mobilization was observed in the amorphous regions due to the hydration, while no significant changes in the rigidity was noticeable in the crystalline (double) helices. $^{13}$C NMR relaxation time in the rotating frame, $T_{1\rho}(C)$ can provide site-specific information on the molecular motions in the mid-kilohertz regime [110]. Therefore, $T_{1\rho}(C)$ can be interpreted in terms of chain flexibility. Spin-lattice and spin-spin processes can be responsible for the loss of magnetization from the rotating frame. Spin-lattice relaxation comes from the modulation of inter-nuclear dipolar interaction by molecular motion at the rotating frame Larmor frequency. Spin-spin relaxation arises from static $^{1}$H-$^{1}$H interaction and proton flip-flops [116]. Previous studies revealed that spin-lattice relaxation due to the molecular motion is the dominant process in demagnetization of amorphous polymers in the rotating frame [101, 110] while relaxation is spin-spin dominated in crystalline polymers [116]. Therefore, the

$T_{1\rho}(C)$ characteristics between amorphous polymers can be used as indication of their mobility where shorter $T_{1\rho}(C)$ would indicate greater average mobility [101, 110].

$^{13}C$ NMR relaxation time in the rotating frame, $T_{1\rho}(C)$, determined using standard cross-polarization magic angle spinning experiment, was used as the measure of chain flexibility. Chain flexibility information obtained from TMDSC near $T_g$ was compared to analysis obtained by solid-state NMR at ambient condition.

The objectives of this study were to investigate the effect of acetylation on the chain dynamics and molecular mobility at moderate temperature (Quasi-isothermal TMDSC and heat cool mode TMDSC) and ambient temperature conditions (VFT model predictions and SS-NMR). Acetylated starch with two different degree of substitution (DS), DS1.5 (partial replacement of hydroxyl groups with acetyl groups) and DS3 (complete substitution of hydroxyl groups by acetyl groups), were selected. Crystallinity characteristics were obtained by wide angle X-ray diffraction. The glass transition temperature ($T_g$) was obtained by three different techniques, conventional DSC, Quasi-isothermal TMDSC and heat-cool mode TMDSC.

## 4.3. Experimental Section

### 4.3.1. Materials

Corn starch was purchased from local Ontario market (BulkBarn®, product code: 000260). Amylose content of starch was estimated to be 25.4±1.6 wt% (Mahmood et al.'s method[59]). Acetylated starch was produced by mixing corn starch with acetic anhydride at a pre-determined molar ratio of acetic anhydride/starch and acetic acid, with or without a catalyst in a 250 mL 3-neck round bottom flask. A reflux condenser was attached to the middle neck of the flask, while a thermometer and a nitrogen-purge inlet were connected to the two side necks. The flask was submerged into a preheated oil bath placed on a magnetic heating plate. The reaction mixture was agitated by continuously stirring with a magnetic stir bar under nitrogen protection. For each experiment, the duration of the reaction was started when the inner temperature of the reactor flask reached 135ºC. The reaction was terminated after 3 hours. The reaction mixtures were precipitated into non-solvent and the precipitate was filtered in a Buchner funnel and further washed under vacuum filtration with non-solvent to remove any residual acetic acid. The recovered precipitate

was dried overnight in a vacuum oven setting at 45°C to remove any residual solvent. The degree of substitution (DS) represents the number of hydroxyl groups that are replaced by acetyl groups on a glucose unit of starch molecule (from 0 to 3). Acetylated starch with two DS, 1.5 and 3, was prepared according to the above procedure. Table 4-1 presents the molecular weight and density characteristics of starch and acetylated starch.

Table 4-1. Molecular weight ($MW$) and density ($\rho$) characteristics of starch and acetylated starch.

| Degree of substitution (DS) | $\boldsymbol{MW}^{\mathbf{a}}$ [g/mol] | $\boldsymbol{\rho}^{\mathbf{b}}$ [g/cm$^3$] |
|---|---|---|
| 0 | 17500000 | 1.49 |
| 1.5 | 3500000 | 1.41 |
| 3 | 320000 | 1.28 |

[a]measured by dilute solution viscometry and intrinsic viscosity. [b]measured by suspension method.

### 4.3.2. Wide Angle X-ray Diffraction (WAXRD)

The crystalline structure of acetylated starch was characterized by wide angle X-ray diffraction (WAXRD) (D8 focus, Bruker) with CuK$\alpha_1$ radiation and 1.5406 Å wavelength operated at 40 kV and 30 mA. The X-ray diffraction patterns were recorded in a $2\theta$ angle range of 3-40 with a step of 0.02° and a speed of 1 sec/step at ambient condition.

### 4.3.3. Differential Scanning Calorimetry (DSC)

The thermal transitions of acetylated starch were investigated with a Q2000 (TA instrument, USA). The acetylated starch (15-20 mg) was placed in an aluminum pan. A hole was poked in the lid of each pan to allow evaporation of any residual solvent or adsorbed water. Nitrogen with a 30 mL/min flowrate was used as purge gas. The sample was initially heated from 25°$C$ to 200°$C$ at 10°$C$/min heating rate to eliminate any residual solvent, adsorbed water or thermal history. Next, the samples were cooled to 25°$C$ and then heated again to 250°$C$ (10°$C$/min heating rate). An empty pan was employed as a reference. Glass transition temperature and melting enthalpy were calculated using the TA Universal Analysis version v5.5.20 software.

### 4.3.4. Temperature modulated differential scanning calorimetry (TMDSC)

TMDSC measurements were carried out on a Q2000 (TA Instruments, USA), calibrated with indium and sapphire disk standards, using standard Tzero. Nitrogen with a 30 mL/min flow rate was used as purge gas. The sample mass was about 5 mg, placed in aluminum plans. The amplitude of modulation was selected such that steady state was maintained with changes in heating rate. TMDSC experiments were conducted in two different modes:

(a) Quasi-isothermal mode: (i) heating to the starting temperature of the experiment at 20°C/min, (ii) equilibration at that temperature to erase any thermal history, and (iii) cooling to the final temperature with 2°C steps each held constant for 20 min. The temperature range was 170 to 120°C for DS1.5 and 180 to 130°C for DS3. The modulation amplitudes were 0.5, 1.0, and 1.5°C, coupled to periods of 30, 60, and 90 s, respectively, to achieve the same maximum heating rate of 6.3°C/min for all experiments. The heat capacity for each temperature at each frequency was recorded every 5 s. Data was recorded during the final 10 min of step (iii) and used to calculate the relaxation time of hole formation ($\tau_h$). Figure 1 of Appendix II shows the Lissajous plots (modulation heat flow versus modulation temperature) at one temperature. Insets show the Lissajous plot of the final 10 min of data collection. Super imposition of the ellipsoids indicated that steady state was reached and maintained during the final 10 min of step (iii) [105]. Therefore, 120 data points were collected and averaged. The heat capacity data for each quasi-isothermal experiment were normalized with the maximum change of the apparent heat capacity during the glass transition ($\Delta C_{p_0}$). Normalized heat capacity was used to estimate $\tau_h$ according to Equation 4.3 for each temperature. Finally in order to eliminate the effect of modulation, $\tau_h$ was extrapolated to zero amplitude of modulation.

(b) Heat-cool mode: (i) heating to 180°C and then cooling to 100°C at 20°C/min, (ii) heating to 180°C with an underlying heating rate of 1°C/min using the similar modulation amplitude and period as for the quasi-isothermal mode. The data collected for 1.5°C amplitude coupled to 90 s period were selected for the estimation of the real and imaginary parts of the heat capacity because these conditions provided the highest signal to noise ratio. Baseline correction procedure proposed by Weyer et al. [117] was selected to obtain the in-phase ($C'$) and out-of-phase ($C''$) components of the heat capacity and a Gaussian peak was fitted to the out-of-phase component of the heat capacity using OriginPro 8.5.

### 4.3.5. Solid State Nuclear Magnetic Resonance (SS-NMR) Spectroscopy

SS-NMR spectroscopy was performed with a Bruker AV6-700 spectrometer operating at 700 MHz for $^{1}H$. In order to obtain high-resolution $^{13}C$ spectra, cross-polarization (CP) and proton decoupling were combined with magic-angle spinning (MAS) for all measurements. Each sample was tightly packed in a double-bearing CP/MAS probe with 4 mm rotor. All relaxation and contact time measurements were performed with a 4 s recycle delay and at 5 kHz spinning speed. For the $^{13}C$ spin-lattice relaxation experiment, a 14 kHz radio-frequency field strength was used. The $^{13}C$ relaxation time in the rotating frame, $T_{1\rho}(C)$, was obtained by using the standard CP sequence and by varying the carbon spin lock time from 0 to 10 ms in 10 steps without proton irradiation after CP (2 ms contact time).

The $^{13}C$ relaxation time in the rotating frame was obtained by fitting a stretched exponential to the measured intensity, $M(\tau_{sl})$ [100, 118]:

$$\frac{M(\tau_{sl}) - M_{\infty}}{M_0 - M_{\infty}} = e^{-(\tau_{sl}/T_{1\rho})^{\beta}} \tag{4.4}$$

where $M_0$ is the initial magnetization, $M_{\infty}$ is the magnetization when the spin system and the lattice reach a quasi-equilibrium, $\tau_{sl}$ is the spin-lock time, and $\beta$ is the non-exponentiality parameter or stretch exponent which contains information on the distribution of the relaxation times.

## 4.4. Results and Discussion

### 4.4.1. Crystalline Structure

The crystalline structure of native starch (DS0) and DS1.5 and DS3, obtained by WAXRD, indicates that some of the crystalline structure of native starch (DS0) disappeared while the emergence of a new crystalline structure was observed for DS3, with a set of peaks between $2\theta$=5° and 10° (Figure 4-1). Similar emergence of new crystalline structure was observed previously in yellow ginger acetylated starch with DS of 2.67 [73]. The new crystalline structure observed for DS3, where all hydroxyl groups have been replaced by acetyl groups leading to the absence of hydrogen bonding and consequently easier fusion, should be different than the crystalline structure of native starch where all hydroxyl groups are present leading to significant hydrogen bonding.

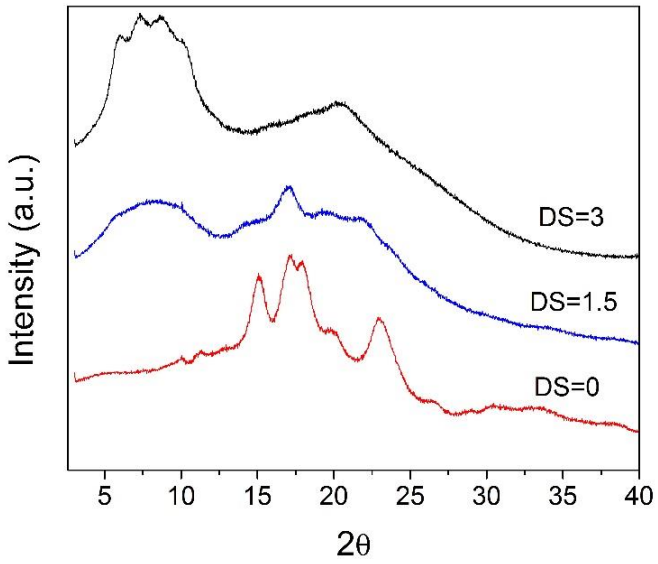


Figure 4-1. WAXRD diffraction patterns of acetylated starch according to DS.

### 4.4.2. Thermal Analysis and Molecular Mobility near the Glass Transition Region (moderate temperature conditions)

The thermal transitions of acetylated starch, obtained by DSC analysis (Figure 4-2), indicate that no glass transition was observed for native starch. The inter and intramolecular hydrogen bonding and the high degree of crystallinity prevent starch from showing any thermal transition before decomposition. In contrast, acetylated starch showed a glass transition temperature, 142°C for DS1.5 and 154°C for DS3. The substitution of hydroxyl groups with acetyl groups during acetylation reduces hydrogen bonding in starch allowing for a glass-rubber transition to occur. A similar glass transition temperature has been reported previously, around 150°C for pea amylose acetate (DS=2.7) and amylopectin acetate (DS=2.6) [10]. At temperature higher than 210°C, native starch (DS0) and DS1.5 exhibited thermal decomposition, while DS3 remained stable up to about 250°C. An endothermic peak around 210°C was observed for DS3. Such peak was previously attributed to the crystallization of amylose [10].

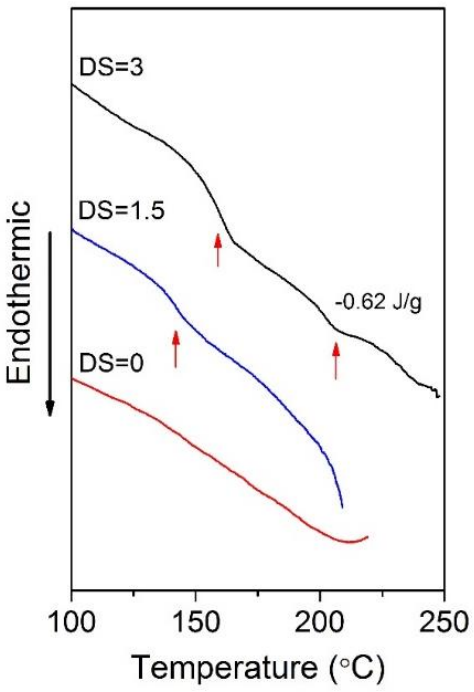


Figure 4-2. DSC profile near the glass transition region of acetylated starch according to DS.

The emergence of a new crystalline structure in DS3 suggests the formation of new junction among the chains. Replacement of acetyl groups with hydroxyl groups on the glucose units of starch alters the chain intermolecular interactions. To investigate these effects, Quasi-isothermal TMDSC experiments were conducted to probe the dynamic behavior of acetylated starch chains near the glass transition region. The normalized change of heat capacity ($\Delta C_p/\Delta C_{p_0}$) for three different modulation conditions, presented in Figure 4-3a and c, indicates higher variation of $\Delta C_p/\Delta C_{p_0}$ according to temperature for DS1.5 compared to DS3. These results were used to estimate the relaxation time of hole formation (Equation 4.3) according to temperature (Figure 4-3b and d).

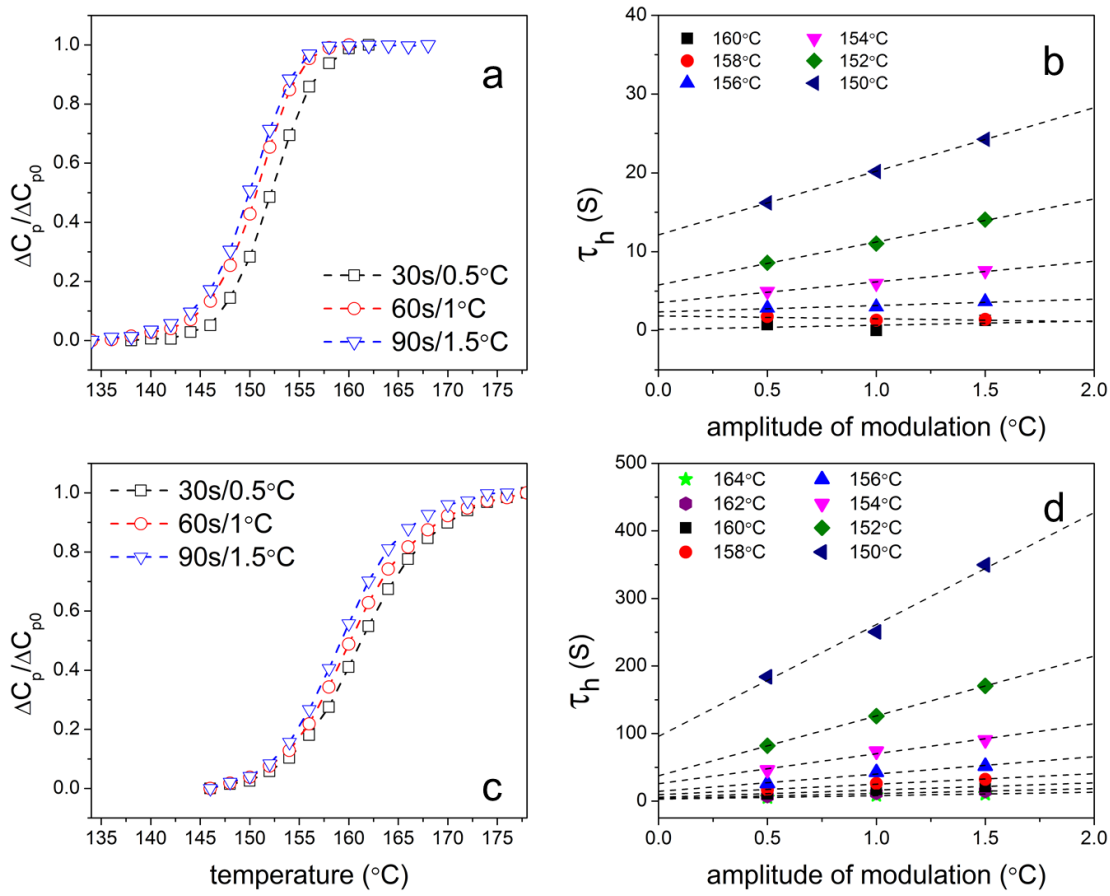


Figure 4-3. Relative change of heat capacity of acetylated starch with (a) DS1.5 and (c) DS3 and calculated relaxation time for hole formation ($\tau_h$) at different temperatures for (b) DS1.5 and (d) DS3. Dashed lines represent a guide (a and c) and linear fit (b and d).

As indicated earlier, chain relaxation in an amorphous material is the prerequisite for hole formation during the glass transition. Thus the behavior of the relaxation time for hole formation ($\tau_h$) may be related to that of the $\alpha$-relaxation time. With this in mind, we have evaluated the behavior of the relaxation time for hole formation using models developed for the $\alpha$-relaxation time. Generally, the temperature dependence of the $\alpha$-relaxation time for polymers depicts a deviation from Arrhenius behavior. This deviation can be captured by the empirical Vogel-Fulcher-Tammann (VFT) equation [119-121]:

$$\tau_h(T) = \tau_0 \exp\left(\frac{B}{T - T_0}\right) \tag{4.5}$$

where $\tau_0$ is the relaxation time at infinite temperature, $B$ is the fitting parameter, and $T_0$ is the reference Vogel temperature.

The good fit of the relaxation time of hole formation ($\tau_h$) with the VFT model ($R^2$, Table 4-2), presented in Figure 4-4 supports the analogy between the two types of relaxation time.

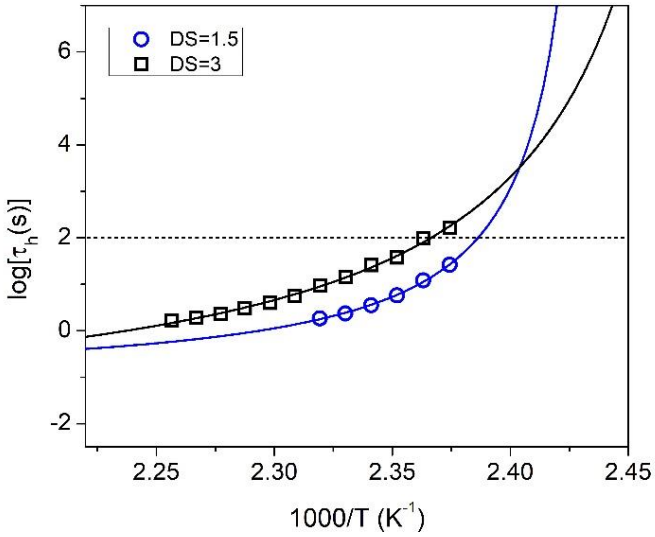


Figure 4-4. Relaxation time of hole formation as a function of the inverse temperature (Arrhenius diagram) for DS1.5 and DS3. Solid lines represent the fit of the experimental data to the VFT model (Equation 4.5). The horizontal dotted line represents the relaxation time of hole formation of $T_g$ considered as $\tau_h$ is equal to 100s.

The VFT model and its estimated parameters from the relaxation time of hole formation were used to calculate the glass transition temperature as the temperature at which $\tau_h$ is 100 s (by definition [122]). The estimated $T_g$ for DS1.5 and 3 with the VFT model is similar to the experimentally measured $T_g$ by DSC, reinforcing the analogy between the relaxation time of hole formation ($\tau_h$) and the $\alpha$-relaxation time. The estimated and measured $T_g$ of DS3 was higher than for DS1.5. The high content of acetyl groups in DS3 may reflect lower intra and intermolecular polar interactions and hydrogen bonding but could also reflect changes in the conformation of the backbone. Intra and intermolecular polar interactions and hydrogen bonding can increase the conformational energy barrier and reduce the backbone flexibility as well as steric hindrance like bulky side groups [123] and geometric restrictions like crystals or crosslinking junctions [124]. The higher $T_g$ of DS3 may also reflect the presence of new crystalline regions as observed by WAXRD (Figure 4-1). These regions may be acting as physical junctions, increase the conformational energy barrier, and reduce the chain flexibility. It should be pointed out that for polymers, the influence of polar interactions on chain flexibility near $T_g$ is affected by the magnitude of the glass transition

temperature and is less pronounced for polymers with high $T_g$. It is a consequence of the lower polar interactions compared to the thermal fluctuations ($k_B T$) at elevated temperatures [123].

Table 4-2. Fitted parameters ($T_0$ (K) and $B$ (K)) of the VFT model (Equation 4.5), fragility index ($m$) and $T_g$ for acetylated starch according to DS.

| Degree of substitution (DS) | $B$ [K] | $T_0$ [K] | $R^2$ | $m$ | $T_{g(\tau=100s)}$ [K] | $T_g$ (DSC) [K] | $T_g$ (Heat-cool mode TMDSC) [K] |
|---|---|---|---|---|---|---|---|
| 0 | - | - | - | 151[a] | - | - | 358[a] |
| 1.5 | 67 | 410 | 0.9980 | 139 | 419 | 415 | 424 |
| 3 | 217 | 399 | 0.9963 | 70 | 422 | 427 | 434 |

[a] data are extracted from reference [125] for starch with 13 wt% water.

The deviation of the temperature dependence of the $\alpha$-relaxation time for hole formation near $T_g$ was analyzed with the fragility index $m$, introduced by Angell [126, 127]. The fragility index is defined by the following equation [128]:

$$m = \frac{d \log[\tau_h(T)]}{d(T/T_g)} \Big|_{T=T_g} \tag{4.6}$$

With $\tau_h(T)$ given by Equation 4.5.

The fragility index can be used to classify the properties of a material [124, 129]. Fragile systems exhibit sharp and narrow glass transitions, presenting rapid increase in heat capacity and $\alpha$-relaxation time near $T_g$. In other words, materials called "fragile", exhibit steep deviation from the Arrhenius temperature dependence of the $\alpha$-relaxation time near $T_g$, while "strong" materials show linear temperature dependence of the $\alpha$-relaxation time. The fragility index determines the vitrification properties of a glass-forming system and can provide information on the relaxation environment of macromolecules [130]. According to the extensive review conducted by Kunal et al. [131] for several polymers with distinct side groups and backbone structures, the fragility index is primarily influenced by the packing efficiency of the amorphous chains in the glassy state and the chain flexibility. Low packing efficiency and low chain flexibility lead to higher fragility index (fragile), while polymers with high packing efficiency and flexible chains have lower fragility index (strong). Although limited studies have investigated the effect of polar interaction on

fragility index, initial results indicate that the polar interactions would increase the fragility index of polymers [123]. The fragility index may be related to the glass transition temperature of a material but the effect remains unclear and up for debate.

The fragility index of acetylated starch, estimated from Equation 4.6 and presented in Table 4-2, indicates higher fragility index for DS1.5 has compared to DS3. The magnitude of the estimated fragility index agrees with the reported value, 151, for potato starch (amylose content 20 wt%) containing 13 wt% moisture [125]. The lower fragility index of DS3 compared to DS1.5 suggests higher packing efficiency and chain flexibility in DS3 which seems counter-intuitive considering that acetyl groups are bulkier than hydroxyl groups.

### 4.4.3. Cooperative Rearranging Region Characteristics

The concept of cooperative rearranging regions (CRR), the smallest amorphous domain where a conformational rearrangement may occur independently from its environment, was used to understand the dynamic heterogeneities in acetylated starch according to DS. CRR regions were investigated by heat-cool mode TMDSC experiments and used to estimate the associated cooperativity length. In recent years, the cooperativity length scale has been extensively studied to understand its molecular characteristics [124, 129].

In our study, two approaches have been considered and compared for the estimation of the size of CRR. The first approach, Donth's model, is based on the temperature fluctuations of the amorphous regions. In this approach, the cooperativity length $\xi_a$ associated with the volume of a CRR ($V_a$) [53] can be calculated as follows:

$$V_a = \xi_a^3 = \frac{\Delta(C_p^{-1}) k_B T_a^2}{\rho(\delta T)^2} \tag{4.7}$$

where $\Delta(C_p^{-1})$ is the change of the inverse heat capacity between the liquid state and the glass state, $k_B$ is the Boltzmann constant, $\rho$ is the density of the amorphous phase and $\delta T$ corresponds to the standard deviation of the out-of-phase component of the heat capacity, $C"(T)$, fitted by a Gaussian peak ($\delta T$= Full width at half maximum/2.35).

The cooperativity degree or the number of relaxing structural units in a CRR, $N_a$, was estimated using the following relation [53]:

$$N_a = \frac{N_A \Delta\left(C_p^{-1}\right) k_B T_a^2}{m_0 (\delta T)^2} \tag{4.8}$$

Where $\Delta(C_p^{-1})$, $k_B$, $\rho$, $N_A$ and $\delta T$ are defined as above, $m_0$ is the molar mass of the relaxing structural unit, and $T_a$ corresponds to the temperature maximum of the Gaussian peak. For the estimation of $\xi_a$ and $N_a$, $\Delta(C_p^{-1})$ was obtained from heat capacity data of heat-cool TMDSC. The parameters $\delta T$ and $T_a$ were estimated by fitting a Gaussian peak to the out-of-phase heat capacity component of the heat-cool TMDSC (Figure 4-5). A repeating unit of chain was considered as the relaxing structural unit in the $N_a$ calculation.

The estimated $\xi_a$ of DS3 was lower than for DS1.5 (Table 4-3). This difference may be explained by the disruption of intermolecular bonds as suggested previously [132-134]. In the case of acetylated starch, the disruption of hydrogen bonding in DS3 would be a direct consequence of the replacement of hydroxyl groups with acetyl groups.

The second approach used to estimate the size of CRR was based on the temperature dependence of the relaxation time in the glass transition region and the model proposed by Matsuoka and Quan [135]. In their model, the segmental relaxation is based on the concept of intermolecular cooperativity where a domain of cooperativity is defined as a group of segments that must relax simultaneously. The size of this domain is specified by the number $z$ of the interlocked relaxing structural units. The estimation of the interlocked relaxing structural units relies on the basic concepts of Adam and Gibbs' theory [136]. An expression of the $\alpha$-relaxation time according to temperature is developed by comparing the conformational entropy of interlocked and isolated structural relaxing units:

$$\tau(T) = \tau^* \exp\left(\frac{\Delta\mu^*}{k}\frac{1}{T - T_0} - \frac{\Delta\mu^*}{kT^*}\right) \tag{4.9}$$

In this equation $\Delta\mu^*$ is the activation energy of the relaxation of isolated structural relaxing units, $T^*$ the temperature at which the conformational entropy of interlocked units is zero and $\tau^*$ the relaxation time at $T^*$. Fitting Equation 4.9 to the experimental results of $\tau(T)$ for many polymers showed a value of 500°C for $T^*$ [106, 137]. Note that Equation 4.9 can be transformed to the VFT equation (4.5) by defining $B = \Delta\mu^*/k$ and $\tau_0 = \tau^* \exp(-\Delta\mu^*/kT^*)$.

The number of interlocked relaxing structural units ($z$) is a function of temperature and was estimated as follows:

$$z = \frac{(T^* - T_0)T}{(T - T_0)T^*} \tag{4.10}$$

The value of $z$, presented in Table 4-3, was calculated with the parameters of the VFT model obtained with the relaxation time of hole formation (Table 4-2) at $T_g$. The estimated z and $N_a$ are lower for DS3 compared to DS1.5 while z is slightly lower than $N_a$ for DS1.5. In our analysis, we assumed that the repeating unit of a chain is the relaxing structural unit, however this definition is debatable. Rijal et al. [129] questioned the selection of the monomer as the relaxing structural unit for polymers with several benzene rings in their repeating units.

Table 4-3. Molar mass of the relaxing structural unit $m_0$, center peak of the fitted Gaussian peak on out-of-phase heat capacity component $T_{a(\tau=90s)}$, mean temperature fluctuation in a CRR ($\delta T$), the cooperativity length ($\xi_a$), number of relaxing structural units ($N_a$) and number of interlocked relaxing structural units ($z$) at $T_g$ (Equations 8, 9 and 11) of DS1.5 and DS3.

| Degree of substitution | $\boldsymbol{m_0}$ [g/mol] | $\boldsymbol{T_{a(\tau=90s)}}$[K] | $\boldsymbol{\delta T}$ [K] | $\boldsymbol{\xi_a}$ [nm] | $\boldsymbol{N_a}$ | $\boldsymbol{z\ (T = T_g)}$ |
|---|---|---|---|---|---|---|
| 0 | 162 | 358($\boldsymbol{\tau = 60s}$)[a] | 10[a] | 0.8[a] | 2.83 | - |
| 1.5 | 225 | 424.46 ± 0.02 | 4.21 ± 0.02 | 2.02 | 11.39 | 8.1 |
| 3 | 288 | 434.06 ± 0.02 | 8.43 ± 0.02 | 1.50 | 3.38 | 3.6 |

[a] data are extracted from reference [125] for starch with 13 wt% water.

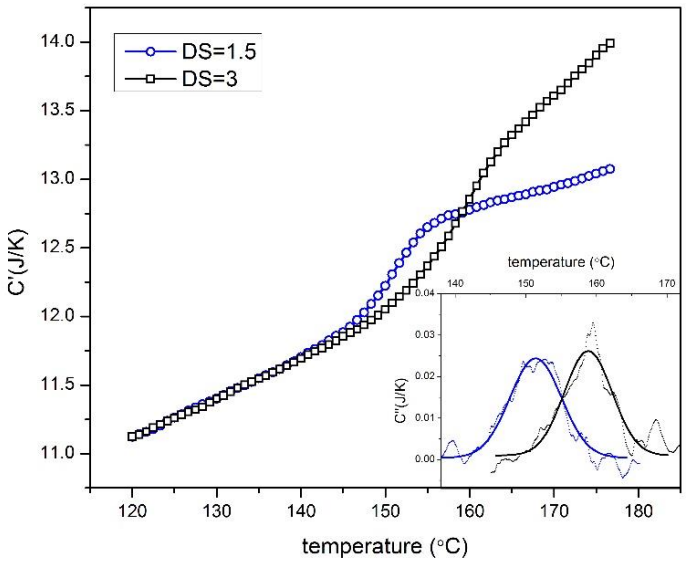


Figure 4-5. In-phase and out-of-phase of heat capacity components of heat-cool TMDSC. Solid line in inset represent the fitted Gaussian peaks.

Another means of evaluating $T_g$ was obtained from the heat-cool mode TMDSC data (Table 4-2). Somewhat higher $T_g$ estimates were obtained for DS1.5 and DS3 compared to the other two $T_g$ estimates. Such differences may be attributed to the high frequency of modulation of heat-cool mode TMDSC compared to the conventional DSC method.

### 4.4.4. Dynamics and Chain Flexibility at Ambient Condition

The flexibility of chains at room temperature was investigated by SS-NMR spectroscopy. Figure 4-6 shows the $^{13}C$ CP/MAS spectra of DS1.5 and DS3 at various spin-lock times along with the chemical structure and associated chemical shift of each carbon. Peak assignments was based on the reported literature data [138]. There was no significant difference between DS1.5 and DS3 except for smoother spectra of DS3 which could be attributed to the lower degree of crystallinity (Figure 4-1). The peak at 21 ppm (methyl group) was selected for representing the relaxation behavior of the chains as this peak was distinct from the other peaks and had no spinning side bands.

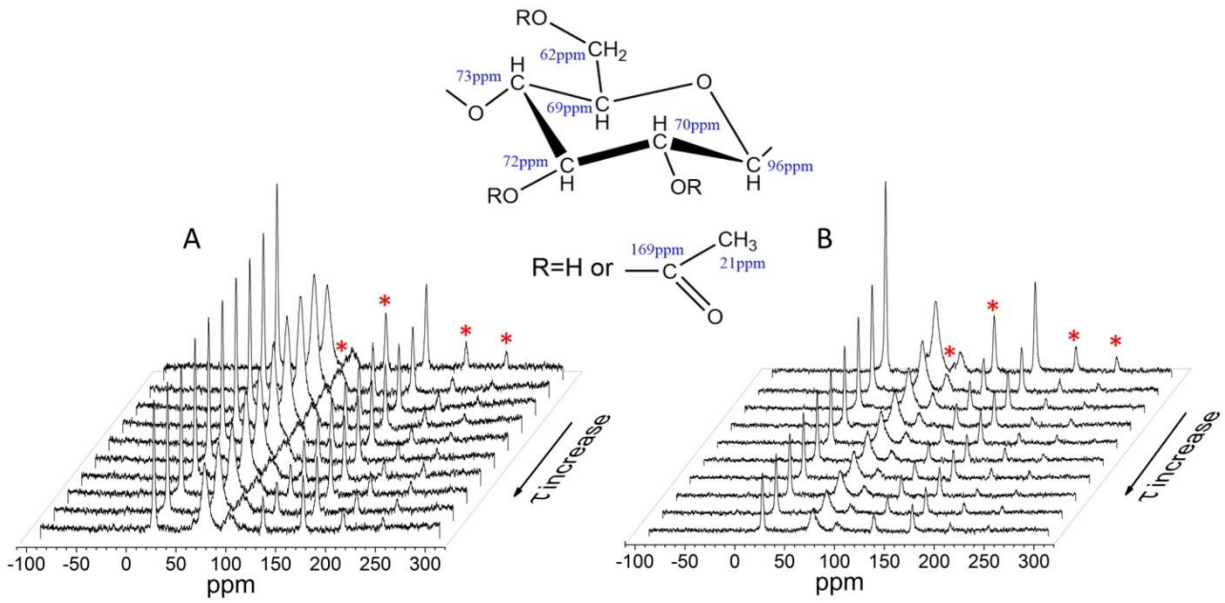


Figure 4-6. $^{13}C$ CP/MAS spectra of DS (A) 1.5 and (B) 3 at various spin-lock times. Spinning sidebands are marked with an asterisk. For better visualization of data spectra were plotted with reverse chemical shift axis.

The normalized magnetization decay in the rotating frame for the methyl carbon peak of DS1.5 and DS3 and its exponential fit according to Equation 4.4 is presented in Figure 4-7.

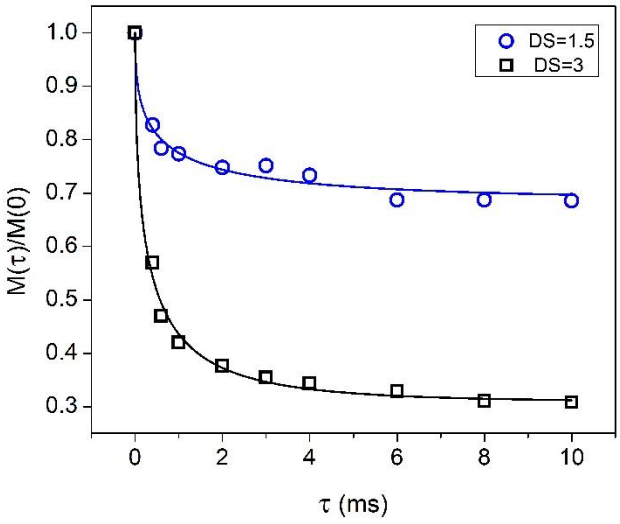


Figure 4-7. Normalized magnetization decay in the rotating frame of methyl carbon peak (21ppm) for DS1.5 and DS3 at room temperature. Solid lines are the fitted stretched exponential function (Equation 4).

Shorter $T_{1\rho}(C)$ of the methyl carbon peak was associated to DS3 compared to DS1.5, suggests higher chain flexibility (Table 4-4). The lower molecular flexibility of DS1.5 could be due to intra and intermolecular interactions as reported previously for the relaxation data of a linear polymer, poly(ethyleneoxide) (PEO) complexed with $Ba(ClO_4)_2$ and pure PEO [139]. In the context of acetylated starch, the hydrogen bonding present in DS1.5 may explain the restrictions in molecular mobility. These observations suggest that the chain dynamics of DS3 are faster than for DS1.5 at ambient temperature conditions.

Table 4-4. Spin-lattice relaxation time in the rotating frame for carbon, $T_{1\rho}(C)$ (ms) and $\beta$, the non-exponentiality parameter (Equation 4) for DS1.5 and DS3.

| Degree of substitution | $T_{1\rho}(C)$ (ms) | β |
|---|---|---|
| **1.5** | 0.59 ± 0.24 | 0.43 ± 0.14 |
| **3** | 0.34 ± 0.08 | 0.49 ± 0.10 |

Dynamic heterogeneity can be reflected by correlations between the range of the glass transition temperature as determined by $\delta T$ and the broadness of the distribution of relaxation times for the amorphous phase [124]. For acetylated starch, higher $\delta T$ was observed for DS3 compared to DS1.5 which shows enhanced dynamic heterogeneity of the amorphous phase (Table 4-3). The estimated $\beta$ obtained by SS-NMR at room temperature also supports this conclusion (Table 4-4).

### 4.4.5. Effect of Temperature Conditions on the Dynamics and Chain Flexibility

The effect of temperature conditions on the chain flexibility was obtained by comparing the experimental observations of TMDSC at moderate temperatures (near the glass transition region) to the predictions of VFT model and the experimental observations of SS-NMR at ambient temperature. The evolution of the relaxation time for hole formation $\tau_h(T)$, obtained from the TMDSC experimental data, was shown to change according to DS and temperature (Figure 4-4). In the moderate temperature region, the $\tau_h(T)$ was lower for DS1.5 compared DS3 while in the ambient temperature region (temperature lower than 416 K), the predicted $\tau_h(T)$ was higher for DS1.5. The presence of an intersection point in the $\tau_h(T)$ curve for DS1.5 and DS3 is an indication of the change in the chain dynamic behavior. The different dynamic behavior according to temperature conditions may explain the lack of correlation between $T_g$ and $m$ observed in this

study where higher $T_g$ was observed for DS3 compared to DS1.5 and lower fragility index for DS3 compared to DS1.5. At ambient temperature, one can envision that few crystalline junctions in DS3 and much more hydrogen bonds in DS1.5 is limiting the molecular mobility. At moderate temperatures (near $T_g$), one can envision that temperature is disrupting hydrogen bonding in DS1.5 while crystalline junctions in DS3 remain intact. Figure 4-8 proposes a schematic representation of potential structural changes in acetylated starch which could lead to different chain dynamic behavior according to DS and temperature.

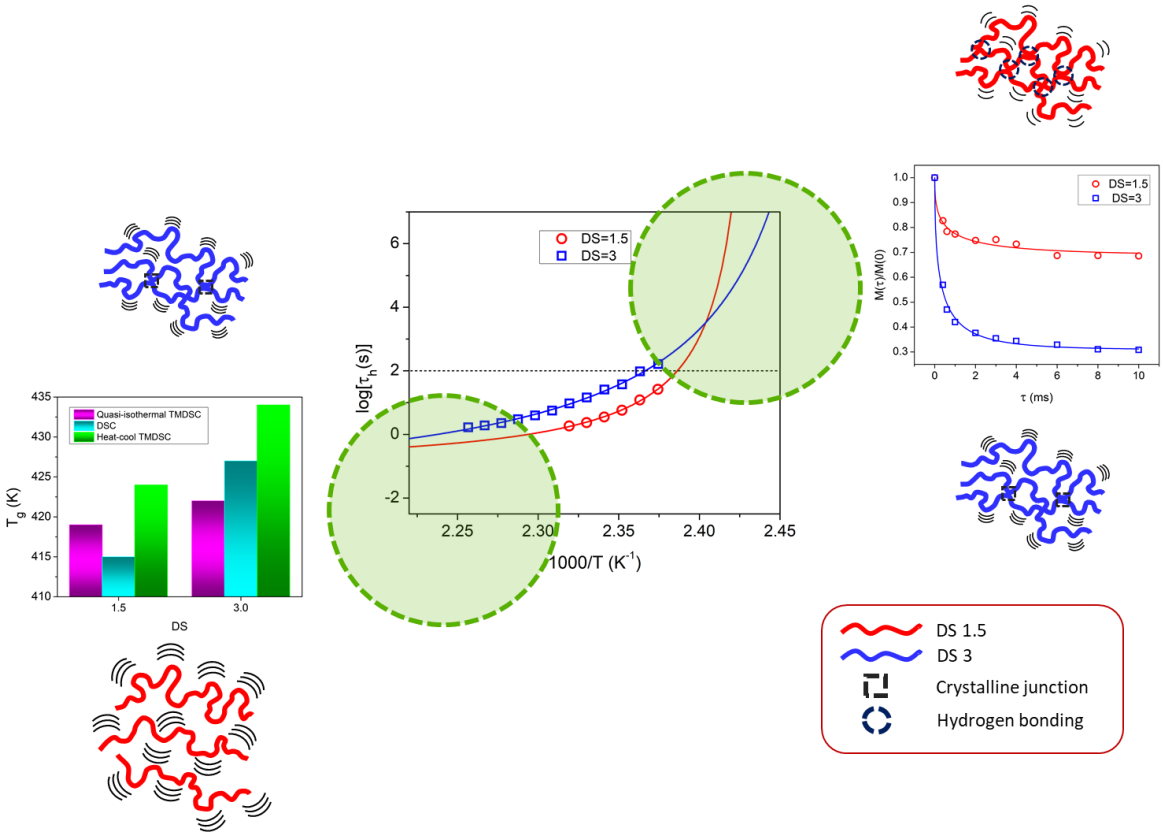


Figure 4-8. Schematic representation of potential structural changes according to temperature that could induce changes in dynamic behavior.

It is important to note that carbons in a given material could display different relaxation times indicating different dynamic behaviors (Appendix II Figure 2). For example, the carbons in the backbone have longer $T_{1\rho}$ and higher $\beta$ than the pendant carbons for DS3 (Appendix II Table 1). It means that the dynamics of the carbons in the backbone are slower and more heterogeneous than the pendant carbons. Similar analysis could not be done for DS1.5 because the signal to noise ratio was inappropriate for analysis.

## 4.5. CONCLUSION

In this study, the effect of acetylation, where hydroxyl groups are replaced by acetyl groups, on chain dynamics and mobility was investigated. Of particular interest was the investigation of the effect of introducing acetyl groups on hydrogen bonding, steric hindrance, packing efficiency and chain flexibility in acetylated starch. The chain dynamics of acetylated starch with two distinct DS, 1.5 and 3 and for moderate and ambient temperature conditions were investigated by adopting techniques and concepts developed for synthetic polymers. At moderate temperature conditions, TMDSC and the concepts of relaxation time for hole formation and cooperative rearranging regions (CRR) were selected. At ambient temperature conditions, SS-NMR was used.

Based on its evolution with temperature, the relaxation time for hole formation estimated from Quasi-isothermal TMDSC heat capacity data was found to be an appropriate representation of the $\alpha$-relaxation time near the glass transition temperature region. Together with the VFT model, the relaxation time for hole formation, was used to estimate the $T_g$ and the fragility index (m). A slightly lower $T_g$ for DS1.5 was observed compared to DS3 while the fragility index was higher for DS1.5 compared to DS3. DS1.5 was characterized by higher size CRR compared to DS3 which could reflect the hydrogen bonding present in DS1.5.

At ambient temperature conditions, SS-NMR results indicated higher chain flexibility for DS3 compared to DS1.5. The SS-NMR results at ambient conditions supported the predicted differences of the relaxation time for hole formation according to DS that were deduced from Quasi-isothermal TMDSC. TMDSC along with solid-state NMR results showed more heterogeneous dynamics of DS1.5 compared to DS3. Since the hydroxyl and acetyl groups are randomly distributed on the repeating units for DS1.5, this distribution can cause heterogeneity in the dynamics of the chains and could explain the higher dynamic heterogeneity of DS1.5 compared to DS3 (only acetyl groups present).

The next steps should focus on the development of PLA/AS blends to confirm the benefits of acetylation. Chapter 3 indicates two different ranges of DS domains in terms of processability improvement. In the first DS domain (0-1.5), there is a drastic reduction of the degree of crystallinity while, in the second DS domain (1.5-3), the crystallinity decreased slowly with increasing DS. The glass transition behavior (DSC) and the second thermal degradation peak

(DTG) which was observed for acetylated starch with a DS higher and equal to 1.5 are indicative of processability improvement. Materials with higher fragility index (fragile) show more rapid change of relaxation time with changing temperature and as a consequence faster change of viscosity. In contrast, strong materials (materials with lower fragility index) exhibit slow change of viscosity with changing temperature. Therefore, lower fragility index is in the favor of thermal processability. Results of chapter 4 showed that acetylation of starch reduces its fragility index and that the higher degree of substitution leads to lower fragility index. It can be concluded that DS1.5 is the threshold where improvement in processability of acetylated starch is noticeable. On the other hand, interfacial tension calculation in chapter 3 indicated that more effective compatibility with PLA can be achieved for acetylated starches with higher DS. Consequently, the most promising acetylated starch characteristics for blending applications should have DS of at least 1.5.

In the next chapter, interfacial properties of PLA/AS will be investigated. Thickness of the interphase and dynamics of PLA chains at interfacial region will be studied as the first step toward better understanding of the PLA/AS blend properties.

# 5. Effect of Degree of Substitution on the Interphase Region of Poly(lactic acid)/Acetylated Starch Blends

Rasool Nasseri[a], Christine Moresoli [b], Aiping Yu[c], Zhongshun Yuan[d] and Chunbao (Charles) Xu[f]

Description of contributions:

[a]: performing all the experimentations and writing the manuscript.

[b] and [c]: main and co-supervisors.

[d] and [f]: providing the acetylated starch samples.

This manuscript is prepared for submission to "Macromolecules" journal under ACS publication.

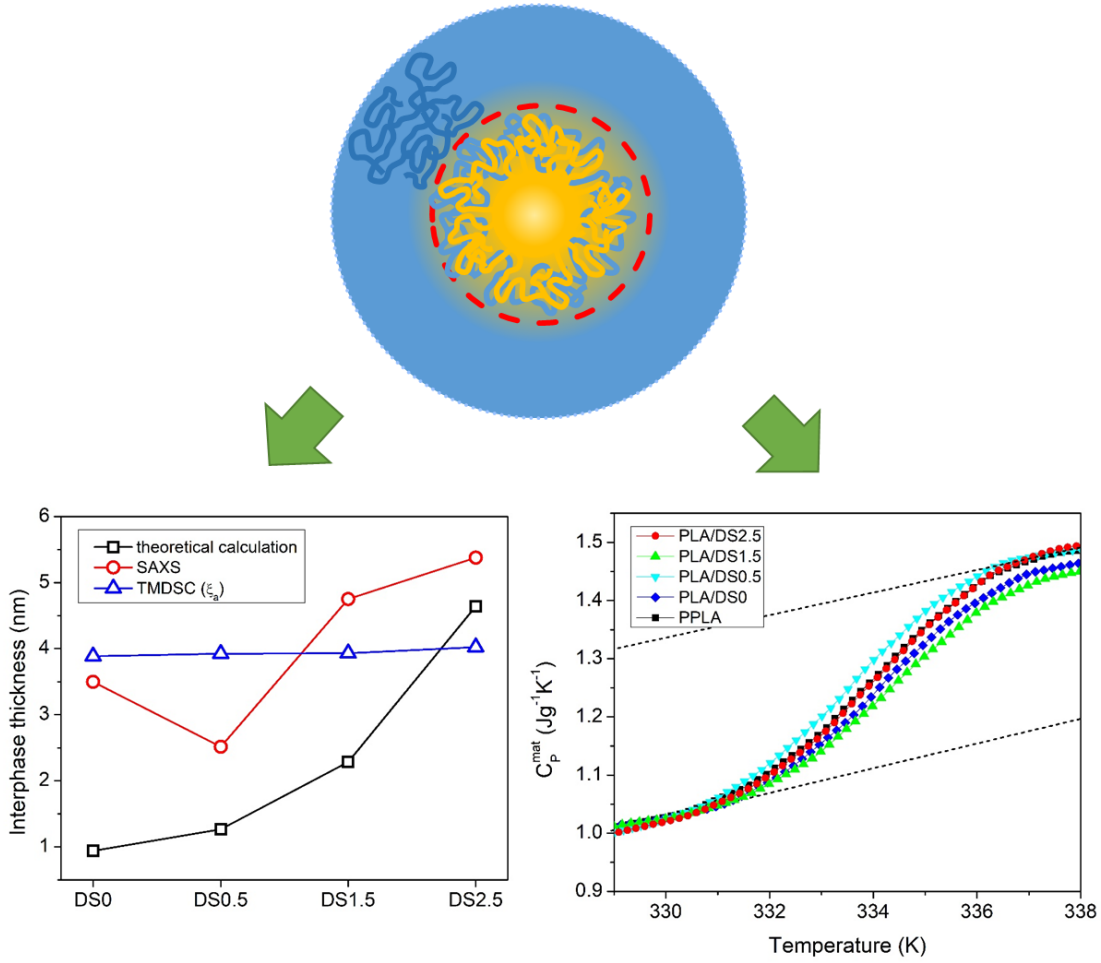

## 5.1. Synopsis

The effect of starch acetylation on the interfacial properties of poly(lactic acid) (PLA)/acetylated starch (AS) was investigated by comparing model predictions with experimental observations. The theoretical thickness of the interphase for PLA/AS blends estimated from pure component properties was compared to experimental estimates obtained by small angle X-ray scattering (SAXS). The interphase thickness increased with increasing degree of substitution (DS) of AS in PLA/AS blend. Satisfactory accordance was observed between the length scale of dynamic heterogeneity of the PLA matrix in PLA/AS blends, estimated by temperature modulated DSC (TMDSC), and the interphase thickness estimated by a theoretical approach and SAXS measurements. TMDSC result revealed the slowdown of the PLA chain dynamics at the interphase region for the PLA/DS0 and PLA/DS1.5 blends. Hydrogen bonding between PLA chains and AS was observed in theses samples by FTIR as the reason of dynamic slowdown at the interphase region.

## 5.2. Introduction

Poly(lactic acid) (PLA) is a promising biodegradable polymer for the replacement of synthetic polymers in some applications. Despite its good mechanical performance and permeability, the applications of PLA are limited by its relatively high cost and slow rate of degradation. The high cost of PLA materials may be alleviated by blending PLA with low cost biodegradable polymers. A promising low cost, abundant and renewable polymer is starch [7] but its high degree of crystallinity and poor compatibility with PLA limit the blending capability of native starch with PLA [8]. The improvement of the properties of PLA/starch blends can be achieved by different strategies, including: additive plasticization, mixture softening, elastomer toughening and interphase compatibilization [140]. The interphase compatibilization strategies can be further classified as chemical crosslinking [141], amphiphilic bridging [142], interfacial transitioning [143], and componential chemical modification [57]. Between the two components, chemical modification of starch is much more convenient. Among all chemical modifications, acetylation of starch is a relatively simple chemical modification that could be used to improve its processability and compatibility with PLA. The substitution of hydroxyl groups on the glucose repeating units of starch molecules with acetyl groups should alter the interactions between starch

and PLA ultimately leading to improved blend properties. The degree of acetylation is generally expressed as the degree of substitution (DS) which is the number of hydroxyl groups on a glucose unit of a starch molecule that has been replaced by acetyl groups (from 0 to 3).

Due to thermodynamic considerations, most polymer blends are immiscible [34]. Therefore, the properties and performance of polymer blends reflect the properties of the pure components and their interphase characteristics (thickness, dynamics, and interfacial interactions) [35]. While the morphology of polymer blends has been extensively studied, there is limited information available on the polymer-polymer interphase due to the limited number and complexity of techniques suitable for the direct investigation of the interphase [36]. Generally the role of the interphase in a blend will be specific to the given property. For example, the influence of the interphase is generally much more pronounced for mechanical properties measured at large deformation [37]. It is agreed that a thick and soft interphase (no vitrification of the chains of the matrix exists in the interfacial region) is generally necessary to achieve high strength [37]. The contributions of the interfacial interactions to the crystallization kinetics remains unclear. The interfacial interactions might restrict the movement of the polymer chains for conformational ordering required for nucleation. Alternatively, interfacial interactions might be beneficial for the adsorption of polymer chains [38].

Theoretical efforts to investigate the interphase have focused on the development of models to estimate its thickness and composition profile since early 1970s. Helfand et al. [39-43] have developed a quantitative theoretical framework in which enthalpic penalty of interdiffusion of immiscible components balances out with the entropic gain for widening the interphase. The best energetic balance finally defines the composition and thickness of the interphase.

The experimental investigation of the interphase has generally relied on sophisticated techniques of the mutual diffusion of immiscible polymers [44-48]. Many of these techniques need careful sample preparation or labeling and typically measure the thickness of the interphase in a stacked bilayer of polymer films [49]. In contrast, the SAXS [50] and TMDSC [51] methods can be used for a pre-processed polymer blend without any special sample preparation.

In this study, the effect of the degree of starch acetylation on the properties of the interphase in PLA/acetylated starch (AS) blends was investigated. The ultimate goal of this work was to evaluate the potential of AS with different degrees of substitution (DS) in modulating key properties of

PLA/AS blend. First, the thickness of the interphase of biphasic PLA/AS blends was estimated with the Helfand model and compared to experimental measurements obtained by SAXS. Next, the properties of the interphase for PLA/AS blends were examined by TMDSC and FTIR.

## 5.3. Materials and Methods

### 5.3.1. Materials

PLA 4032D ($M_n$=58000 g/mol, D-content 1.8 %) was provided by NatureWorks Inc (USA). Corn starch was acquired from local Ontario market (BulkBarn®, product code: 000260). Corn starch and acetic anhydride were mixed with pre-determined molar ratios of acetic anhydride/starch and acetic acid in order to produce acetylated starch. The mixture was stirred and heated to 135°C using an oil bath for 3 hours. Precipitation of the reaction mixtures into a non-solvent followed by filtration and washing the precipitant with non-solvent were carried out in this sequence. The recovered SA product was vacuum dried overnight in an oven at 45°C. Acetylated starch with four DS, 0.5, 1.5, 2.5, and 3 were synthesized according to the above mentioned procedure.

### 5.3.2. Methods

#### 5.3.2.1. Blend Preparation

Prior to their mixing, PLA and AS were dried in a vacuum oven at $80°C$ over night. A SJSZ-07A lab-scale twin screw extruder (Ruiming Plastics Machinery, Wuhan city, China) was used for melt-blending of PLA with AS. In order to prevent degradation, preliminary experiment were preformed to identify the mixing temperature, speed and duration for minimizing degradation. The extrusion was performed at $180°C$ with screw speed of 30 rpm for 7 min. The extruded samples were then pelletized. Pellets were compression molded to make a thin sheet using a hot press at 200°C with 10000 lbs pressure for 4 minutes (PHI, Pasadena Hydraulic Inc., USA). The compression molded sheets were then placed in an oven at $190°C$ and quenched with liquid nitrogen to produce completely amorphous blends for SAXS analysis. A small portion of the quenched sheets was grinded to produce a fine powder for FTIR analysis. Table 5-1 presents the code and composition of the PLA and PLA/AS blends.

Table 5-1. Code, composition, and processing time of the samples.

| Sample | PLA (wt%) | AS (wt%) | DS of AS |
|---|---|---|---|
| **PPLA (processed)** | 100 | 0 | - |
| **PLA/DS0** | 85 | 15 | 0 |
| **PLA/DS0.5** | 85 | 15 | 0.5 |
| **PLA/DS1.5** | 85 | 15 | 1.5 |
| **PLA/DS2.5** | 85 | 15 | 2.5 |
| **PLA/DS3** | 85 | 15 | 3 |

### 5.3.2.2. Small-Angle X-ray Scattering (SAXS)

Small-angle X-ray scattering measurements were performed using a SAXSess $mc^2$ instrument (Anton Paar, Austria) equipped with a Kratky block-collimation system and a sealed-tube Cu K$\alpha$ X-ray generator with the wavelength, $\lambda$= 0.154 nm, operating at 40 kV and tube current = 50 mA. All the measurements were performed at ambient temperature using transmission geometry. The scattered X-ray intensities were measured by a 2D charge coupled detector located 264.5 mm apart from the sample. The scattering intensities, $I(q)$, measured as a function of the half of scattering angle, $\theta$, were first desmeared and then corrected for the background absorption and transformed to a plot of scattering intensity vs scattering vector, $q$ ($q = 4\pi sin\theta/\lambda$) using the saxsImage software (Utah SAXS Tools, David P. Goldenberg, September 2012).

### 5.3.2.3. Temperature Modulated Differential Scanning Calorimetry (TMDSC)

TMDSC measurements were carried out with a Q2000 (TA Instruments, USA), calibrated with indium and sapphire disk standards, using standard Tzero. Nitrogen, with a 30 mL/min flow rate, was used as purge gas. The sample mass, about 10 mg, was placed in aluminum plans. The temperature procedure was (i) heating to 190°C at 20°C/min heating rate, (ii) constant heating at 190°C for 5 min in order to eliminate thermal history, (iii) cooling to 40°C at 20°C/min cooling rate of to avoid recrystallization of PLA and (iiii) heating to 70°C at 2°C/min heating rate and amplitude of 1.5°C coupled to 90 s period. Peak deconvolution was obtained with the procedure proposed by Weyer et al. [117] to obtain the in-phase ($C'$) and out-of-phase ($C''$) components of the heat capacity and a Gaussian peak was fitted to the out-of-phase component of the heat capacity using OriginPro 8.5.

#### 5.3.2.4. Fourier Transform Infrared (FTIR) Spectroscopy

FTIR spectra were recorded on a Tensor-27 Fourier IR spectrometer (Bruker, USA). Samples were prepared by mixing fine powder of PLA/AS blends with KBr and pressed into KBr pellets. The wave number range of FTIR was 4000-500 $cm^{-1}$ with a resolution of 1 $cm^{-1}$. Number of 32 scans were accumulated to reduce spectra noise.

## 5.4. Results and Discussions

### 5.4.1. Thickness of the interphase

Predictions of compressible regular solution (CRS) model along with the SEM observations reported in Chapter 6 confirmed the presence of two distinct phases for all PLA/AS blends except for the PLA/DS3 blend. Consequently in all blends except PLA/DS3 an interphase region exists and interphase properties like thickness and chain dynamics can be investigated.

The thickness of the interphase for biphasic PLA/AS blends according to DS at room temperature ($298K$) was estimated by three different methods, one theoretical method and two experimental methods namely SAXS and TMDSC. The theoretical estimates of the thickness are based on the approach proposed by Helfand et al. and the properties of the pure components [39-42]. In this approach, the thickness of the interphase ($a_{I\infty}$) is related to the interaction parameter by the lattice model considering infinite chain length:

$$a_{I\infty} = 2\left[\frac{\beta_A^2 + \beta_B^2}{2\chi_{AB}(\rho_{0A}\rho_{0B})^{1/2}}\right]^{1/2} \tag{5.1}$$

with

$$\beta_i^2 = \frac{\rho_{0i} b_i^2}{6} \tag{5.2}$$

where $b_i$ is the Kuhn segment length and $\rho_{0i}$ is the segment density of component $i$ (considered equal to the density of the polymer) and $\chi_{AB}$ is Flory-Huggins interaction parameter. The subscript $A$ and $B$ represent PLA and AS, respectively. Broseta et al. corrected $a_{I\infty}$ for entropic effects and suggested an expression that goes beyond the approximation of infinite molecular weight:

$$a_I = a_{I\infty}[1 + (1/\omega_a + 1/\omega_b) ln2] \tag{5.3}$$

where $\omega_i = \chi_{AB} N_i$ is the degree of incompatibility. Kong et al. [144] combined the interaction energy of the Flory-Huggins theory with the CRS model [145] to develop a modified Flory-Huggins interaction parameter as follows:

$$\chi_{AB} = \frac{v}{kT}\left(\tilde{\rho}_A \delta_{A,0} - \tilde{\rho}_B \delta_{B,0}\right)^2 \quad (5.4)$$

where $v$ is the geometric average of segment volumes:

$$v = \sqrt{v_A v_B} \quad (5.5)$$

The hard core segment is defined as:

$$v_i = M_i / N_{Av} \rho_i^* \quad (5.6)$$

$M_i$ is the molecular weight of the repeating unit and $N_{Av}$ is Avogadro's number. The parameter $\rho_i^*$ is the hard core density and is estimated from density at temperature $T$ through the following relation:

$$\rho_i(T) = \rho_i^* exp(-\alpha_i T) \quad (5.7)$$

The hard core density and the density at temperature $T$ was used to calculate reduced density at temperature $T$:

$$\tilde{\rho}_i(T) = \rho_i / \rho_i^* \quad (5.8)$$

The parameter $\delta_{i,0}$ was obtained from the reduced density and solubility parameter at $298K$:

$$\delta_{i,0}^2 = \delta_i^2(298) / \tilde{\rho}_i(298) \quad (5.9)$$

The pure component properties of AS were measured experimentally in our previous work and the pure component properties of PLA were obtained from the literature. Those properties, summarized in Table 5-2, were used to estimate the interphase thickness of the PLA/AS blends.

Table 5-2. Pure component properties of AS and PLA.

| Material | $\rho$ (g/cm$^3$) | $\alpha$ ($10^{-4}$ K$^{-1}$) | $\delta$(298) (J.cm$^{-3}$)$^{1/2}$ | $M_i$ (g/mol) | molecular weight (g/mol) | Kuhn segment length (nm) |
|---|---|---|---|---|---|---|
| **PLA** | 1.25[a] | 7.4[a] | 21.73[b] | 76 | 58000 | 0.72[c] |
| **Native starch (DS0)** | 1.49 | 0.52 | 44.25 | 162 | 17500000 | 2.4[d] |
| **DS0.5** | 1.46 | 0.67 | 37.21 | 183 | 19200 | 2.4[d] |
| **DS1.5** | 1.40 | 1.82 | 29.12 | 225 | 3500000 | 2.4[d] |
| **DS2.5** | 1.36 | 2.24 | 24.38 | 267 | 1800000 | 2.4[d] |
| **DS3** | 1.28 | 3.36 | 22.63 | 288 | 323000 | 2.4[d] |

[a] reference [94]; [b] reference [146]; [c] reference [147]; [d] reference [148, 149]

The Porod analysis was employed to determine the interphase thickness. The original Porod's law was developed for an ideal two-phase system with sharp boundary between the two phases and without background effect. The original Porod's law has been modified to be able to analyze real polymer systems. First, the scattering intensity should be corrected for the effect of thermal density fluctuations [150]. Second, the effect of diffuse interface boundary (interphase) should be accounted for such as proposed by Vonk [151] and Ruland [152]. Therefore, the scattered intensity can be expressed as:

$$I(q) - I_{background} = \frac{K_p}{q^4}\exp(-4\pi^2\sigma^2 q^2) \tag{5.10}$$

where $K_p$ is a constant. The interphase thickness is then $a_I = 12^{\frac{1}{2}}\sigma$. The parameter $I_{background}$ can be estimated from the slope of a plot of $q^4 I(q)$versus $q^4$ at large scattering vectors. The interphase thickness can then be estimated from the slope of a plot of $\ln[(I - I_{background})q^4]$ versus $q^2$, (Figure 5-1).

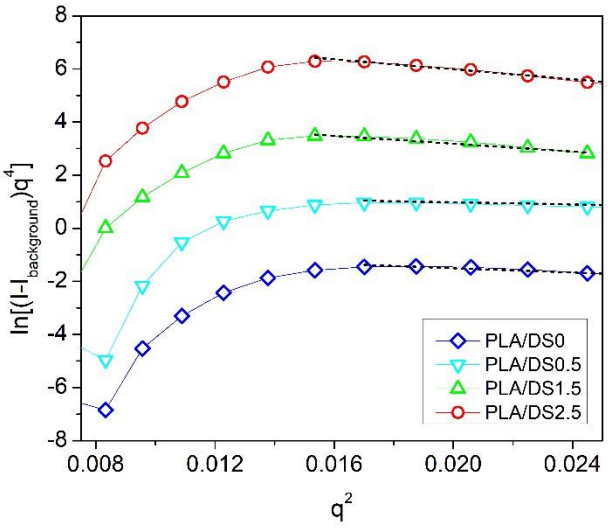


Figure 5-1. Porod plots of PLA/AS blends at room temperature. Slop of dashed black lines where used to estimate the interphase thickness. Plots are vertically shifted for better visualization.

The existence of potential relationships between the minimum thickness of the interphase and the characteristic length scale $\xi_a$ of the dynamic heterogeneities or cooperative rearranging regions (CRR) has been proposed for the matrix of biphasic structures [36]. Relationship between the thicknesses of the interphase of a thin polymer film with air and dynamic heterogeneity or CRR length scale has also been suggested in theory [153] and simulation [154] studies. In the context of the PLA/AS blends investigated in this study, the existence of potential relationships between the thickness of the interphase and $\xi_a$ of the blends at $T_g$ was investigated. The CRR size was estimated from the temperature fluctuation of the amorphous regions based on Donth's approach. In this approach, the cooperativity length scale $\xi_a$ is associated with the volume of a CRR ($V_a$) [53] and was calculated as follows:

$$V_a = \xi_a^3 = \frac{\Delta(C_p^{-1}) k_B T_a^2}{\rho(\delta T)^2} \tag{5.11}$$

where $\Delta(C_p^{-1})$ is the change of the inverse heat capacity between the liquid and the glass states, $k_B$ is the Boltzmann constant and $\rho$ is the density of the amorphous phase. When the out-of-phase component of the heat capacity, $C"(T)$, is fitted by a Gaussian peak, $\delta T$ corresponds to the standard deviation of this Gaussian peak ($\delta T$= Full width at half maximum/2.35) and $T_a$ corresponds to the temperature maximum of the Gaussian peak, (Appendix III, Table1).

The estimates of the thickness of the interphase for biphasic PLA/AS blends according to DS, is presented in Figure 5-2. The estimates of thickness are in the same order of magnitude of reported data for immiscible polymer blends in the literature. For instance, Perrin and Prud'homme reported a value of 1.8 nm for the interphase thickness of poly(styrene)/poly(methyl methacrylate) blend which was measured by SAXS [50]. For the same blend, Farinha et al. measured a value of 2.5 nm as the thickness if the interphase by ellipsometry [155]. More examples of interphase thickness for various polymer blends which were measured with various techniques are presented in Appendix III (Table 2). The estimates of the interphase thickness deduced from the TMDSC experimental measurements seem to be in a good agreement with the calculated and SAXS derived interphase thickness of the blends and showed negligible effect (gradual increase) due to the DS of the acetylated starch. It is worth mentioning that $\xi_a$ is calculated at $T_g$ and would increase at ambient condition. In contrast, the theoretical and SAXS derived estimates showed increased thickness of the interphase with increasing DS except for the PLA/DS0 blend (SAXS estimates). The theoretical estimates of the thickness of the interphase are generally lower than those deduced from the SAXS experimental measurements. These differences seem reasonable considering that the theoretical calculations are for thermodynamic equilibrium conditions which may be far away from the actual processing conditions due to the kinetic limitations of the system and that a number of approximations were considered. These approximations include the calculation of the Flory-Huggins interaction parameter using the properties of the pure components, the calculation of the Kuhn segment length using the properties of amylose only while AS contains both amylose and amylopectin and that AS with different DS possess different chain flexibilities due to the replacement of hydroxyl groups with acetyl group. Presence of visible gaps observed by SEM (chapter 6) in the PLA/DS0 blend may explain the higher measured interphase thickness by SAXS for the PLA/DS0 blend compared to the PLA/DS0.5.

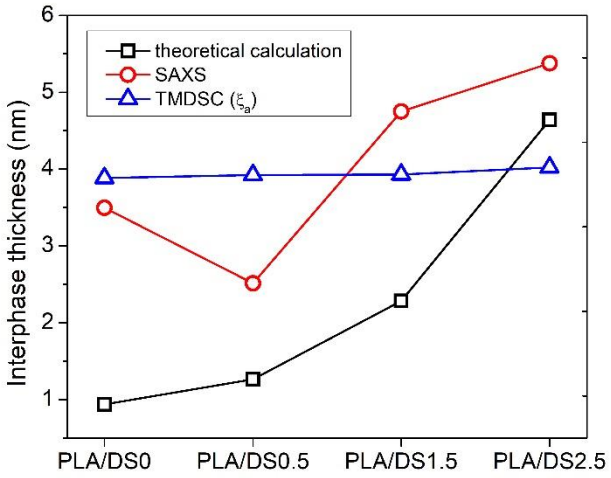


Figure 5-2. Thickness of the interphase of PLA/AS blends according to DS and estimated by three methods (theoretical calculation, SAXS and TMDSC).

## 5.4.2. Dynamics of the Interphase

The dynamics of the interphase are known to be strongly influenced by the interactions between the chains of the matrix and the dispersed phase [81]. These interactions can be investigated by examining the behavior of the specific heat capacity at the glass transition temperature and can provide information on the fraction of the chains of the matrix contributing to the glass transition. By comparing the behavior of the pure matrix to the blends, one can estimate the fraction of the chains of the matrix that has slower dynamics due to the interaction with the dispersed phase and that do not contribute to the glass transition [156]. We have used TMDSC to investigate these effects by accurately estimating the heat capacity while avoiding kinetic effects such as solvent evaporation, crystallization, and enthalpic recovery [81]. The normalized heat capacity of the PLA/AS blends was calculated as:

$$C_p^{mat} = \frac{C_p^{blend} - C_p^{AS} m_{AS}}{1 - m_{AS}} \tag{5.12}$$

where, $C_p^{blend}$ and $C_p^{AS}$ are the specific heat capacity of the blend and AS (Appendix III, Figure 1), and $m_{AS}$ is the weight fraction of AS in the blend. Figure 5-3A depicts the normalized specific heat capacity of the PLA/AS blends and pure PLA.

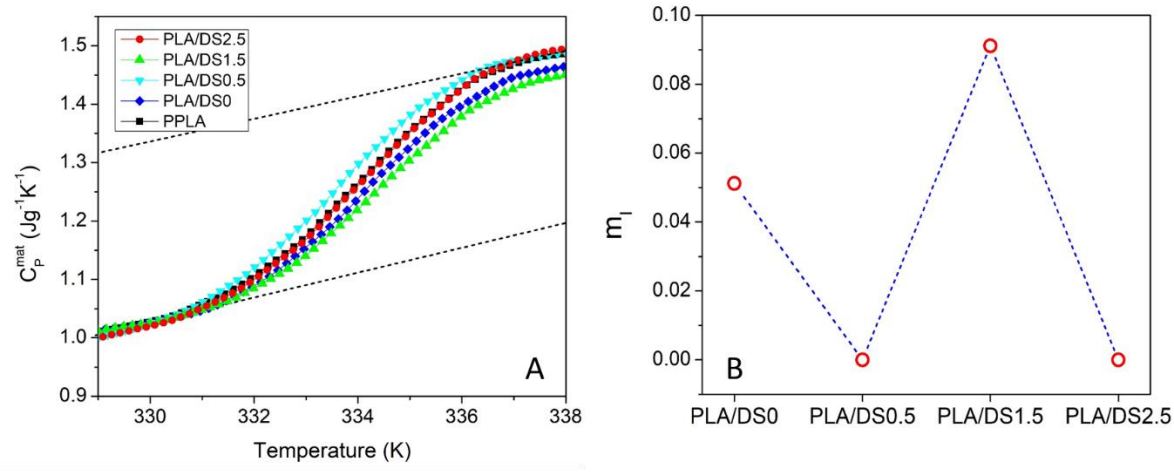


Figure 5-3. (A) Specific heat capacity of the PLA/AS blends. The curves are vertically shifted to align at lower temperatures and illustrate the change of specific heat capacity increment at glass transition. The dotted lines are presented to guide the eye. (B) The volume fraction of the PLA matrix with slower dynamics.

The difference between the specific heat capacity increment at $T_g$ of neat PLA ($\Delta C_p$) and that of the PLA matrix in the blends ($\Delta C_p^{mat}$), $\delta C_p = \Delta C_p - \Delta C_p^{mat}$, was used to estimate the weight fraction of the PLA matrix in the blends with slower dynamics as follows:

$$m_I = \frac{\delta C_p}{\Delta C_p} \tag{5.13}$$

The calculated $m_I$ for the biphasic PLA/AS blends, presented in Figure 5-3B, indicate that the PLA/DS0 and PLA/DS1.5 have an interphase with slower dynamics ($m_I \neq 0$). There is no fraction with slower dynamics for PLA/DS05 and PLA/DS2.5 blends ($m_I = 0$).

## 5.4.3. Interfacial Interactions

FTIR was used to probe the physical interactions between the PLA matrix and the AS dispersed phase in the PLA/AS blends (Figure 5-4).

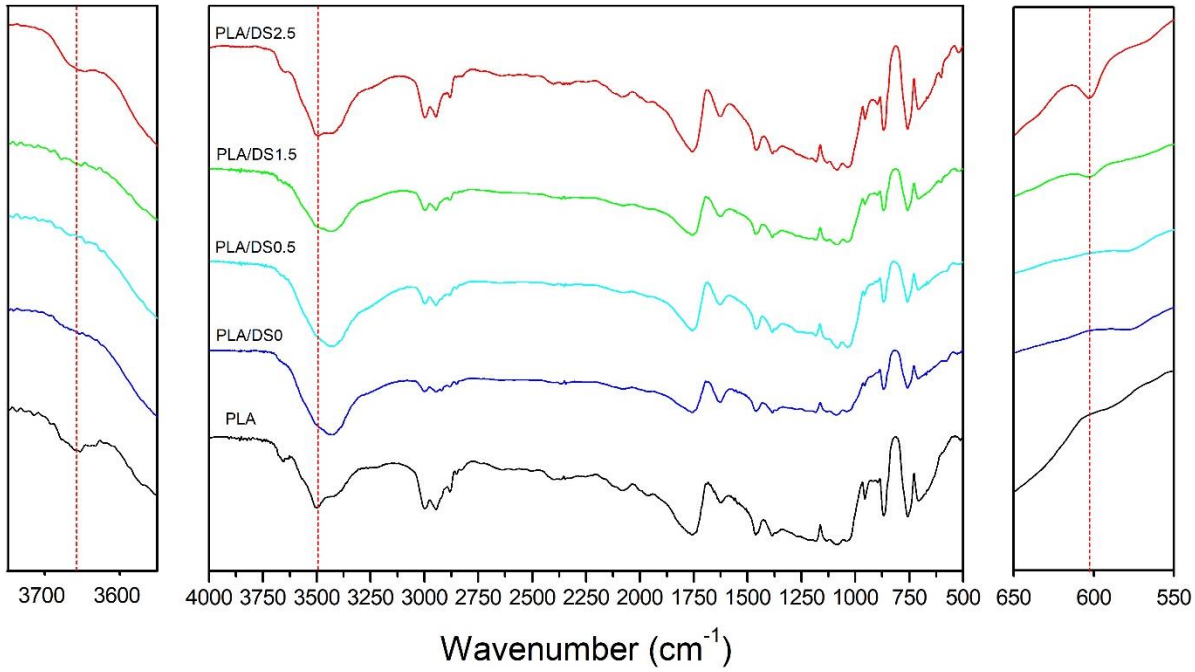


Figure 5-4. FTIR spectra of PLA/AS blends. Two regions of spectra are enlarged: 3550 $cm^{-1}$ to 3750 $cm^{-1}$ (left hand side) and 550 $cm^{-1}$ to 650 $cm^{-1}$ (right hand side).

The FTIR spectra of PLA and the PLA/AS blends are very similar to each other except for two regions (marked with a dashed line). The first difference is the emergence of a peak at 601$cm^{-1}$ in the spectra of PLA/AS blends with DS greater than 0.5. The emergence of this peak may reflect weak hydrophobic interactions between the PLA matrix and the AS dispersed phase. The second difference was in the region of –OH stretching. Three peaks were observed in the PLA spectrum. The first peak is a broad peak appearing at 3446 $cm^{-1}$, which may possibly correspond to $\nu$(C–O···H) [157]. The second and third peaks at 3506 $cm^{-1}$ and 3653 $cm^{-1}$ are located in the region of the free –OH stretching [157]. The disappearance of these peaks in PLA/DS0, PLA/DS0.5 and PLA/DS1.5 blends indicates higher level of hydrogen bonding in these blends compared to the PLA/DS2.5 blend. This may explain the slower dynamics of the interphase in PLA/DS0 and PLA/DS1.5 blends. The higher volume fraction of the PLA matrix with slower dynamics in PLA/DS1.5 compared to PLA/DS0 may be attributed to the higher thickness of the interphase in PLA/DS1.5. The inter-diffusion of phases followed by hydrogen bonding could lead to an interphase with slower dynamics. The lower number and random distribution of the available hydroxyl groups may explain the lower volume fraction of the PLA matrix with slower dynamics in PLA/DS0.5 compared to PLA/DS0. This might also explain the higher thickness of the

interphase in PLA/DS0 compared to PLA/DS0.5 deduced from SAXS experimental measurements. The absence of slowdown of the dynamics for PLA/DS2.5 suggests that inter-diffusion of PLA in starch acetate is not sufficient to alter the dynamics in the interphase region. Strong physical interactions such as hydrogen bonds may contribute to the slowdown of the dynamics in the interphase region for PLA/AS blends.

It is worth mentioning that we tried to use solid-state nuclear magnetic resonance (SSNMR) to study the dynamics of the interfacial region. Carbon spin-lattice relaxation time in the rotating frame, $T_{1\rho}(C)$, can be employed to study the change in molecular mobility of the matrix chains in the presence of the dispersed phase [158]. In order to do so, the presence of a carbon with a completely resolved NMR peak in the molecular structure of the matrix is necessary. Change in molecular mobility of the matrix chains cannot be probed if all the NMR peaks of the matrix carbons overlapped those of dispersed phase [158]. Although literature data of solution $^{13}C$ NMR reported different values for the chemical shift of methyl carbons in PLA and AS (16.7 ppm [159] and 21 ppm [138], respectively), our SSNMR measurement revealed a broad peak from 16 ppm to 22 ppm, (Appendix III, Figure 2). Therefore, it was not possible for us to study the dynamics of the interfacial region using SSNMR.

## 5.5. Conclusion

The objective of this chapter was to investigate the effect of the degree of substitution in acetylated starch on the interphase region in biphasic PLA/AS blends. The thickness of the interphase region, deduced from theoretical and SAXS experimental measurements, increased with increasing DS of AS in PLA/AS blends. Satisfactory accordance was observed between cooperativity length $\xi_a$ of PLA matrix in PLA/AS blends and the interphase thickness estimated using theoretical approach and SAXS measurements. Therefore, $\xi_a$ can be used as a measure of the minimum interphase thickness. TMDSC results revealed the slowdown of the PLA chain dynamics at the interphase region for PLA/DS0 and PLA/DS1.5 blends while no slowdown was observed for PLA/DS0.5 and PLA/DS2.5 blends. FTIR results showed that the strong physical interaction (hydrogen bonding) is the main reason of dynamic slowdown at the interphase region and inter-diffusion of phases is the less prominent factor.

Next chapter will be focused on some important properties of PLA/AS blends including thermal transitions and stability and mechanical and water transport properties. We will try to use results of this chapter to explain the observed properties of the blends.

# 6. Poly(lactic acid)/acetylated Starch Blends: Effect of Starch Acetylation on the Material Properties

Rasool Nasseri[a], Robert Ngunjiri[b], Christine Moresoli[c], Aiping Yu[d], Zhongshun Yuan[e] and Chunbao (Charles) Xu[f]

Description of contributions:

[a]: performing most of the experimentations and writing the manuscript.

[b]: performing dilute viscometry for measuring molecular weights.

[c] and [d]: main and co-supervisors.

[e] and [f]: providing the acetylated starch samples.

This manuscript is prepared for submission to "Carbohydrate Polymers" journal under Elsevier publication.

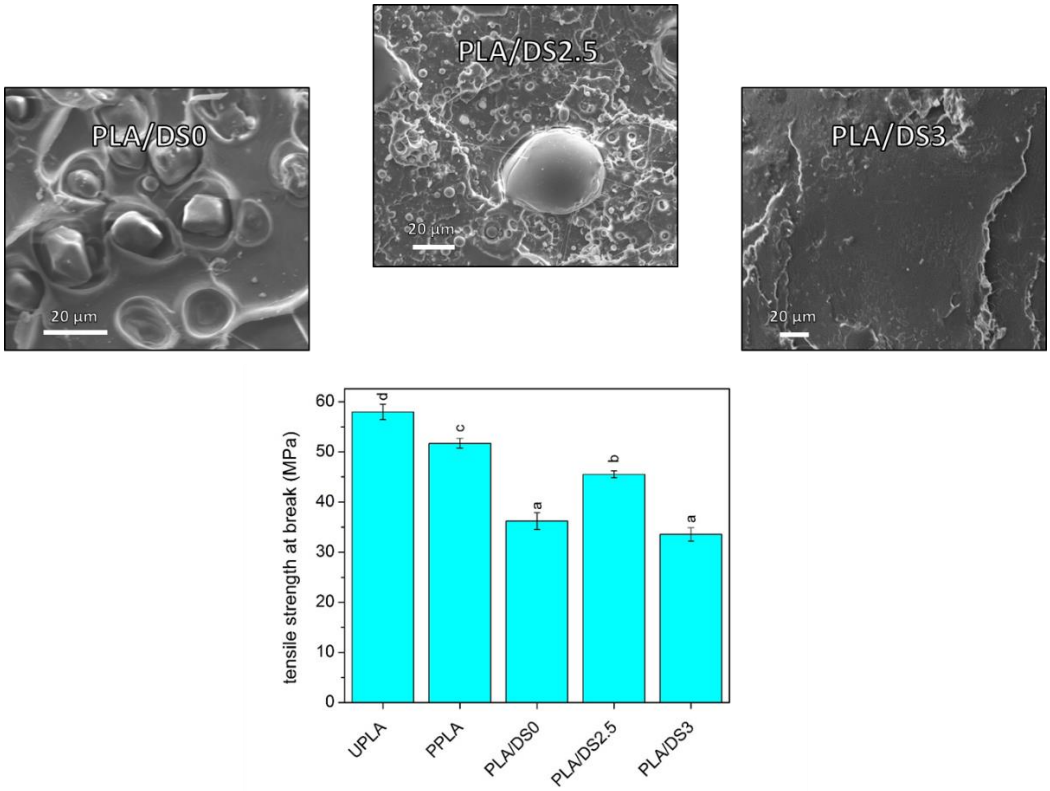

## 6.1. Synopsis

The effect of the degree of substitution (DS) of acetylated starch (AS) on the properties of poly(lactic acid) (PLA)/AS blends was investigated. A biphasic morphology was observed for all PLA/AS blends, except PLA/DS3. According to thermogravimetrical analysis (TGA), the thermal stability of PLA/AS blends was improved compared to neat PLA. Differential scanning calorimetry (DSC) results indicated that AS had a plasticization and nucleation effect in the PLA/AS blends. The highest tensile strength, toughness, and impact strength was achieved when DS2.5 was added to PLA which may reflect the biphasic structure and the thick diffused interphase of this blend. The diffusion coefficient of water and the water vapor permeability (WVP) of PLA/AS blends were influenced by the presence of AS. The diffusion coefficient of water decreased while the WVP increased for PLA/AS blends by incorporation of AS.

## 6.2. Introduction

The increasing consumption of synthetic polymers creates significant environmental concerns and impact [1-4]. Alternatives to address these environmental concerns are currently being developed. One alternative is the development of biodegradable polymers such as poly(lactic acid) (PLA), poly(hydroxyalkanoates) (PHAs), polycaprolactone (PCL) and polyesteramide (PEA). Among these biodegradable polymers, PLA is one of the most promising candidates due to the renewability of its feedstock, its compostability, and adequate mechanical properties and permeability [5, 6]. The relatively high cost of PLA and its slow degradation rate, however, limit its application in daily usages. Blending PLA with low-cost biodegradable polymers can alleviate these shortcomings. Starch has received significant attention as a promising biodegradable material due to its low cost, abundance and renewability [7]. Native starch is biosynthesized in the form of semi-crystalline granules with crystallinity in the range of 15 to 45% and density around 1.5 g/cm$^3$ [17]. The high degree of crystallinity of starch is the main obstacle in its thermal processing due to the lack of thermal transition before degradation [8] while its hydrophilic characteristics and poor compatibility limit its application in PLA blends. The plasticization of starch can improve its thermal processability by reducing the glass transition temperature [8] and can considerably improve blend properties [21, 23]. However, the use of plasticizer to improve the thermal processing of starch has drawbacks such as starch retrogradation and embrittling, leads to

phase separation, and produces materials with heterogeneous characteristics. Furthermore, the limited interfacial interactions between starch and PLA remain a limitation. The effectiveness of nonreactive compatibilizers such as amphiphilic molecules [24] or reactive compatibilizers such as maleic anhydride (MA) [25], epoxidized soybean oil [26] and tung oil anhydride [27] in improving the interfacial interactions between starch and PLA and the properties of PLA/starch blends has been reported. Alternatively, the compatibility between starch and PLA can be increased by chemical modification of starch which is expected to improve its processability as well. Butyl-etherification and silane modification of starch [28, 29] have been reported to improve the interfacial interactions between starch and PLA and the properties of PLA/starch blends. An alternative chemical modification, the acetylation of starch, is a relatively simple process. The acetylation of starch can be adjusted such as to produce acetylated starch having a wide range of hydrophobicity by manipulating the degree of substitution of hydroxyl groups with acetyl groups [9]. The acetylation of starch weakens the intermolecular hydrogen bonding and decreases crystallinity, thus facilitating the mobility of the molecules and providing them with an opportunity to participate in the glass transition [10]. Therefore, acetylation of starch can improve its thermal processability.

The main purpose of this study was to evaluate the effectiveness of the acetylation of starch as a means of improving the compatibility of starch with PLA. Acetylated starch (AS) with different degrees of substitution (DS) was investigated and used to prepare PLA/AS blends. The morphology of the PLA/AS blends was studied by scanning electron microscopy imaging. The effect that the DS of AS ha on the thermal stability and transitions of the PLA/AS blends was investigated. The influence of the morphology and the interfacial interactions between AS and PLA on the mechanical properties, water uptake and water vapor permeability of the blends was also scrutinized.

# 6.3. Materials and Methods

## 6.3.1. Materials

PLA 4032D ($M_n$=58000 g/mol, D-content 1.8 %) was provided by NatureWorks Inc (USA). Corn starch was purchased from a local Ontario market (BulkBarn®, product code: 000260). The amylose content of the starch was estimated to be 25.4±1.6 wt% (Mahmood et al's method [59],

details in Appendix I). Acetic anhydride (≥ 97.0%) and acetic acid (≥ 99.7%) were obtained from CALEDON laboratory chemicals (Canada). Dimethyl sulfoxide (HPLC grade, ≥ 99.9%) was purchased from Sigma-Aldrich (Canada).

## 6.3.2. Methods

### 6.3.2.1. Acetylation of Starch

Corn starch was vacuum-dried at 55 ℃ for 24 hours prior to acetylation. AS with different DS, 0.5, 1.5, 2.5 and 3 was produced. A typical acetylation reaction would be initiated by placing 15 g vacuum-dried corn starch an amount of acetic anhydride defined by the molar ratio between starch and acetic anhydride and desired DS in a 250 mL three neck glass reactor. A mass of 0.375 g of catalyst would be mixed with acetic acid and subsequently adding the mixture to the 250 mL three neck glass reactor equipped with a nitrogen stream. The reactor was heated at 135 ℃ in an oil bath with magnetic stirring. After 180 min, the reaction was stopped by placing the reactor in water. The cooled mixture was transferred into a 500 mL beaker and was precipitated with non-solvent. The residual viscous product was rinsed with non-solvent and recovered into a 500 mL beaker. The precipitated AS was filtered and rinsed with an additional 200 mL of non-solvent in a 500 mL beaker. The mixture was filtered again and the final AS was vacuum-dried at 45℃.

### 6.3.2.2. Determination of the degree of substitution (DS) for acetylated starch (AS)

DS was estimated by proton nuclear magnetic resonance ($^1$H NMR) spectra as the ratio between the area of acetyl $CH_3$ at 2.15 ppm to the area of starch CH at 3.5-5.5 ppm [60]. All spectra were obtained with a Varian Inova 600 NMR spectrometer equipped with a Varian 5 mm triple-resonance indirect-detection HCX probe at $25°C$ using DMSO as the solvent. An example of a typical $^1$H NMR spectra of AS (DS3) is presented in Appendix I (Figure 1).

### 6.3.2.3. Wide Angle X-ray Diffraction (WAXRD)

The degree of crystallinity of AS was measured by WAXRD (D8 focus, Bruker) with $CuK\alpha_1$ radiation and 1.5406 Å wavelength operated at 40 kV and 30 mA. The X-ray diffraction patterns were recorded in a $2\theta$ angle range of 3-40 with step of 0.02° and speed of 1 sec/step.

The degree of crystallinity was estimated with the method reported in reference [61]. The area under the diffractogram was assigned to the crystalline and the amorphous domains by creating a smooth curve that connected the baseline of the peaks using the OriginPro 8.5 software (Appendix I Figure 2). The area above the smooth curve was considered as the crystalline domain and the area between the smooth curve and the linear baseline was considered as the amorphous domain. The degree of crystallinity ($\chi_{c_{AS}}$) was calculated from the area of the peaks for the crystalline domain and the sum of the area of the crystalline domain and the amorphous domain:

$$\chi_{c_{AS}}\,(\%) = \frac{A_c}{A_c + A_a} \times 100 \qquad (6.1)$$

where $\chi_{c_{AS}}$ is the degree of crystallinity, $A_c$ the area of the peak assigned to the crystalline domain and $A_a$ the area of the peak assigned to the amorphous domain.

#### 6.3.2.4. Preparation of PLA/AS blends

PLA and AS were dried overnight at 80°$C$ in a vacuum oven. The PLA/AS blends were produced in a SJSZ-07A lab-scale twin screw extruder (Ruiming Plastics Machinery, Wuhan city, China) where the blend components were mixed at 180°$C$ with a screw speed of 30 rpm for 7 min. The mixing temperature, speed and time were identified from preliminary experiments such as to minimize changes in the color of PLA as an indication of its degradation. The extruded PLA/AS blends were then pelletized and compression molded into tensile and impact specimens using a hot press (PHI, Pasadena Hydraulic Inc., USA) at 200°C with 10000 lbs pressure for 4 minutes. Thin films (~100 μm) of PLA/AS were prepared for water vapor permeability analysis using the same compression molding procedure. The different neat PLA and PLA/AS samples are presented in Table 6-1.

Table 6-1. Code, composition, and processing time of the samples.

| Sample | PLA (wt%) | AS (wt%) | DS of AS | Processing time (min) |
|---|---|---|---|---|
| **UPLA (unprocessed)** | 100 | 0 | - | 0 |
| **PPLA (processed)** | 100 | 0 | - | 7 |
| **PLA/DS0** | 85 | 15 | 0 | 7 |
| **PLA/DS0.5** | 85 | 15 | 0.5 | 7 |
| **PLA/DS1.5** | 85 | 15 | 1.5 | 7 |
| **PLA/DS2.5** | 85 | 15 | 2.5 | 7 |
| **PLA/DS3** | 85 | 15 | 3 | 7 |

### 6.3.2.5. Scanning electron microscopy (SEM)

The cross-sectional morphology of the samples was investigated using a SEM equipment (Quanta FEG 250, USA) with an electron voltage of 10 kV. The specimens were frozen under liquid nitrogen, then fractured, mounted, coated with gold and observed. The ImageJ software was used to measure the diameter of the dispensed phase. At least 10 particles of the dispersed phase were selected for the size analysis.

### 6.3.2.6. Thermogravimetric analysis (TGA)

Thermogravimetric analysis was performed in a Q500 TA instrument (USA). Each sample (about 20 mg) was heated from 25°$C$ to 600°$C$ at a 10°$C$/min heating rate under nitrogen atmosphere (40.0 mL/min) to prevent thermo-oxidative degradation. The mass change over time profile was analyzed with the TA Universal Analysis version v5.5.20 software to estimate the temperature for the onset of degradation ($T_{5\%}$) and the temperature at the maximum rate of degradation ($T_{max}$) of the PLA/AS blends and their associated AS component.

### 6.3.2.7. Differential Scanning Calorimetry (DSC)

The thermal transitions of the PLA/AS blends were investigated with a Q2000 TA instrument (USA). A sample (15-20 mg) was placed in an aluminum pan. The sample was initially heated from 25°$C$ to 190°$C$ at a 10°$C$/min heating rate to eliminate any residual thermal history. Next, the sample was cooled to 25°$C$ and then heated again to 190°$C$ (10°$C$/min heating rate). An empty pan was used as a reference. The glass transition temperature ($T_g$), crystallization temperature ($T_c$) and melting temperature (peak) ($T_m$) were determined from the second heating scan of the thermogram

using the TA Universal Analysis version v5.5.20 software. When multiple endothermic peaks were present, the peak temperature of the biggest endotherm was taken as $T_m$. The degree of crystallinity ($\chi_c$) was defined as follows [29, 160]:

$$\chi_c(\%) = \left(\frac{\Delta H_m}{\Delta H_m^0 \times \delta_{PLA}}\right) \times 100 \quad (6.2)$$

where $\Delta H_m$ is the enthalpy of melting for the second heating scan, $\Delta H_m^0$ the melting enthalpy for 100 % crystalline PLA (93.6 J/g [161]), and $\delta_{PLA}$ is the mass fraction of PLA in the PLA/AS blends.

### 6.3.2.8. Tensile properties

The tensile properties were measured at 25°$C$ using an Instron 3369 tensile tester (USA), according to ASTM D1708 with crosshead speed of 10 mm/min. Ten specimens of each material were analyzed. All samples were conditioned at ambient conditions for 24h before testing.

### 6.3.2.9. Izod impact strength

The Izod impact strength of the notched specimens was measured in an Instron CEAST 9050 impact tester (USA), according to ASTM D256. At least six specimens of each material were tested. All samples were conditioned at ambient condition for 24 h before testing.

### 6.3.2.10. Water absorption test

Each specimen (30 mm×13 mm×3 mm) was dried overnight at 50°$C$ in a convection oven. Each specimen was then immersed in a water bath at 30°$C$. The weight change was recorded at different time intervals, after removing the specimens from the water bath and removing the surface water, using a balance with a precision of $10^{-4}$ g. The water uptake was calculated as:

$$M_t\ (\%) = \frac{w_t - w_0}{w_0} \times 100 \quad (6.3)$$

where $w_0$ and $w_t$ are the initial weight of the specimen before immersion and the weight of the specimen after exposure to water, respectively. The water uptake at time $t$, was expressed as [162]:

$$\frac{M_t}{M_\infty} = 1 - \sum_{n=0}^{\infty} \frac{8}{(2n+1)^2\pi^2} \exp\left[\frac{-D(2n+1)^2\pi^2 t}{d^2}\right] \quad (6.4)$$

where $M_\infty$ is the equilibrium water uptake of the samples, $d$ the thickness of the sample, and $D$ the diffusion coefficient. At short times then, $D$ can be calculated as:

$$D = \frac{\pi d^2 \theta^2}{16 M_\infty} \tag{6.5}$$

where $\theta$ is the slope of the linear portion of $M_t$ versus $t^{1/2}$ curve [163, 164].

#### 6.3.2.11. Water vapor permeability (WVP)

The WVP test was conducted according to ASTM E96/E96M. Circular thin films of the samples were mounted and sealed on the open mouth of cylindrical cups containing about 100 g of calcium chloride. The test cups were measured to determine their initial weight before being kept in an environmental chamber (Sanyo versatile environmental test chamber, Japan) at relative humidity of 50 % and temperature of 23°$C$. The cups were weighed at regular intervals until the equilibrium state was reached. After reaching equilibrium, the increase in the weight of the cups over time were measured and WVP was calculated as:

$$WVP = \frac{m \times d}{A \times t \times P} \tag{6.6}$$

where $m$ (g) is the mass increase of the container and film, $d$ (m) the film thickness (in the range of $0.08\times10^{-3}$ to $0.13\times10^{-3}$ m), $A$ ($m^2$) the exposed area of the film ($29.22\times10^{-4}$ $m^2$), $t$ (h) is the duration of permeation, and $P$ (Pa) is the water vapor partial pressure difference across the films (1396 Pa). Three films of each material were analyzed and the average results were presented in (g/h.m.Pa).

### 6.3.3. Statistical analysis

Multiple-comparison Bonferroni t-test at a significance level of $\alpha$=0.1 was employed to evaluate the significance of the difference between means of properties that have replicate measurements. All reported error bars represent standard error.

## 6.4. Results and Discussion

### 6.4.1. Phase Behavior and Morphology

The predictions of phase behavior of PLA/AS blends were obtained with the compressible regular solution (CRS) model [145]. In the CRS model, the total change in free energy upon mixing per unit volume is given by [145]:

$$\Delta g_{mixing} = k_B T \left( \frac{\phi_A \tilde{\rho}_A}{N_A \nu_A} \text{Ln}\, \phi_A + \frac{\phi_B \tilde{\rho}_B}{N_B \nu_B} \text{Ln}\, \phi_B \right) + \phi_A \phi_B \left( \tilde{\rho}_A \delta_{A,0} - \tilde{\rho}_B \delta_{B,0} \right)^2 \quad (6.7)$$

where $k_B$ is the Boltzmann constant, $\phi_i$ the volume fraction, $v_i$ the hard core segment volume, $\tilde{\rho}_i$ the reduced density at temperature $T$, $N_i$ the number of segments and $\delta_{i,0}$ the solubility parameter at zero Kevin for component *i*. *A* and *B* denote PLA and AS, respectively. The hard core segment is defined as:

$$\nu_i = M_i / N_{Av} \rho_i^* \quad (6.8)$$

$M_i$ is the molecular weight of the repeating unit and $N_{Av}$ is Avogadro's number. The parameter $\rho_i^*$ is the hard core density and is estimated from the density at temperature $T$ through the following relation:

$$\rho_i(T) = \rho_i^* exp(-\alpha_i T) \quad (6.9)$$

The hard core density and the density at temperature $T$ was used to calculate reduced density at temperature $T$:

$$\tilde{\rho}_i(T) = \rho_i / \rho_i^* \quad (6.10)$$

The parameter $\delta_{i,0}$ was obtained from the reduced density and solubility parameter at $298K$:

$$\delta_{i,0}^2 = \delta_i^2(298) / \tilde{\rho}_i(298) \quad (6.11)$$

The solubility parameter at room temperature were estimated by the Van Krevelen and Hoftyzer (VKH) [165] group contribution method. A compressible blend should be stable with respect to the composition and the volume fluctuations for phase stability. Since the simplified free energy expression given by the CRS model is based on the properties of the pure components, the effect of the volume fluctuation was neglected. Therefore, the criterion for local stability in a binary polymer mixture can be presented by [166]:

$$\frac{\partial^2 \Delta g_{mix}}{\partial \phi_A^2} = kT\left(\frac{\tilde{\rho}_A}{\phi_A N_A \nu_A} + \frac{\tilde{\rho}_B}{\phi_B N_B \nu_B}\right) - 2\left(\tilde{\rho}_A \delta_{A,0} - \tilde{\rho}_B \delta_{B,0}\right)^2 > 0 \quad (6.12)$$

At the spinodal condition, which is the limit of local stability, this value equals zero.

The pure component properties of AS were measured experimentally (details are provided in Supporting Information) and the pure component properties of PLA were obtained from the literature. Those properties, summarized in Table 6-2, were used to estimate $\Delta g_{mixing}$ and the corresponding phase behavior of the PLA/AS blends.

Table 6-2. Pure component properties of AS and PLA.

| Polymer | $\rho$ ($g/cm^3$) | $\alpha$ ($10^{-4}\ K^{-1}$) | $\delta(298)$ $(J.cm^{-3})^{1/2}$ | $M_i$ (g/mol) | molecular weight (g/mol) |
|---|---|---|---|---|---|
| **Poly(lactic acid)** | 1.25[a] | 7.4[a] | 21.73[b] | 76 | 58000 |
| **Native starch (DS0)** | 1.49 | 0.52 | 44.25 | 162 | 17500000 |
| **DS0.5** | 1.46 | 0.67 | 37.21 | 183 | 19200 |
| **DS1.5** | 1.40 | 1.82 | 29.12 | 225 | 3500000 |
| **DS2.5** | 1.36 | 2.24 | 24.38 | 267 | 1800000 |
| **DS3** | 1.28 | 3.36 | 22.63 | 288 | 323000 |

[a] reference: [94]; [b] reference: [146].

The phase diagram of the PLA/AS blends is shown in Figure 6-1. The estimated volume fraction of PLA in the blends was in the range of 0.85-0.87 based on the density of the pure components. The phase behavior estimates predict immiscibility for all blends except PLA/DS3 at processing (453K) and room (298K) temperature conditions.

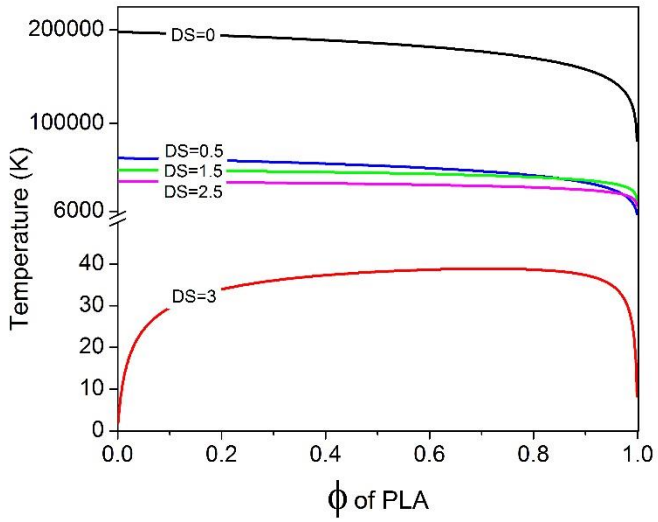


Figure 6-1. Phase diagram predictions of PLA/AS blends according to PLA volume fraction for different DS of AS.

The morphology, at two different magnifications, for cryo-fractured bars of PLA/AS blends is presented in Figure 6-2. Two distinct phases were clearly observed for all PLA/AS blends except for PLA/DS3. The model predictions are in agreement with the morphology of the cross-section of PLA/AS blends. The interfacial region of the dispersed and continuous phases, depicted with an arrow, indicates a visible gap in the PLA/DS0 blend (Figure 6-2B) while no visible gap was observed in the other biphasic blends (Figure 6-2D, F, and H). The presence of a visible gap in PLA/DS0 could reflect the high degree of crystallinity in DS0 (36.2%, Table 6-3) preventing interdiffusion of the phases at the interface. The interdiffusion of the phases in the other biphasic blends may have been sufficient to prevent the formation of a visible gap at the interface.

Table 6-3. Diameter of the dispersed phase of PLA/AS blends and degree of crystallinity of their associated AS ($\chi_{c_{AS}}$), glass transition temperature ($T_g$), cold crystallization temperature ($T_c$), melting temperature ($T_m$), and degree of crystallinity of the matrix ($\chi_c$).

| Sample | AS properties | | Blend properties | | | |
|---|---|---|---|---|---|---|
| | $\chi_{c_{AS}}$ (%) | Diameter of the dispersed phase (μm) | $T_g$ (°C) | $T_c$ (°C) | $T_m$ (°C) | $\chi_c$ (%) |
| **PPLA** | - | - | 62 | 112 | 170 | 40.5 |
| **PLA/DS0** | 36.2 | 13.95±0.70[a] | 61 | 106 | 169 | 45.3 |
| **PLA/DS0.5** | 22.9 | 9.98±0.68[b] | 60 | 103 | 169 | 47.4 |
| **PLA/DS1.5** | 7.1 | 23.14±1.39[c] | 60 | 108 | 169 | 43.6 |
| **PLA/DS2.5** | 4.8 | 5.91±1.86[d] | 61 | 108 | 169 | 45.1 |
| **PLA/DS3** | 3.8 | - | 61 | 109 | 170 | 42.6 |

Different letters denote statistically significant different samples (Bonferroni t-test at a significance level of α=0.1)

The average equivalent diameter of the dispersed phase (assuming spherical geometry) is presented in Table 6-3. In the PLA/DS2.5 blend, some small size dispersed phase was observed together with larger size dispersed phase. Average equivalent diameter of PLA/DS2.5 blend is 5.91±1.86. Big relative standard deviation reflects the presence of small and big droplets at the same time. AS previously reported for immiscible molten polymer blends one can envision that the reduced interfacial tension between PLA and DS2.5 may have caused an effective tension transfer from the PLA matrix to the large AS droplets during the processing and their subsequent breaking into smaller droplets [167]. Similar observations have been reported for PLA/silane modified cassava starch blends [28] and PLA/maleic anhydride grafted wheat starch blends [25].

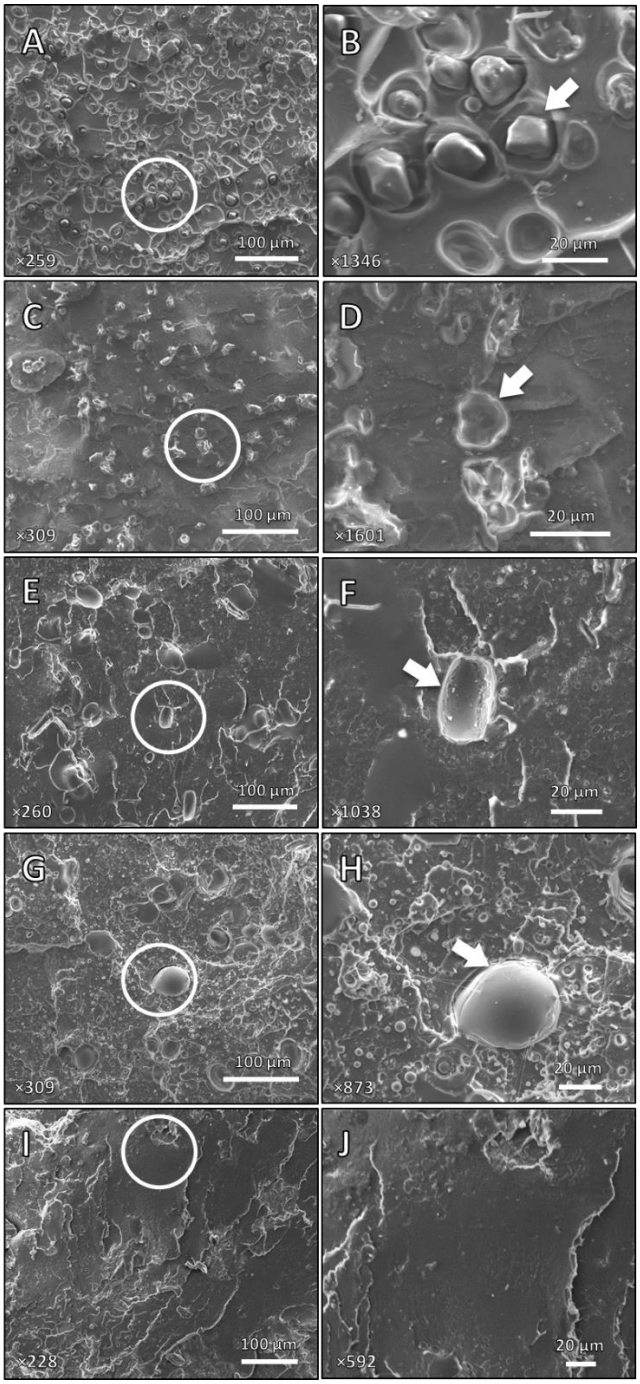


Figure 6-2. SEM images from cryofractured cross-section of (A, B) PLA/DS0, (C, D) PLA/DS0.5, (E, F) PLA/DS1.5, (G, H) PLA/DS2.5, and (I, J) PLA/DS3 at two magnifications. The circled region in the lower magnification image (left hand side) is shown in the right hand side image at higher magnification. Arrows pointed to the interface.

## 6.4.2. Thermal stability

The TGA and the DTGA characteristics (steps of mass loss and the temperature of the DTGA peaks ($T_{max}$)) of AS with different DS will be discussed first and will be used to understand the impact of AS on the thermal stability of PLA in PLA/AS blends.

### 6.4.2.1. Acetylated starch

The TGA (Figure 6-3A and B) and DTGA (Table 6-4) for starches with different DS illustrate the effect of acetylation on the thermal stability. Native starch (DS0) showed one minor and one major mass losses. The first mass loss (minor), observed in the 25-140°$C$ temperature range, was related to the release of physically adsorbed water [86]. The second mass loss (major), observed in the 245-600°$C$ temperature range, was related to starch decomposition. The TGA of AS (DS0.5 to 2.5) showed three potential different mass losses. The minor first mass loss (25-140°$C$) was attributed to the release of physically adsorbed water. The second mass loss (200-300°$C$) was attributed to the condensation of the hydroxyl groups while the third mass loss (315-415°$C$) was assigned to the decomposition of the acetyl groups. For DS0.5 decomposition of acetyl groups was observed as a shoulder in the right hand side of the hydroxyl group decomposition peak. The shift of the peak of the second mass loss to lower temperatures for AS could reflect the degradation of starch occurring during the acetylation reaction [86]. The TGA of DS3 showed a minor mass loss in the range of 25-140°$C$ due to the release of water and a major mass loss in the range of 315-415°$C$ due to the degradation of the acetyl groups. The absence of the mass loss in the 200-300°$C$ temperature range for DS3 (Figure 6-3A) supports the removal of the hydroxyl groups. $T_{max}$ of DS3 occurred at 367°$C$, about 50°$C$ higher than the temperature at which the highest rate of mass loss was observed for native starch (DS0). The TGA analysis presented in this study indicated that acetylation of starch increased its thermal stability which is in agreement with previous work [71, 79, 86].

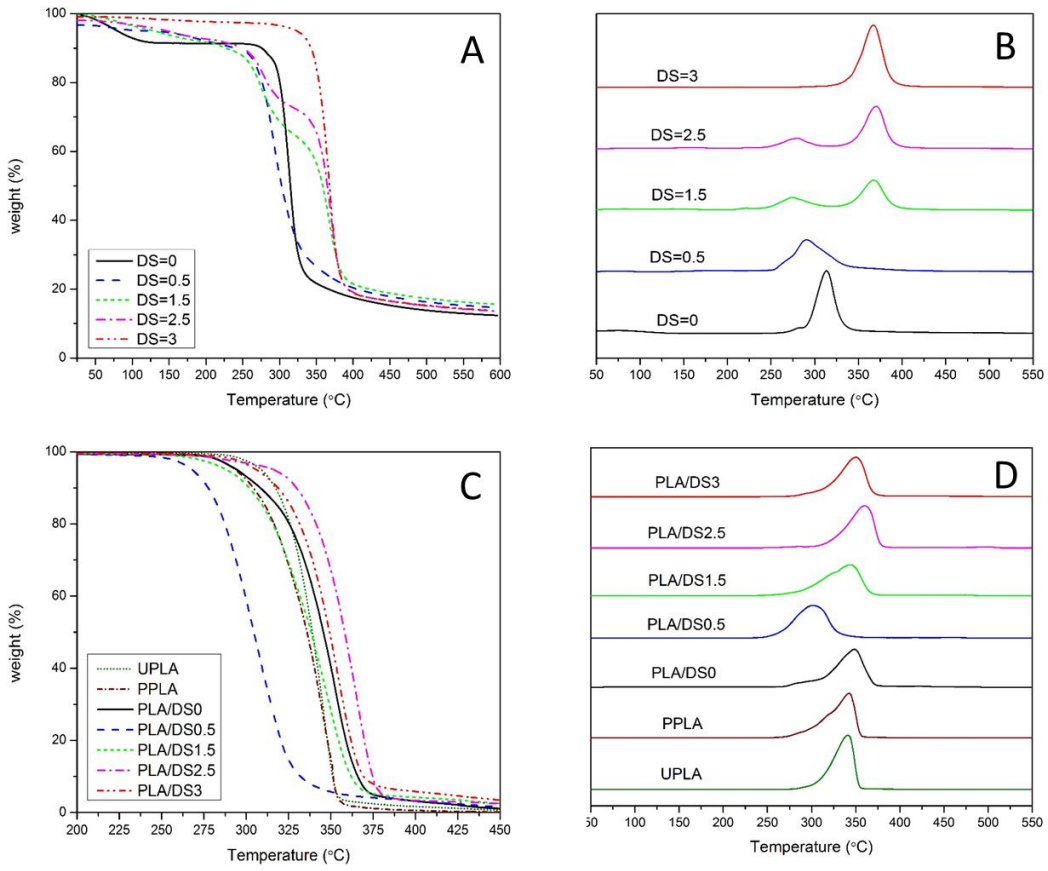


Figure 6-3. TGA (A and C) and DTGA (B and D) curves of PLA and PLA/AS blends containing AS with different DS (10°C /min heating rate, nitrogen conditions).

### 6.4.2.2. PLA/AS blends

The effect of starch acetylation on the thermal stability of PLA/AS blends, investigated by TGA, is presented in Figure 6-3C and D and the corresponding temperature of the onset of degradation ($T_{5\%}$) and the temperature at the maximum degradation rate ($T_{max}$) are presented in Table 6-4. Note that the temperature of the onset of degradation for the processed PLA (PPLA) was lower compared to the unprocessed PLA (UPLA), reflecting the thermal and shear induced degradation taking place during the processing, while the temperature at the maximum rate of degradation remained unchanged. The addition of native starch to PLA did not affect $T_{5\%}$ but increased slightly the $T_{max}$. In contrast, $T_{5\%}$ decreased significantly for the PLA/DS0.5 blend and decreased moderately for the PLA/DS1.5 blends compared to the PLA/DS0 blend while the $T_{max}$ decreased significantly for the PLA/DS0.5 blend and remained relatively constant for the PLA/DS1.5 blend.

These observations reflect the differences in hydroxyl and acetyl content of the AS. The degradation of hydroxyl groups in DS0.5 and DS1.5 was observed at lower temperatures compared to native starch (DS0) reflecting the effect of the acetylation reaction on the starch chains. The higher acetyl content of DS1.5 compared to DS0.5 may explain the higher $T_{5\%}$ and $T_{max}$ of PLA/DS1.5 blends compared to the PLA/DS0.5 blend. The PLA/DS2.5 and PLA/DS3 blends displayed higher $T_{5\%}$ and $T_{max}$ compared to PPLA and other PLA/AS blends. The higher thermal stability of these two PLA/AS blends reflect the positive effect of acetylation in improving the thermal stability of PLA materials. The minor hydroxyl content in DS2.5 (minor degradation peak observed at 279°$C$, Figure 6-3B) did not seem to affect and contribute significantly to the thermal stability of the PLA/DS2.5 blend.

Table 6-4. Temperature of the onset of degradation ($T_{5\%}$) and temperature at the maximum rate of degradation ($T_{max}$) of AS, PLA and PLA/AS blends.

| Sample | $T_{5\%}$ (°$C$) | $T_{max}$ (°$C$) |
|---|---|---|
| **DS0** | 80 | 313 |
| **DS0.5** | 126 | 291 |
| **DS1.5** | 130 | 274/368 |
| **DS2.5** | 148 | 279/370 |
| **DS3** | 324 | 367 |
| **UPLA** | 308 | 341 |
| **PPLA** | 293 | 342 |
| **PLA/DS0** | 294 | 349 |
| **PLA/DS0.5** | 268 | 302 |
| **PLA/DS1.5** | 288 | 344 |
| **PLA/DS2.5** | 316 | 360 |
| **PLA/DS3** | 306 | 350 |

## 6.4.3. Thermal transitions

The effect of AS as disperse phase on the thermal transitions and thermal properties of PLA/AS blends was studied by DSC. The DSC thermograms of PLA and PLA/AS blends are presented in Figure 6-4A and the associated characteristics (glass transition temperature ($T_g$), cold crystallization temperature ($T_c$), melting temperature ($T_m$) degree of crystallinity of the matrix ($\chi_c$), and degree of crystallinity of their associated AS ($\chi_{c_{AS}}$)) are presented in Table 6-3. The $T_g$ of the PLA/AS blends decreased by 1 to 2 °C compared to PLA due to the plasticization effect of AS

(Table 6-3). PLA/DS0 and PLA/DS0.5 displayed an exothermic peak prior to the endothermic peak associated for melting, which was previously attributed to the PLA crystal transformation from the disordered $\alpha'$ form to the more ordered $\alpha$ form [15]. The small peak or shoulder at $162°C$ prior to the main melting peak for all blends reflects the characteristic melt-recrystallization behavior of the $\alpha$ form [168].

The $T_c$ of all PLA/AS blends decreased compared to PLA. It is inferred that AS acts as a nucleating agent for PLA which facilitates its crystallization and reduces the cold crystallization temperature. The efficiency of a nucleating agent is affected by several factors, its size (available surface area), the smoothness of its surface, its crystalline lattice structure and its thermodynamic affinity to the matrix. The nucleation effect is promoted when the nucleating agent is small, has high surface roughness, has similar crystalline lattice structure to the matrix and has high affinity with the matrix, [169-172]. Considering these factors, the role of AS as nucleating agent in PLA/AS blends was analyzed. The degree of crystallinity of AS in the blend might be different from $\chi_{c_{AS}}$ before blending but still can be employed for qualitative comparison of the nucleants. The affinity of AS with PLA increased with increasing DS. The PLA/DS0.5 and PLA/DS3 blends showed the highest and lowest $\chi_c$, respectively. The AS in the PLA/DS0.5 blend that has a small average equivalent diameter, rough surface (Figure 6-2D), and high degree of crystallinity, is expected to be associated with the most efficient PLA nucleation. The absence of the dispersed phase in PLA/DS3 which was visible by SEM imaging (Figure 6-2J) may explain the lowest $\chi_c$ of all blends. The AS in the PLA/DS2.5 blend has the smallest average equivalent diameter of all blends and its thermodynamic affinity with the PLA matrix is higher than PLA/DS0.5 but the low degree of crystallinity ($\chi_{c_{AS}}$) and smooth surface (Figure 6-2H) of DS2.5 dispersed phase may have predominated and suppressed its nucleation efficiency.

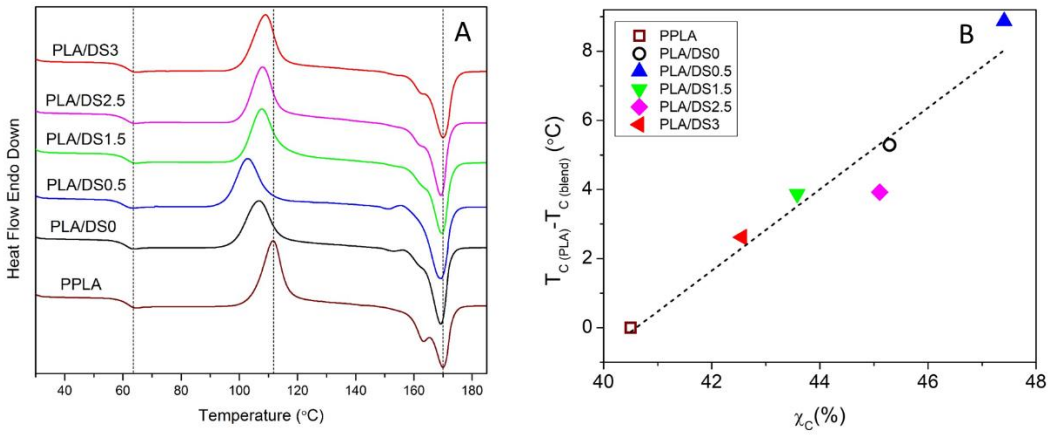


Figure 6-4. (A) DSC thermograms of PLA and PLA/AS blends and (B) linear correlation between the lowering of the temperature of cold crystallization compared to PLA and degree of crystallinity of PLA and PLA/AS blends. Dashed line represents the linear fit ($R^2$=0.96).

A similar effect of DS for AS in PLA/AS blends was observed for the lowering of the temperature of cold crystallization compared to PLA and the degree of crystallinity of the blends as illustrated by the linear correlation between these two parameters (Figure 6-4B).

### 6.4.4. Mechanical properties

The effect of starch acetylation on the mechanical properties of PLA/AS blends was investigated for those blends that had distinct thermal features and morphology. The PLA/DS2.5 blend was selected for its high thermal stability and its biphasic morphology with a thick interphase layer. The PLA/DS3 blend was also selected for its thermal stability and because of its unique single-phase morphology. The properties of these two blends were compared to the properties of PLA and PLA/DS0. The lower thermal stability (lower $T_{5\%}$) of the PLA/DS0.5 and PLA/DS1.5 blends induced degradation during compression molding and created visible air bubbles in the material. The manipulation of the temperature, pressure and time conditions for the compression molding was unable to alleviate the problem. The mechanical properties of PLA and PLA/AS blends are summarized in Figure 6-5 and Table 6-5.

Table 6-5. Mechanical properties of PLA and PLA/AS blends.

| Sample | Tensile strength at break (MPa) | Elongation at break (%) | Young's modulus (GPa) | Toughness ($mJ/mm^3$) | Impact strength ($KJ/m^2$) |
|---|---|---|---|---|---|
| **UPLA** | $57.98\pm1.56^{d}$ | $4.99\pm0.13^{d}$ | $1.64\pm0.02^{a}$ | $1.49\pm0.07^{c}$ | $3.34\pm0.17^{c,b}$ |
| **PPLA** | $51.73\pm0.99^{c}$ | $4.48\pm0.07^{c}$ | $1.64\pm0.02^{a}$ | $1.22\pm0.03^{b}$ | $2.46\pm0.04^{a}$ |
| **PLA/DS0** | $36.20\pm1.67^{a}$ | $3.81\pm0.13^{b}$ | $1.62\pm0.06^{a}$ | $0.83\pm0.04^{a}$ | $2.47\pm0.15^{a}$ |
| **PLA/DS2.5** | $45.53\pm0.70^{b}$ | $4.20\pm0.08^{b}$ | $1.65\pm0.04^{a}$ | $1.07\pm0.03^{b}$ | $2.73\pm0.21^{b,a}$ |
| **PLA/DS3** | $33.56\pm1.34^{a}$ | $3.23\pm0.18^{a}$ | $1.69\pm0.02^{a}$ | $0.70\pm0.05^{a}$ | $2.38\pm0.05^{a}$ |

Different letters denote statistically significant different samples (Bonferroni t-test at a significance level of $\alpha=0.1$)

By comparing UPLA and PPLA samples it can be inferred that extrusion of PLA for 7 minutes affected negatively all of its mechanical properties except its modulus. The addition of native starch (DS0) also decreased the mechanical properties of the PLA/DS0 blend. Its tensile strength, elongation at break and toughness dropped by 30%, 15% and 32%, respectively compared to PPLA. The lower mechanical properties observed for the PLA/DS0 blend can be explained by the visible gap observed by SEM between the native starch dispersed phase and the PLA matrix (Figure 6-2B) which acted as stress concentration points. In contrast, the PLA/DS2.5 blend showed significantly higher tensile strength, elongation at break, toughness and impact strength, increased by 26%, 10%, 29% and 10.5%, respectively, compared to the PLA/DS0 blend. The higher mechanical properties of the PLA/DS2.5 blend most probably reflect the absence of visible gap observed by SEM between the AS dispersed phase and the PLA matrix (Figure 6-2H). The effective tension transfer from the PLA matrix to the AS dispersed phase could explain the enhanced mechanical properties of the PLA/DS2.5 blend compared to the PLA/DS0 blend.

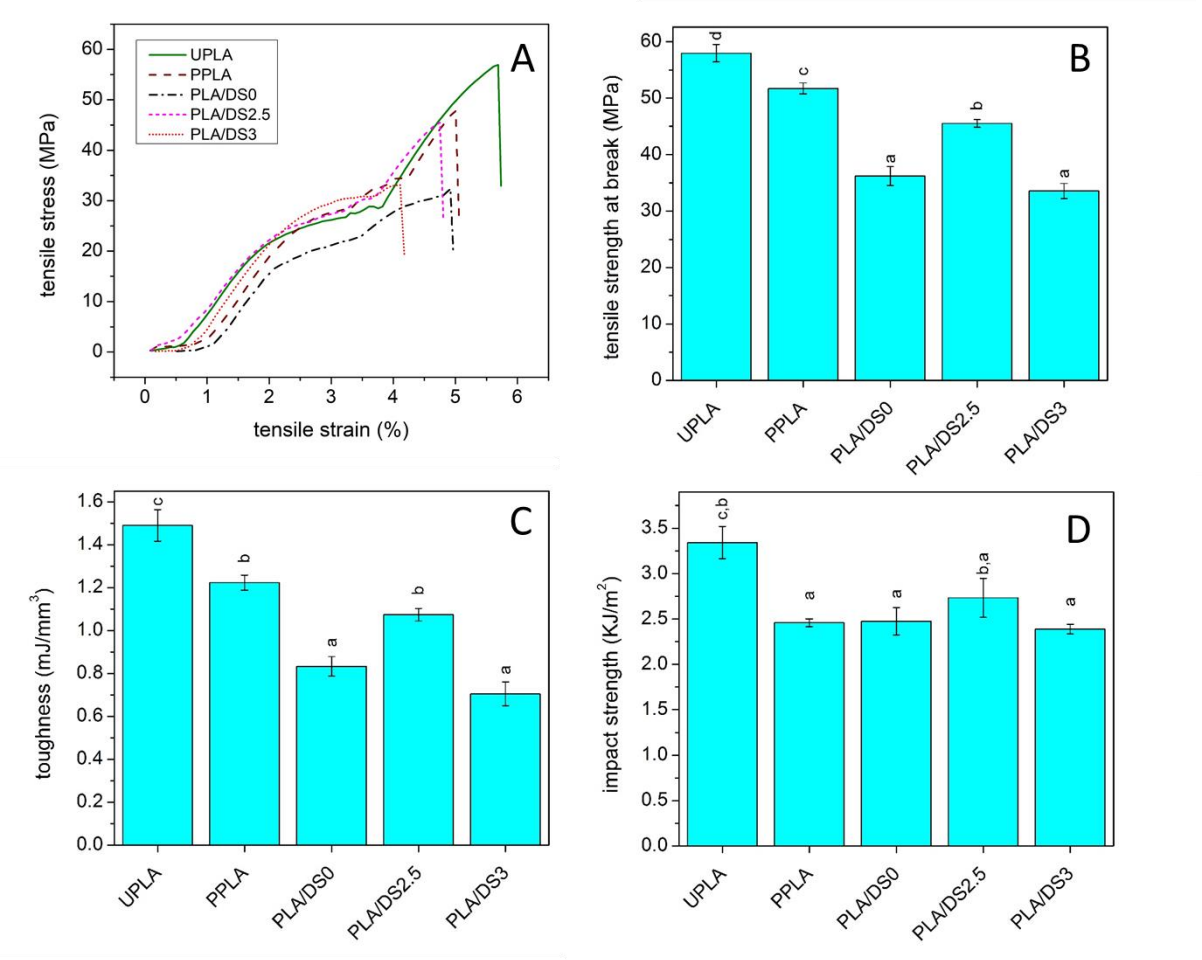


Figure 6-5. Mechanical properties of PLA and PLA/AS blends; (A) stress-strain curves, (B) tensile strength, (C) toughness and (D) impact stress. Different letters denote statistically significant differences (Bonferroni t-test, $\alpha$=0.1).

The mechanical properties of the PLA/DS3 blend, containing fully acetylated starch, were significantly lower than for the PLA/AS2.5 blend and similar to the PLA/DS0 blend containing native starch except for its modulus. The observed mechanical properties of PLA/DS3 reflect its morphology with no visible biphasic structure (Figure 6-2J). The presence of DS3 in the PLA blend could interfere with the continuity of the PLA matrix and reduce the mechanical performance of the blend. Similar observations have been reported previously for poly(propylene carbonate)/AS blends where changes of the microstructure from biphasic to single phase due to the increase of DS reduced the tensile and impact strength of the blend [58].

### 6.4.5. Water transport properties

The water transport properties of PLA and PLA/AS blends with sufficient thermal stability for compression molding are presented in Figure 6-6. An abrupt change in the slope of the water uptake curves was observed around 15 days for PLA/DS0 and PLA/DS2.5 blends which could be ascribed to the biphasic microstructure of these blends (Figure 6-2). The equilibrium water uptake of the PLA/AS blends was significantly higher than PPLA and decreased with increasing DS (Table 6-6).

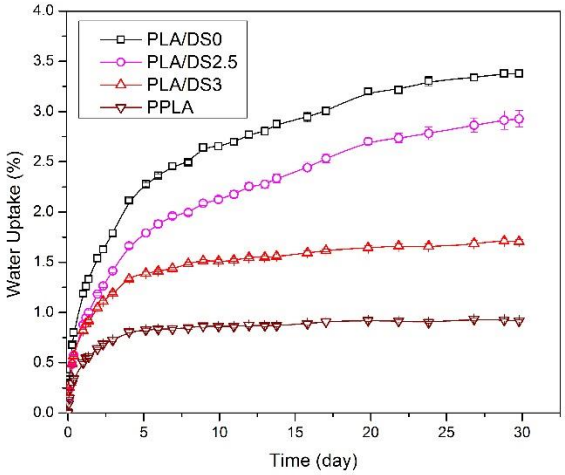


Figure 6-6. Water uptake of PLA and PLA/AS blends.

The water diffusion coefficient, calculated using Equation 6.5, is presented in Table 6-6. The water diffusion coefficient of the PLA/DS0 and PLA DS2.5 blends, displaying biphasic microstructure, is significantly lower than for the PLA/DS3 single phase blend. The water transport mechanisms in blend materials will be influenced by the microstructure of the dispersed phase and matrix and the degree of crystallinity. In the PLA/DS0 blend, the lower water diffusion coefficient may be related to the high crystallinity of the native starch which could act as an impermeable barrier preventing the diffusion of the water molecules and forcing these molecules to follow longer and more tortuous paths for diffusion [173]. Additionally, the presence of crystalline regions in the matrix can immobilize adjacent amorphous chains and make a rigid amorphous phase which is less permeable [173]. The diffused interphase may also be less permeable forcing the water molecules to follow a tortuous path [174]. The presence of a biphasic microstructure in the

PLA/DS2.5 blend together with the smaller size and larger number of acetylated starch dispersed phase may increase the tortuosity and explain the lower water diffusion coefficient compared to the PPLA and PLA/DS0 blend. Since the water diffusion mechanisms in PPLA and PLA/DS3 should reflect their single phase morphology, the degree of crystallinity will be the predominant factor influencing the water transport properties in these materials. In the PLA/DS3 blend, PLA has the higher capability of crystallization (Table 6-3) reflecting its smaller water diffusion coefficient compared to PPLA.

Table 6-6. Equilibrium water uptake, water diffusion coefficient and WVP of PPLA and PLA/AS blends.

| Sample | Diffusion coefficient ($\times 10^{12}$ $m^2/s$) | Equilibrium water uptake (%) | WVP ($\times 10^7$ $gh^{-1}m^{-1}Pa^{-1}$) |
|---|---|---|---|
| **PPLA** | $7.23 \pm 0.55^{c}$ | $0.92 \pm 0.01^{a}$ | $0.67 \pm 0.02^{a}$ |
| **PLA/DS0** | $2.91 \pm 0.25^{a}$ | $3.38 \pm 0.03^{d}$ | $1.16 \pm 0.12^{b}$ |
| **PLA/DS2.5** | $2.02 \pm 0.13^{a}$ | $2.93 \pm 0.08^{c}$ | $1.52 \pm 0.08^{b}$ |
| **PLA/DS3** | $5.32 \pm 0.33^{b}$ | $1.71 \pm 0.02^{b}$ | $2.48 \pm 0.09^{c}$ |

Different letters denote statistically significant different samples (Bonferroni t-test at a significance level of $\alpha$=0.1)

The permeation of gases through a polymer film includes four steps: sorption of gas molecules on the surface of the film; dissolution of the gas in film; diffusion through the film; and, desorption of the gas from opposite surface of the film [173, 175].

The water vapor permeability (WVP) for films prepared with PLA and PLA/AS blends is reported in Table 6-6. The WVP for all PLA/AS blends is higher compared to PPLA and increases with DS. The higher WVP permeability may reflect the contribution of the individual steps to the overall water vapor transport through the films. In the PLA/AS blends, the higher equilibrium water uptake (Table 6-6) could enhance the solubility of water and allow for faster permeability of the water vapor in these blends. Despite of their higher water solubility compared to other materials, due to the low diffusion coefficient of water in PLA/DS0 and PLA/DS2.5 blends, they have the second lowest WVP. The highest WVP obtained for PLA/DS3 was most probably due to the combination of high water solubility and diffusion. Slightly lower WVP of PLA/DS0 compared to PLA/DS2.5 despite of the higher water solubility and diffusion coefficient, may be attributed to the trapping of the water molecules by the starch granules which reduces the permeation rate.

## 6.5. Conclusion

This study demonstrates the potential of starch acetylation as a means to improve its compatibility with PLA by alleviating the limitations in the processing of starch and by producing materials with improved properties. CRS model predictions and SEM observations confirmed the presence of biphasic microstructure for all PLA/AS blends except PLA/DS3. The replacement of hydroxyl groups with acetyl groups enhanced the thermal stability of starch and PLA/AS blends. The plasticization and nucleation effect of AS altered the glass transition and crystallization behavior of PLA. The PLA/DS2.5 blend had the highest mechanical performance which could be explained by its biphasic microstructure and the presence of the thickest diffused interphase. The water transport properties of PLA were influenced by the presence of AS. The water diffusion coefficient of PLA/AS blends decreased while its WVP increased.

Better understanding of the effect of acetylation on properties of PLA/AS blends might be achieved by precisely controlling the morphology through adding the pre-formed AS particles into the blend. Other influential factor on blend properties such as crystallization behavior need to be further investigated before employing this blend in real applications. Crystallization can influence the mechanical and barrier properties and degradation rate of PLA. Increasing the degree of crystallinity can enhance the mechanical properties of PLA such as strength and modulus and reduce the rate of enzymatic degradation. Higher degree of crystallinity also leads to the improved barrier properties of PLA [13]. Therefore, investigation of the crystallization behavior of PLA in the presence of AS is very important. Investigation of the isothermal crystallization behavior of semicrystalline polymers is more convenient compared to non-isothermal, however, real industrial processing conditions are more non-isothermal. In the next chapter isothermal and non-isothermal crystallization behavior of PLA/AS blends will be studied.

# 7. Effect of degree of Substitution on Isothermal and Non-isothermal Crystallization Behavior of Poly(lactic acid)/Acetylated Starch Blends

Rasool Nasseri[a], Christine Moresoli [b], Aiping Yu[c], Zhongshun Yuan[d] and Chunbao (Charles) Xu[f]

Description of contributions:

[a]: performing all the experimentations and writing the manuscript.

[b] and [c]: main and co-supervisors.

[d] and [f]: providing the acetylated starch samples.

This manuscript is prepared for submission to "Polymer" journal under Elsevier publication.

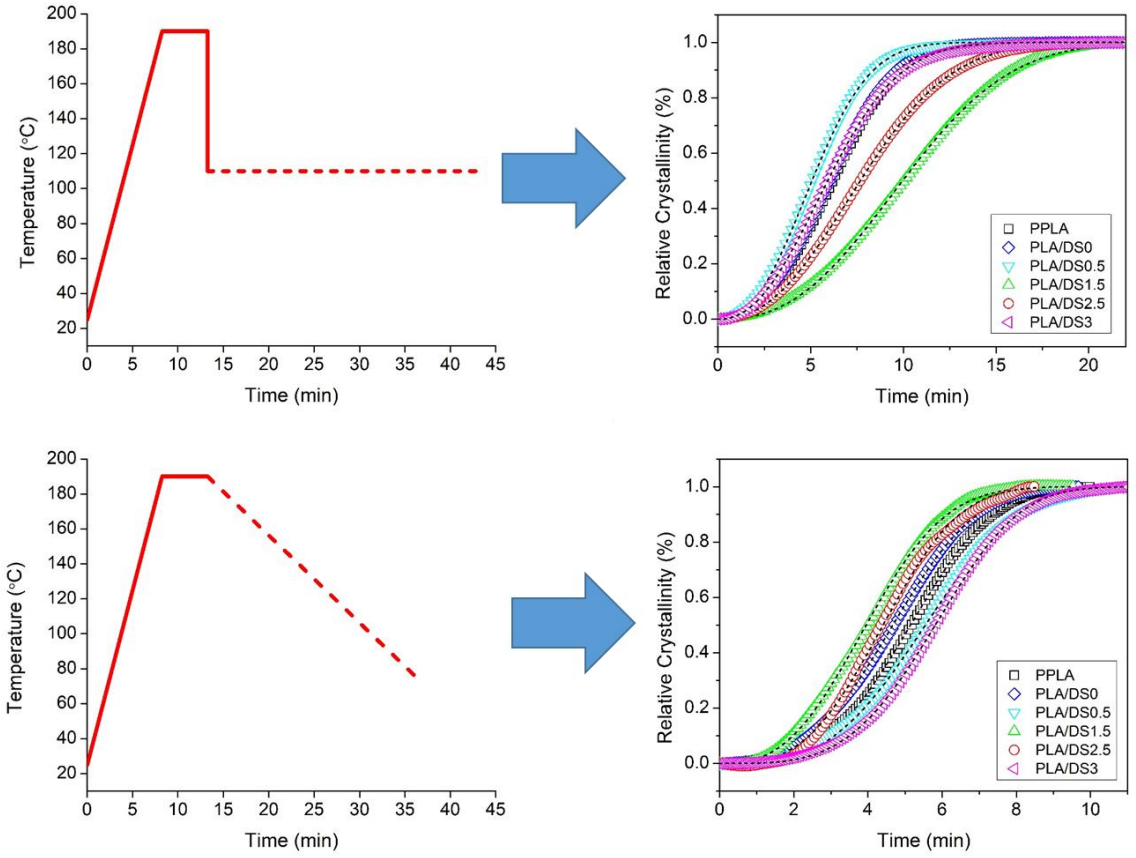

## 7.1. Synopsis

The rate of crystallization of pure poly(lactic acid) PLA and blends of PLA/acetylated starch (AS) with different degrees of substitution (DS) were investigated. The PLA/DS0.5 and PLA/DS1.5 blends showed the highest and the lowest rate of crystallization in isothermal crystallization conditions, respectively. The highest rate of crystallization in isothermal crystallization conditions for the PLA/DS0.5 blend reflects the highest nucleation activity of DS0.5 along with the faster dynamics of the PLA chains. The highest initial degree of crystallinity for PLA/DS1.5 blends may seem contrary to the lowest crystallization rate of this blend in isothermal crystallization conditions. The non-isothermal crystallization investigation, however, revealed similar rates of crystallization for the PLA/DS1.5 blend compared to the other PLA/AS blends at the lowest cooling rate ($2°C$/min) while having the fastest rate of crystallization at the highest cooling rate ($5°C$/min). The positive activation energy for the crystallization of the PLA/DS1.5 blend may reflect an endothermic process in the crystallization of this blend as a result of interfacial interactions. The SAXS analysis revealed the presence of smaller lamellar structure in PLA/AS blends. The largest amorphous phase among blends was observed for PLA/DS1.5 blend which can be attributed to the interfacial interactions in this blend.

## 7.2. Introduction

Poly(lactic acid) (PLA) has attracted extensive attention because of its biodegradable nature, its good mechanical properties and the renewability of its feedstock [5, 6]. Nonetheless, its slow rate of degradation along with its relatively high cost, have limited its range of applications. The blending of PLA with biodegradable polymers that are less expensive and which possess higher degradation rates can alleviate the limitations of PLA and extend the range of its applications. The biodegradability, abundance, renewability and low price of starch make it an attractive candidate [7]. Starch as a material has its own limitations. The low thermal processability of starch due to the lack of thermal transition before degradation [8] and its poor compatibility due to its hydrophilic characteristics limit its application in PLA blends. The thermal processability of starch can be improved by plasticization [8] but it does not address the poor compatibility with PLA. The compatibility of starch with PLA can be improved with the use of compatibilizers such as maleic anhydride (MA) [25], and epoxidized soybean oil [26]. The processability and compatibility of

starch with PLA can also be obtained by chemical modifications such as butyl-etherification, silane modification [28, 29] and acetylation [9, 10].

Crystallization can influence the mechanical and barrier properties and degradation rate of PLA. Increasing the degree of crystallinity can enhance the mechanical properties of PLA such as its strength and modulus and can reduce its rate of enzymatic degradation. A higher degree of crystallinity can also improve the barrier properties of PLA [13]. Therefore, the investigation of crystallization behavior of PLA in the presence of AS is very important. In the context of polymer blends, the presence of the secondary component will generally affect the crystallization behavior of the base polymer. The addition of a foreign component is known to increase the crystallization rate by increasing the nucleation probability which is a crucial initial step in the crystallization process [176]. The study of polymer crystallization under isothermal conditions is common and provides basic understanding of the crystallization kinetics and mechanisms. However, in practical and industrial applications, polymers typically undergo non-isothermal crystallization during their cooling. Cai et al. [177] reported on the isothermal crystallization behavior of thermoplastic starch (TPS)/PLA composites. Their results indicated that the spherulite growth rate, the overall crystallization rate and the activation energy of TPS/PLA composites were affected significantly by the incorporation of TPS which may have acted as a nucleating agent, improving the crystallinity of PLA in the TPS/PLA composites. They also reported a general constraint of PLA chain mobility in the composite melt due to the presence of TPS. Non-isothermal crystallization of TPS/PLA was investigated by Li et al. [178]. They confirmed the results of the isothermal crystallization study by Cai et al. [177] and indicated the that TPS acted as a nucleating agent that improved crystallinity of PLA and constrained the mobility of the PLA chains.

In the present study, the effect of the degree of substitution (DS) of acetylated starch (AS) on the isothermal and non-isothermal crystallization behavior of PLA/AS blends is presented. The main objective of this work was to understand how the crystallization of PLA was affected by the presence of AS with different DS. The crystalline structure of AS and fast-cooled PLA/AS blends was investigated by wide angle X-ray diffraction (WAXRD). The isothermal crystallization kinetics and mechanisms of the PLA/AS blends was investigated by differential scanning calorimetry (DSC) and discussed with Avrami's model. The effect of cooling rate on the crystallization kinetics and mechanisms of PLA/AS blends was investigated with non-isothermal

crystallization. The impact of DS on the nucleation activity and activation energy of the crystallization of PLA/AS blends also investigated. In order to clarify the effect of interfacial interactions on crystallization, the lamellar structure of PLA/AS blends was studied with small angle x-ray scattering (SAXS).

## 7.3. Materials and Methods

### 7.3.1. Materials

PLA 4032D ($M_n$=58000 g/mol, D-content 1.8 %) was provided by NatureWorks Inc (USA). Corn starch was purchased from a local Ontario market (BulkBarn®, product code: 000260). Acetylated starch (AS) was produced by mixing corn starch with acetic anhydride at a pre-determined molar ratio of acetic anhydride/starch and acetic acid. The mixture was stirred and heated to 135°$C$ using a preheated oil bath for 3 hours. The reaction mixture was precipitated into non-solvent and the precipitate was filtered and washed with non-solvent to remove any residual acetic acid. The recovered AS products were dried overnight in a vacuum oven at 45°C to remove any residual solvent. The degree of substitution (DS) represents the number of hydroxyl groups on a glucose unit of a starch molecule that are replaced by acetyl groups (from 0 to 3). AS with four DS of 0.5, 1.5, 2.5, and 3 were prepared according to the above mentioned procedure.

### 7.3.2. Methods

#### 7.3.2.1. Blend preparation

Prior to mixing, PLA and AS were dried at 80°$C$ in a vacuum oven overnight. A SJSZ-07A lab-scale twin screw extruder (Ruiming Plastics Machinery, Wuhan city, China) was employed for melt-blending of PLA with AS. The PLA/AS blends were prepared at 180°$C$ using a screw speed of 30 RPM for 7 min. In order to identify conditions that prevented degradation, preliminary experiments were preformed to identify the mixing temperature, speed and time. The extruded samples were then pelletized and compression molded to make a thin sheet using a hot press (PHI, Pasadena Hydraulic Inc., USA) at 200°C with 10000 lbs pressure for 4 minutes. The compression molded samples were then cooled rapidly using steel sheets precooled in an ice bath. The samples to be used for the small angle X-ray scattering analysis, were cooled slowly. All samples were

stored in a desiccator for further analysis. Table 7-1 presents the code and composition of the samples.

Table 7-1. Composition, code and processing time of the PLA and PLA/AS blends.

| Sample | PLA (wt%) | AS (wt%) | DS of AS |
|---|---|---|---|
| **PPLA (processed)** | 100 | 0 | - |
| **PLA/DS0** | 85 | 15 | 0 |
| **PLA/DS0.5** | 85 | 15 | 0.5 |
| **PLA/DS1.5** | 85 | 15 | 1.5 |
| **PLA/DS2.5** | 85 | 15 | 2.5 |
| **PLA/DS3** | 85 | 15 | 3 |

### 7.3.2.2. Wide Angle X-ray Diffraction (WAXRD)

The crystalline structure of AS and PLA/AS blends was investigated by wide angle X-ray diffraction (WAXRD) (D8 focus, Bruker) with CuK$\alpha_1$ radiation and 1.5406 Å wavelength operated at 40 kV and 30 mA. The X-ray diffraction patterns of AS and PLA/AS blends were recorded in $2\theta$ angle range of 3-40 and 10-40, respectively. The step size of the measurements was 0.02° and speed was 1 sec/step.

### 7.3.2.3. Small-Angle X-ray Scattering (SAXS)

Small-angle X-ray scattering measurements were performed using a SAXSess mc$^2$ instrument (Anton Paar, Austria) equipped with a Kratky block-collimation system and a sealed-tube Cu K$\alpha$ X-ray generator with wavelength, $\lambda$= 0.154 nm, operating at 40 kV and tube current = 50 mA. All measurements were performed at ambient temperature using transmission geometry. The scattered X-ray intensity was measured with a 2D charge coupled detector located 264.5 mm apart from the sample. The scattering intensity, $I(q)$, measured as a function of half the scattering angle, $\theta$, was first desmeared and then corrected for the background absorption and transformed to a plot of scattering intensity vs scattering vector, $q$ ($q = 4\pi sin\theta/\lambda$) using the saxsImage software (Utah SAXS Tools, David P. Goldenberg, September 2012).

### 7.3.2.4. Differential Scanning Calorimetry (DSC)

The thermal transitions, isothermal crystallization and non-isothermal crystallization of PLA and PLA/AS blends were investigated with a Q2000 TA instrument (USA) calibrated with indium and sapphire disk standards, using standard Tzero. Nitrogen with a 50 mL/min flowrate was used as purge gas. A sample (approximately 10 mg) was placed in an aluminum pan. DSC experiments were conducted with three different thermal procedures:

(a) Temperature modulated DSC (TMDSC): heating the sample from 40°$C$ to 190°$C$ at constant heating rate (2°$C$/min) coupled with modulation amplitude of 1.5°$C$ and period of 90 s to study the thermal transitions and initial degree of crystallinity of the blends. The initial degree of crystallinity $\chi_{c_0}$ is defined as [179]:

$$\chi_{c_0}(\%) = \left(\frac{\Delta H_{rev} - \Delta H_{nonrev}}{\Delta H_m^0 \times \delta_{PLA}}\right) \times 100 \tag{7.1}$$

where $\Delta H_{rev}$ and $\Delta H_{nonrev}$ is the area under the reversible and non-reversible heat flow respectively, $\Delta H_m^0$ is the melting enthalpy for 100 % crystalline PLA (93.6 J/g[161]), and $\delta_{PLA}$ is the mass fraction of PLA in the blends.

The degree of crystallinity $\chi_c$ after cold crystallization is defined as [29, 160]:

$$\chi_c(\%) = \left(\frac{\Delta H_m}{\Delta H_m^0 \times \delta_{PLA}}\right) \times 100 \tag{7.2}$$

where $\Delta H_m$ is the enthalpy of melting.

(b) Isothermal crystallization: heating the sample to 180°$C$ and maintaining it at 180°$C$ for 5 mins to erase the thermal history followed by fast cooling to 110°$C$ and isotherm for 40 mins.

(c) Non-isothermal crystallization: heating the sample to 180°$C$ and maintaining it at 180°$C$ for 5 mins to erase the thermal history followed by cooling at different cooling rates of 2°$C$/min, 3.5°$C$/min and 5°$C$/min.

## 7.4. Results and Discussion

### 7.4.1. Crystalline structure of AS and PLA/AS blends

The X-ray diffraction patterns of AS presented in Figure 7-1A indicate changes in crystallinity according to DS. By comparing the patterns of AS to those of neat starch, one observes a lower intensity of the peaks characteristic of crystallinity. Similar decrease was reported previously for acetylated corn starch [70]. The reduction of crystallinity during acetylation may reflect the lower inter and intramolecular hydrogen bonding due to the partial replacement of hydroxyl groups with acetyl groups resulting in disordering of the crystalline structure [71, 72]. The WAXRD patterns revealed a new crystalline structure for DS3 where a new set of peaks was observed between $2\theta$=5° and 10° (Figure 7-1A).

Figure 7-1B shows the X-ray diffraction patterns of PLA/AS blends. There is no sign of AS diffraction in the diffraction pattern of the PLA/AS blends. The diffraction peak at $2\theta$=31° from (1010) plane of the $\alpha$-form crystal [180] was observed in all blends. The peak at $2\theta$=16.5° representing the diffraction from (110) and/or (200) planes of the disordered $\alpha'$-form [15] was observed in all blends except PLA/DS0 and PLA/DS2.5. A very low level of crystallinity was observed in all blends except for PLA/DS1.5, most probably due to the fast cooling. The PLA/DS1.5 blend has the highest degree of crystallinity and possesses distinguishing diffraction patterns such as a peak at $2\theta$=19° from (203) plane of the $\alpha$-form crystal [181].

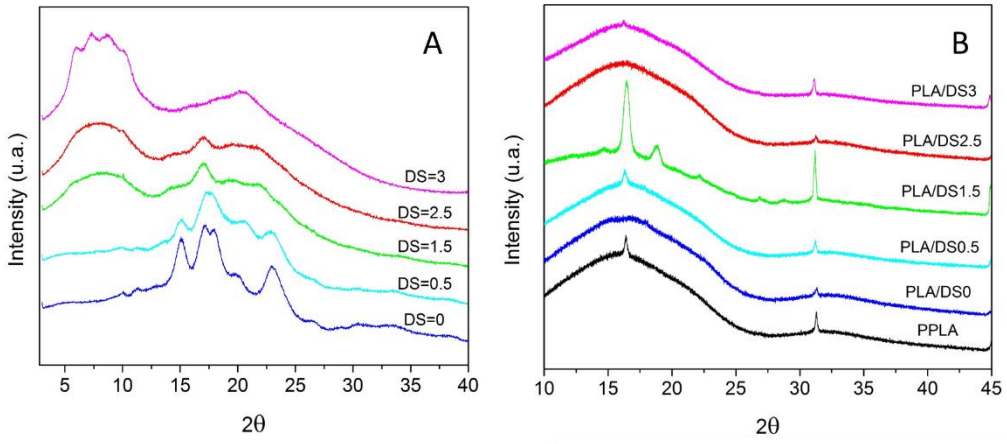


Figure 7-1. WAXRD diffraction patterns of (A) acetylated starch and (B) PLA/AS blends according to DS.

## 7.4.2. Thermal transitions and initial degrees of crystallinity

The influence of AS on the thermal transitions of PLA/AS blends was investigated by TMDSC. Figure 7-2A depicts the TMDSC thermogram of pure PLA and PLA/AS blends. The glass transition temperature ($T_g$) of PLA decreased slightly by incorporation of AS due to the plasticization effect (Table 7-2). The small peak in the $T_g$ region (pointed out by arrows) of the TMDSC thermograms showed that the glass transition included an enthalpy relaxation [182]. Cold crystallization (exothermic peak ($T_c$) around $90°C$) was observed for all samples. A second exothermic peak ($T_{cc}$) was observed prior to the melting temperature ($T_m$) which was attributed to the crystal transformation from the disordered $\alpha'$ form to the more ordered $\alpha$ form [15]. The initial degree of crystallinity before cold crystallization was estimated by deconvolution of the heat flow in its reversible and non-reversible parts (Equation 7.1). An example of the deconvolution of the total heat flow for PPLA is presented in Figure 7-2B. The estimated initial degree of crystallinity is presented in Table 7-2. PLA/DS1.5 blend had the highest initial degree of crystallinity which is supported by the WAXRD results. The degree of crystallinity of all blends was slightly higher than that of PLA. All blends reached the same level of crystallinity after cold crystallization.

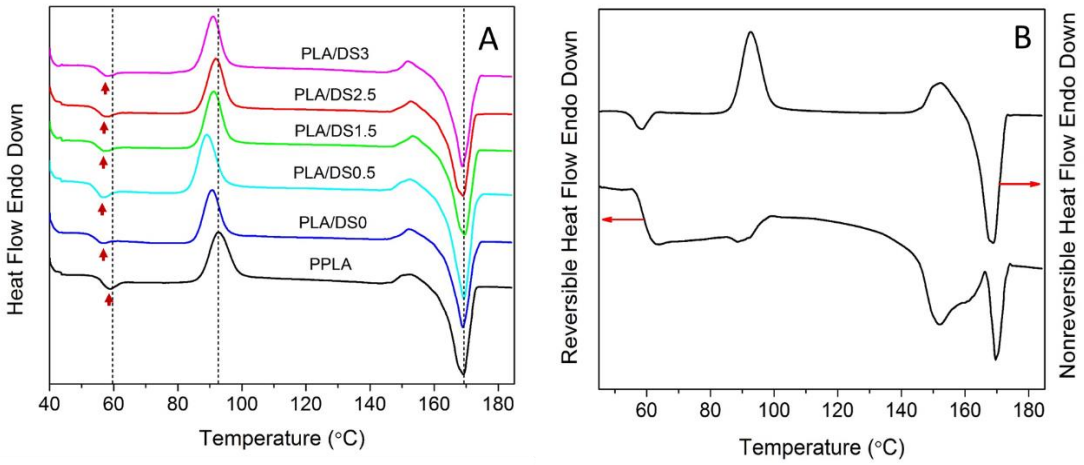


Figure 7-2. (A) TMDSC thermogram of pure PLA and PLA/AS blends, (B) deconvolution of the total heat flow into the reversing and nonreversing contributions for PPLA.

Table 7-2. Glass transition temperature ($T_g$), cold crystallization temperature ($T_c$), $\alpha'$ to $\alpha$ transformation temperature ($T_{cc}$), melting temperature ($T_m$), area under reversing ($\Delta H_{rev}$) and nonreversing ($\Delta H_{nonrev}$) parts of heat flow, initial degree of crystallization ($\chi_{c_0}$) before cold crystallization, and final degree of crystallization ($\chi_c$) after cold crystallization of pure PLA and PLA/AS blends.

| Sample | $T_g$ (°C) | $T_c$ (°C) | $T_{cc}$ (°C) | $T_m$ (°C) | $\Delta H_{rev}$ (J/g) | $\Delta H_{nonrev}$ (J/g) | $\chi_{c_0}$ (%) | $\chi_c$ (%) |
|---|---|---|---|---|---|---|---|---|
| **PPLA** | 59 | 92 | 152 | 169 | 8.49 | 12.52 | 4.3 | 38.6 |
| **PLA/DS0** | 56 | 91 | 152 | 169 | 8.16 | 13.52 | 6.7 | 40.0 |
| **PLA/DS0.5** | 56 | 89 | 152 | 169 | 6.82 | 11.4 | 5.8 | 40.1 |
| **PLA/DS1.5** | 57 | 91 | 153 | 169 | 0.10 | 10.94 | 13.6 | 39.6 |
| **PLA/DS2.5** | 58 | 92 | 152 | 169 | 10.19 | 14.73 | 5.7 | 41.8 |
| **PLA/DS3** | 58 | 91 | 152 | 169 | 8.45 | 14.43 | 7.5 | 43.9 |

## 7.4.3. Isothermal Crystallization

The isothermal crystallization thermograms of PLA and PLA/AS blends obtained at 110°$C$ are shown in Figure 7-3A. The addition of AS affected the crystallization of PLA in the blends. Two opposing effects were observed, an increased rate of crystallization for PLA/DS0, PLA/DS0.5 and PLA/DS3 and slower rate of crystallization for PLA/DS1.5 and PLA/DS2.5. The rate of isothermal crystallization was investigated by analyzing the relative crystallinity ($\chi_t$) at different times ($t$) and calculated as follows:

$$\chi_t = \frac{\int_0^t (\mathrm{dH_c/dt})dt}{\int_0^\infty (\mathrm{dH_c/dt})dt} \tag{7.3}$$

where $\mathrm{dH_c/dt}$ is the rate of heat evolution during a given time period. The relative crystallinity, $\chi_t$, was calculated from the area under the exothermic peak of crystallization (Figure 7-3B). At the beginning of the crystallization process, an induction period was observed which reflects nucleation [183]. Crystallization is generally represented as a two steps process: primary crystallization (linear portion of $\chi_t$) and secondary crystallization (non-linear portion of $\chi_t$) [177]. The first step represents crystal growth until crystals are sufficiently large to touch each other. When crystals touch each other, the second stage starts with slowing down of the crystallization process [184]. The kinetics of the isothermal crystallization process were investigated with the Avrami model:

$$1 - \chi_t = \exp(-Kt^n) \tag{7.4}$$

where $K$ and $n$ are the crystallization rate constant and the Avrami exponent, respectively. The parameter $K$ gives information on the rate of nucleation and crystal growth. The parameter $n$ provides information on the type of nucleation and the dimensionality of the crystal growth. The

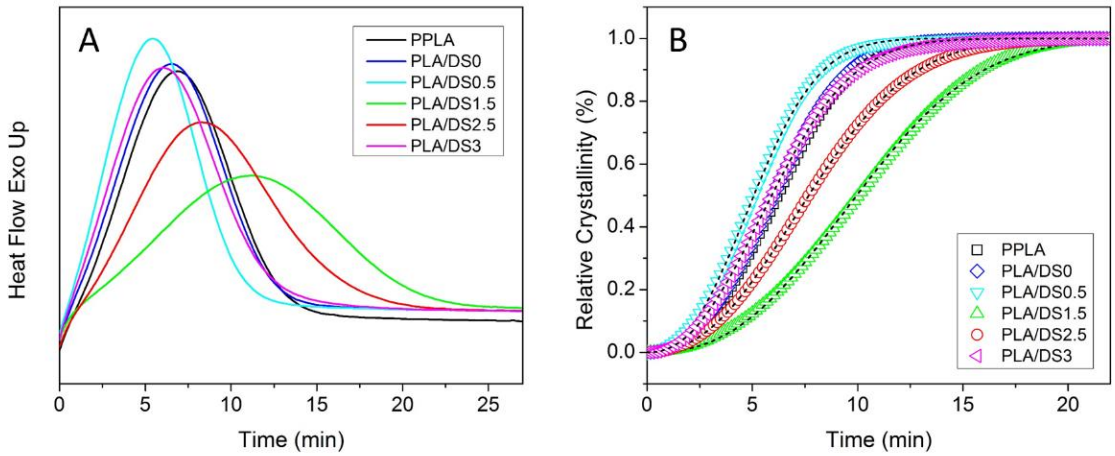


Figure 7-3. (A) Isothermal crystallization thermograms of PLA and PLA/AS blends obtained at 110°$C$, (B) Relative crystallinity of PLA and PLA/AS blends according to time. Black dashed lines show the fitted Avrami equation.

The Avrami equation provided a very good fit of the relative crystallinity determined experimentally (Figure 7-3B). The Avrami parameters, $n$ and $K$ obtained from the least square fitting of the experimental data with MATLAB R2014a, are presented in Table 7-3. The Avrami exponent, related to the nucleation mechanism (simultaneous or sporadic) and the dimensionality of the crystal growth (two or three dimensional) usually has a value between 2 and 4 for polymer crystallization. Large values of the Avrami exponent are indicative of sporadic (or combination of sporadic and simultaneous) nucleation with three-dimensional spherulitic growth while small values are attributed to instantaneous (accompanied with some sporadic) nucleation with two dimensional growth [13, 171]. The Avrami exponent of the PLA/AS blends was slightly smaller than PLA (except for PLA/DS1.5). The addition of AS mildly affected the nucleation mechanism and growth dimensionality of pure PLA. It can be inferred that the crystal growth in PLA/AS blends became more than two dimensional with more simultaneous nucleation compared to PLA. A similar effect has been reported previously for thermoplastic starch on Avrami exponent of PLA/thermoplastic starch blends [177]. Note that the Avrami equation is based on a number of simplifications which limits the conclusions that can be made with regard to microscopic mechanisms of the crystal growth without morphological information [185].

The Avrami parameters were used to estimate the crystallization half-time ($t_{1/2}$), defined as the time required to reach 50% relative crystallinity (Equation 7.5) and the crystallization rate (G) given as the reciprocal of $t_{1/2}$ (Equation 7.6).

$$t_{1/2} = \left(\frac{ln2}{K}\right)^{1/n} \tag{7.5}$$

$$G = 1/t_{1/2} \tag{7.6}$$

Table 7-3. Avrami kinetic parameters of pure PLA and PLA/AS blends for isothermal crystallization. Reported ranges are the 95% confidence interval on the parameter estimates for Avrami model.

| Sample | $n$ | $K$ (min$^{-1}$) | $t_{1/2}$ (min) | $G$ (min$^{-1}$) | $R^2$ |
|---|---|---|---|---|---|
| **PPLA** | 2.51±0.01 | 0.0072±0.0001 | 6.159 | 0.162 | 0.999 |
| **PLA/DS0** | 2.48±0.01 | 0.0082±0.0001 | 5.983 | 0.167 | 0.999 |
| **PLA/DS0.5** | 2.38±0.01 | 0.0146±0.0002 | 5.073 | 0.197 | 0.999 |
| **PLA/DS1.5** | 2.52±0.01 | 0.0021±0.0001 | 9.955 | 0.100 | 0.999 |
| **PLA/DS2.5** | 2.31±0.00 | 0.0062±0.0001 | 7.678 | 0.130 | 1 |
| **PLA/DS3** | 2.26±0.01 | 0.0125±0.0003 | 5.918 | 0.169 | 0.999 |

The PLA/DS0.5 blend had the smallest $t_{1/2}$, i.e. the highest rate of crystallization which could be due to the nucleation effect of DS0.5 or to faster dynamics of the PLA chains in the blend as a result of the lower glass transition. In contrast, the PLA/DS1.5 blend had the highest $t_{1/2}$, i.e. the lowest rate of crystallization which is contrary to the results of WAXRD and TMDSC where the highest initial degree of crystallinity was estimated for this blend after fast cooling (Table 7-2). The effect of DS1.5 on the PLA crystallization behavior was investigated by non-isothermal crystallization and is discussed in the next section.

## 7.4.4. Non-isothermal crystallization

The non-isothermal crystallization thermograms of PLA and PLA/AS blends obtained at three different cooling rates of 2, 3.5 and 5°$C$/min. The thermograms were analyzed with the Avrami equation modified to account for the non-isothermal conditions. The effect of the cooling rate ($\beta$) is accounted for introducing a correction factor to the crystallization rate constant $K$ [186]:

$$\ln K_c = \frac{\ln K}{\beta} \tag{7.7}$$

where $K_c$ is the kinetic crystallization rate constant for non-isothermal crystallization.

The relative crystallinity over time and the fitted Avrami equation according to the cooling rate for PLA  the PLA/AS blends are depicted in Figure 7-4 (A, B, and C) and the Avrami parameters obtained by least square fitting are presented in Table 7-4.

The Avrami exponent $n$ for the non-isothermal crystallization generally decreased with increasing cooling rate indicating a decrease in the dimensionality of the crystal growth while nucleation mechanism is becoming more simultaneous.

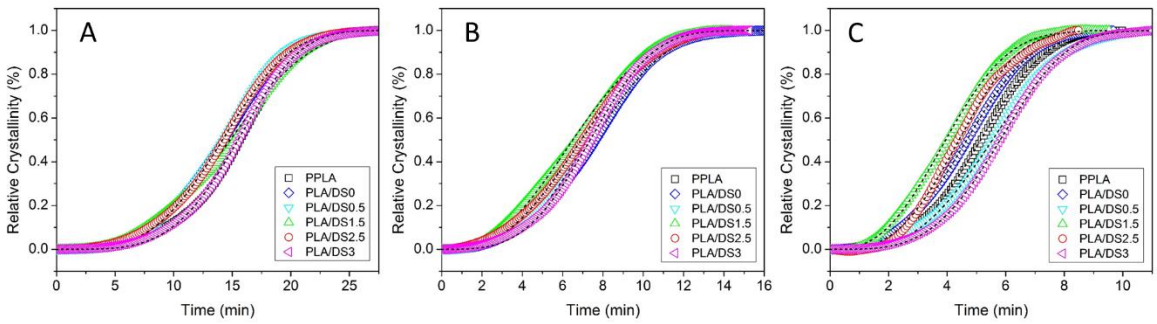


Figure 7-4. Relative crystallinity of PLA and PLA/AS blends at different cooling rates (A) 2°$C$/min, (B) 3.5°$C$/min, and (C) 5°$C$/min. Black dashed lines represent the fitted Avrami equation.

At the lowest cooling rate, 2°$C$/min, $t_{1/2}$ was about 15 mins for PLA and all the blends indicating similar crystallization rate. This could also be inferred from the overlapping between the relative crystallinity versus time curves (Figure 7-4B). Differences in the relative crystallinity versus time between PLA and the PLA/AS blends started to appear at a 3.5°$C$/min cooling rate and were distinct at a 5°$C$/min cooling rate. The PLA/DS1.5 blend showed the highest rate of crystallization at the highest cooling rate while in isothermal crystallization, this blend showed the slowest rate of crystallization. That might explain the highest initial degree of crystallinity for this sample which was observed in WAXRD (Figure 7-1B) and TMSDC (Table 7-2) experiments.

The exothermic peak of crystallization of PLA and PLA/AS blends at different cooling rates, presented in Figure 7-5, shows that $T_p$ (crystallization peak temperature) shifted to lower temperatures as the rate of cooling was increased for all blends except the PLA/DS1.5 blend. The crystallization peak temperature of the PLA/DS1.5 blend shifted to higher temperatures with increasing cooling rate.

Table 7-4. Avrami kinetic parameters, activation energy of crystallization, and nucleation activity parameters of PLA and PLA/AS blends during non-isothermal crystallization.

| Sample | $\beta$ ($^{\circ}C$/min) | $t_{1/2}$ (min) | $G$ ($min^{-1}$) | $n$ | $K_c$ ($min^{-1}$) | $R^2$ | $T_P$ ($^{\circ}C$) | $E_a$ (KJ/mol) | $B$ or $B^*$ ($K^2$) | $\phi_n$ |
|---|---|---|---|---|---|---|---|---|---|---|
| **PPLA** | 2 | 15.56 | 0.064 | 4.10±0.04 | 0.0030±0.0009 | 0.999 | 99.15 | -238.41 | 37403 | - |
| | 3.5 | 7.16 | 0.140 | 3.26±0.01 | 0.1442±0.0043 | 0.999 | 95.53 | | | |
| | 5 | 5.14 | 0.194 | 3.34±0.01 | 0.3115±0.0074 | 0.999 | 95.49 | | | |
| **PLA/DS0** | 2 | 14.19 | 0.070 | 3.45±0.01 | 0.0085±0.0014 | 0.999 | 101.49 | -276.95 | 38748 | 1.03 |
| | 3.5 | 7.56 | 0.132 | 3.10±0.01 | 0.1504±0.0049 | 0.999 | 98.66 | | | |
| | 5 | 4.67 | 0.214 | 3.01±0.01 | 0.3678±0.0090 | 0.999 | 97.76 | | | |
| **PLA/DS0.5** | 2 | 14.07 | 0.071 | 3.61±0.02 | 0.0070±0.0015 | 0.999 | 102.32 | -156.84 | 22170 | 0.59 |
| | 3.5 | 7.23 | 0.138 | 3.22±0.01 | 0.1640±0.0050 | 0.999 | 97.57 | | | |
| | 5 | 5.55 | 0.180 | 3.22±0.01 | 0.3068±0.0068 | 0.999 | 95.45 | | | |
| **PLA/DS1.5** | 2 | 14.82 | 0.067 | 3.18±0.03 | 0.0114±0.0035 | 0.998 | 99.62 | 347.03 | -47851 | -1.28 |
| | 3.5 | 6.51 | 0.015 | 2.53±0.01 | 0.2329±0.0109 | 0.998 | 101.81 | | | |
| | 5 | 3.95 | 0.253 | 2.71±0.01 | 0.4409±0.0137 | 0.999 | 102.49 | | | |
| **PLA/DS2.5** | 2 | 14.16 | 0.070 | 3.53±0.02 | 0.0077±0.0020 | 0.999 | 99.48 | -111.42 | 164263 | 4.39 |
| | 3.5 | 6.92 | 0.144 | 2.72±0.01 | 0.2006±0.0073 | 0.999 | 98.72 | | | |
| | 5 | 4.40 | 0.227 | 3.11±0.02 | 0.3689±0.0148 | 0.998 | 98.68 | | | |
| **PLA/DS3** | 2 | 15.49 | 0.064 | 4.17±0.03 | 0.0027±0.0008 | 0.999 | 100.31 | -220.58 | 33278 | 0.89 |
| | 3.5 | 7.37 | 0.136 | 3.40±0.01 | 0.1292±0.0044 | 0.999 | 96.99 | | | |
| | 5 | 5.81 | 0.172 | 3.70±0.01 | 0.2526±0.0042 | 0.999 | 95.51 | | | |

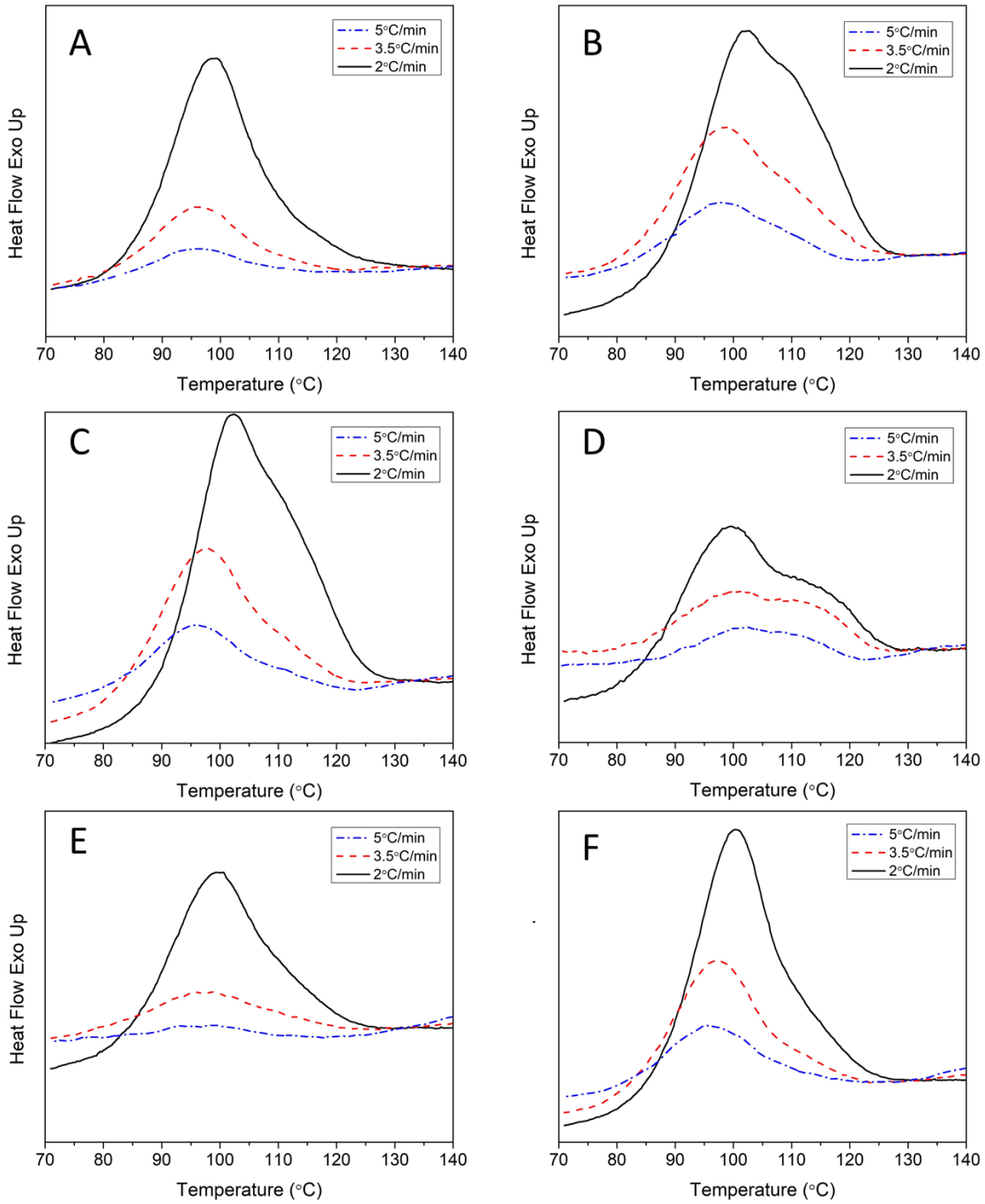


Figure 7-5. Exothermic peaks of crystallization at different heating rates for (A) pure PLA, (B) PLA/DS0, (C) PLA/DS0.5, (D) PLA/DS1.5, (E) PLA/DS2.5 and, (F) PLA/DS3 blends.

The activation energy of non-isothermal crystallization was estimated by using the Kissinger approach [187]:

$$\frac{d\left[\ln\left(\frac{\beta}{T_p^2}\right)\right]}{d\left[\frac{1}{T_p}\right]} = -\frac{E_a}{R} \tag{7.8}$$

where $T_p$, $E_a$, and $R$ are the crystallization peak temperature, the activation energy of crystallization, and is the universal gas constant, respectively.

The Kissinger plots are presented in Figure 7-6A and the estimated activation energy of the crystallization of PLA are summarized in Table 7-4. The exothermic nature of the transition from the melt to the crystalline state leads to negative $E_a$ values. A negative $E_a$ value represents the acceleration of the crystallization mechanisms by decreasing the temperature [187] which was observed for all PLA/AS blends except for the PLA/DS1.5 blend. The positive $E_a$ of the PLA/DS1.5 blend may reflect an endothermic phenomenon such as the disruption of the interfacial bonding between the PLA matrix and the AS dispersed phase during the crystallization process. Further investigation will be required to understand the presence and effect of the interfacial interactions in PLA/AS blends.

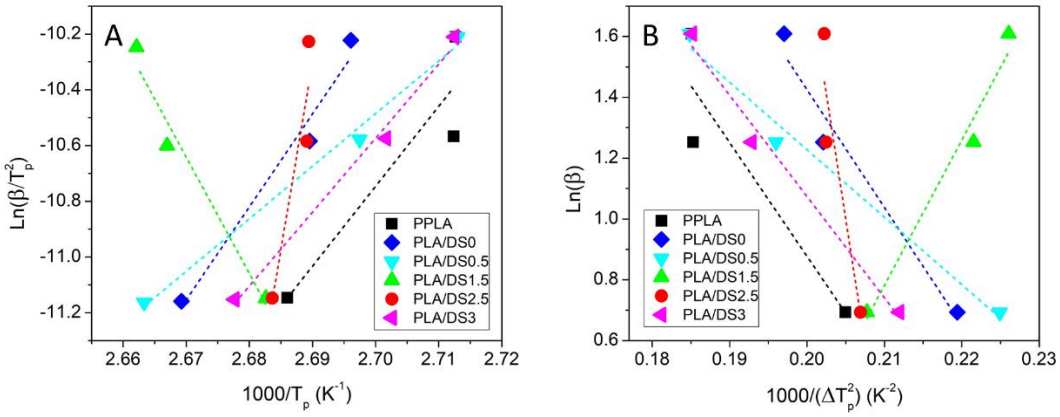


Figure 7-6. (A) Kissinger plot for the estimation of the $E_a$ for the crystallization of PLA and PLA/AS blends. (B) Nucleation activity plots of PLA and PLA/AS blends.

The nucleation activity of the dispersed component in polymer blends ($\phi_n$) defined as a factor by which the work of crystallization of a polymer decreases with the addition of a second component, was evaluated by the method suggested by Dobreva and Gutzow [188]. In this method, the nucleation activity is defined as follows:

$$\phi_n = \frac{B^*}{B} \tag{7.9}$$

where $B^*$ and $B$ are parameters related to the filled and pure polymer, respectively and are calculated with the following equations:

$$\ln(\beta) = C_1 - \frac{B^*}{\Delta T_p^2} \tag{7.10}$$

$$\ln(\beta) = C_2 - \frac{B}{\Delta T_p^2} \tag{7.11}$$

where $\beta$ is the cooling rate, $C_1$ and $C_2$ are constants, and $\Delta T_p = T_m - T_p$ is the supercooling. $B$ and $B^*$ are estimated from the slope of the plot $\ln(\beta)$ versus $1/\Delta T_p^2$ (Figure 7-6B). The estimated nucleation activity for PLA/AS blends is presented in Table 7-4. When the dispersed component in a blend is extremely active for nucleation, the value of $\phi_n$ approaches 0, while for an inert dispersed component, it is about 1. A nucleation activity higher than 1 might be interpreted as an anti-nucleating effect [176]. In the context of PLA/AS blends, the highest nucleation activity was observed for DS0.5, DS0, and DS3 showed inert nucleation activity, whereas DS2.5 displayed an anti-nucleating effect. An unusual nucleation activity was observed for DS1.5 where the nucleation activity was negative. The nucleating activity of DS1.5 may reflect potential endothermic processes occurring during the crystallization as previously concluded from its positive $E_a$ value. The activity of a nucleating agent depends on several factors such as size (available surface area), thermodynamic affinity to the matrix, and crystalline lattice structure. Nucleants that are small, possess high affinity with the matrix, and have matching crystalline lattice structure with the matrix will promote nucleation activity [169-171]. Further investigation of these factors will be required to better understand the nucleation activity of AS.

### 7.4.5. Lamellar structure of PLA and PLA/AS blends

The lamellar structure of PLA and PLA/AS blends was investigated by SAXS. The Lorentz-corrected SAXS data are presented in Figure 7-7 as $Iq^2$ vs $q$, where $q = 4\pi/\lambda \sin(\theta)$ and $\theta$ and $\lambda$ are half of the scattering angles and the wave length of the X-rays, respectively.

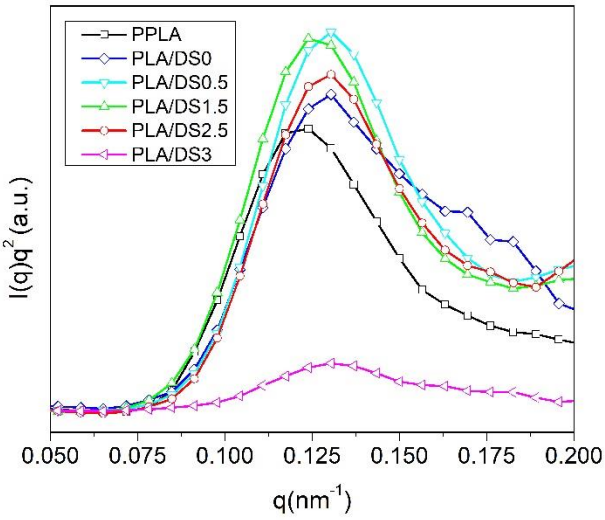


Figure 7-7. Lorentz-corrected SAXS profiles recorded at room temperature for PLA and PLA/AS blends.

The morphological parameters of the lamellar structure including the long period, the average lamellar thickness and the amorphous-phase thickness were estimated from the normalized one-dimensional correlation function calculated from the scattered intensity by using the following equation [189]:

$$\gamma(r) = \frac{\int_0^\infty I(q)q^2 \cos(qr)\, dq}{\int_0^\infty I(q)q^2 dq} \tag{7.12}$$

where $r$ is the direction along which the electron density distribution was measured.

The data were extended from the smallest measured $q$ to zero by linear extrapolation. Large $q$ values were extrapolated to infinite $q$ using a Porod law ($q^{-4}$ decay) [150]. The average long period ($L$) was estimated from the first maximum of the correlation function. The average lamellar thickness ($l_c$) was determined from the r-axis value of the intersection point between the tangent-line at $\gamma(r) = 0$ and the tangent-line at the first minimum in the correlation curve as shown in the inset of Figure 7-8. The thickness of the amorphous phase ($l_a$) was calculated from $L$ and $l_c$ ($l_a = L - l_c$) [189]. The long period can also be estimated from equation $L = 2\pi/q^*$, where $q^*$ is the peak of Lorentz-corrected plot [150]. The normalized one-dimensional correlation functions of PLA and the PLA/AS blends are plotted in Figure 7-8.

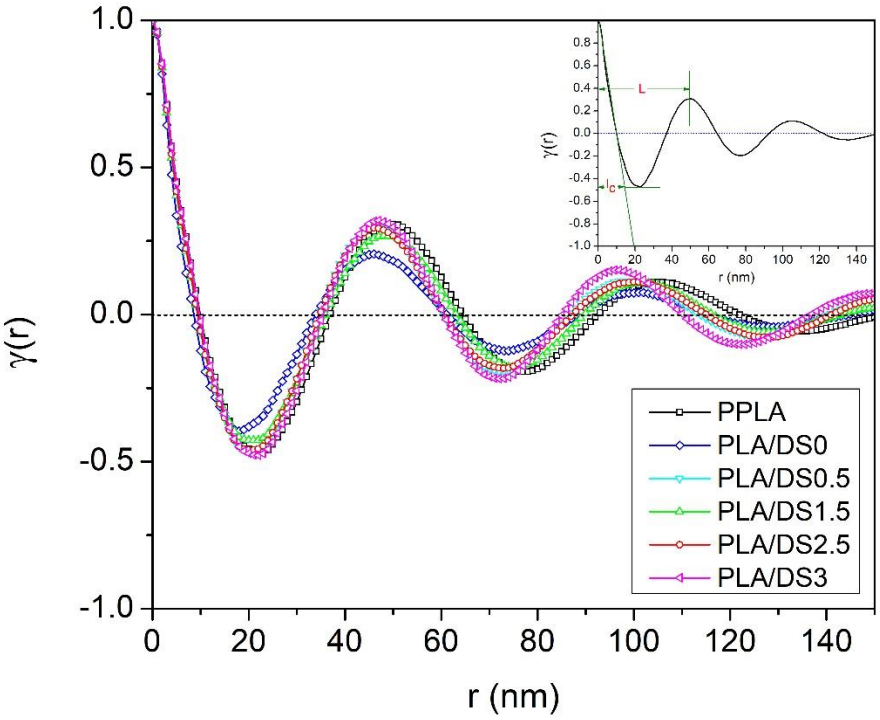


Figure 7-8. One-dimensional correlation functions of PLA and PLA/AS blends.

Table 7-5. Morphological parameters of the lamellar structure of pure PLA and PLA/AS blends.

| **Sample** | ***L* (nm)** | | $l_c$ **(nm)** | $l_a$ **(nm)** |
|---|---|---|---|---|
| | **peak of Lorentz-corrected plot** | **correlation function** | | |
| **PPLA** | 50.7 | 49.9 | 15.2 | 34.7 |
| **PLA/DS0** | 48.2 | 45.9 | 12.9 | 33 |
| **PLA/DS0.5** | 48.2 | 46.3 | 14.2 | 32.1 |
| **PLA/DS1.5** | 50.7 | 48.1 | 14.1 | 34 |
| **PLA/DS2.5** | 48.2 | 46.3 | 14.3 | 32 |
| **PLA/DS3** | 48.2 | 46.8 | 14.9 | 31.9 |

The morphological parameters of the lamellar structure presented in Table 7-5 indicated lower $L$, $l_c$ and $l_a$ estimates for all PLA/AS blends compared to PLA. The PLA/DS1.5 blend displayed the most similar $L$ and $l_a$ parameters to those of PLA. During the crystallization process, the crystallization of the PLA chains compete with the interactions between the PLA and AS chains. This competition will govern the final lamellar structure of the material [190]. The interactions between the PLA and the AS chains interfere with the conformational changes of the PLA chains

that are required for crystallization to occur and which would lead to a smaller lamellar structure. With this in mind, the higher thickness of the amorphous phase ($l_a$) of the PLA/DS1.5 blend may be attributed to the higher interactions taking place between the PLA and AS components in this blend. This is in line with the $E_a$ estimate of the interfacial interaction between PLA and DS1.5.

# Conclusion

The role of AS in the crystallization of PLA in PLA/AS blends investigated by WAXRD , SAXS and isothermal and non-isothermal crystallization analysis. The highest initial degree of crystallinity was observed for PLA/DS1.5. The crystallization characteristics of PLA in PLA/AS blends are affected by the presence of AS. Based on the Avrami exponent $n$ of the isothermal crystallization, the crystal growth is becoming more two dimensional with increased simultaneous nucleation by incorporation of AS to PLA. The fastest rate of crystallization was observed for the PLA/DS0.5 blend. The highest nucleation activity observed for DS0.5 ($\phi_n$=0.59) along with the faster dynamic of PLA chains due to the plasticization effect in the blend compared to PLA are the main reasons for the fastest crystallization of this blend. The PLA/DS1.5 blend showed the lowest rate of crystallization during isothermal crystallization conditions which contradicted its highest initial degree of crystallinity. This discrepancy was explored further by investigating the crystallization behavior of PLA/AS1.5 for non-isothermal conditions. A distinct rate of crystallization were observed for PLA/DS1.5 as a function of the cooling rate. The crystallization rate of the PLA/DS1.5 blend was very similar to the other PLA/AS blends at cooling rate of $2°C$/min. However, at higher cooling rate, $5°C$/min, PLA/DS1.5 blend showed the highest rate of crystallization which may explain the highest initial degree of crystallinity for this blend. The positive $E_a$ estimate for the crystallization of PLA/DS1.5 may reflect an endothermic process during the crystallization of PLA. Further investigation of the interfacial interactions between the AS components and the PLA matrix is required to better understand the potential endothermic process. The lamellar structure of the PLA/AS blends deduced from SAXS experiments, indicated a small lamellar structure for all the PLA/AS blends. The highest amorphous phase thickness was observed for the PLA/DS1.5 blend which supports the presence of significant interfacial interactions in this blend.

# 8. Conclusions and Recommendations

## 8.1. Conclusions

The objective of this PhD was to investigate the acetylation of starch as a means to improve its thermal processability and compatibility with PLA and ultimately widen the range of potential applications for PLA/acetylated starch (AS) blends. The work was divided in two parts: (1) the characterization of AS according to degree of the substitution (DS) and (2) the preparation and characterization of PLA/AS blends.

The analysis of the crystallinity of AS indicated that the substitution of hydroxyl groups with acetyl groups upon acetylation destroyed the native crystalline structure of starch and led to the emergence of a glass transition in AS with DS equal or greater than 1.5. The appearance of a transition from the glassy state to the rubbery state at the glass transition temperature ($T_g$) is desirable as this is a requirement for the thermal processability of AS. The fully substituted AS (DS3) showed the emergence of a new crystalline structure which increased its $T_g$ and a new thermal transition (melting) before degradation. The enhancement of the thermal stability and decrease of the molecular weight upon acetylation for all DS were also observed and should improve the thermal processability of AS. The polar contribution of the surface energy decreased as a result of acetylation of the hydroxyl groups of starch for all DS. Increasing thermal expansion coefficient along with the decrease of density with increasing DS of AS, make starch a more similar material to PLA. Based on its evolution with temperature, the relaxation time for hole formation estimated from Quasi-isothermal TMDSC heat capacity data was found to be an appropriate representation of the $\alpha$-relaxation time near the glass transition temperature region. Together with the VFT model, the relaxation time for hole formation, were used to estimate the $T_g$ and the fragility index (m). I DS of AS indicated that higher DS is more suitable for thermal processing.

The second part of the thesis, which focused on the preparation and characterization of PLA/AS blends, resulted in a number of significant observations. The morphology of all PLA/AS blends was biphasic, except for PLA/DS3 which was uniform, based on the predictions obtained with the compressible regular solution (CRS) model and confirmed experimentally by SEM imaging. The thickness of the interphase for the biphasic blends increased with increasing DS, based on the

theoretical approach developed by Helfand et al. [41-43] and confirmed by SAXS measurements. The length scale of the dynamic heterogeneity of the blends estimated by TMDSC showed similar relationship with DS as observed for the interphase thickness estimates. The vitrification of the PLA chains in the interphase region deduced from TMDSC data was identified for two blends, PLA/DS0 and PLA/DS0.5, and was attributed to the hydrogen bonding of the PLA chains with AS based on FTIR analysis. The thermal stability of PLA in PLA/AS blends was enhanced by the presence of AS. The PLA/DS2.5 blend showed the highest thermal stability.

The effect of the degree of acetylation and the resulting blend morphology and interphase thickness on the mechanical and water transport was investigated. Three blends with distinct characteristics, PLA/DS0 with unsubstituted starch, PLA/DS2.5 with the thickest interphase and PLA/DS3 as a miscible blend were selected. The absence of acetylation in the PLA/DS0 blend and the absence of biphasic structure in the PLA/DS3 blend did not lead to improved mechanical performance. The PLA/DS2.5 blend, with a biphasic structure and large interphase thickness, displayed the best mechanical performance. The diffused interphase may have assisted in facilitating the transfer of the tension from the PLA matrix to the DS2.5 dispersed phase avoiding crack initiation from the interface. The PLA/DS2.5 blend also had the lowest water diffusion coefficient which may be explained by the contributions of the biphasic morphology and the diffused interphase in creating a tortuous path for the movement of the water molecules.

The crystallization of PLA in PLA/AS blends was investigated for isothermal and non-isothermal crystallization conditions. The PLA/DS0.5 blend showed the highest rate of crystallization while PLA/DS1.5 blend had the slowest rate of crystallization for isothermal conditions. The highest rate of crystallization of the PLA/DS0.5 blend may be attributed to the high degree of crystallinity of DS0.5 and effective interfacial interactions. The slow rate of crystallization for the PLA/DS1.5 blend may be related to the dynamic slowdown of the PLA chains in the interphase region. The investigation of crystallization under non-isothermal conditions revealed differences in the rate of crystallization according to cooling rate. At the lowest cooling rate, of $2°C$/min, the rate of crystallization was relatively similar for all blends. At higher cooling rate, $5°C$/min, the PLA/DS1.5 blend showed the fastest rate of crystallization. Two factors could explain the distinct rate of crystallization of the PLA/DS1.5 blend. The first factor is the positive value of the estimated activation energy for the crystallization of the PLA/DS1.5 blend which could reflect an

endothermic process associated with the breakage of the hydrogen bonds of PLA chains with AS. The second factor is the highest thickness of the amorphous phase in lamellar structure, deduced by SAXS, of the PLA/DS1.5 blend which could reflect the significance of the interfacial interactions in this blend.

Finally, results of this study showed that the acetylation of starch is a promising avenue for PLA/starch blends. Increasing the processability of starch and its compatibility with PLA through acetylation, provides the opportunity of making a wide range of materials with different applications. Various mechanical, thermal, and water transport properties, transparency and crystallization behavior can be achieved by incorporating AS with different DS into PLA.

## 8.2. Summary of Contribution

In this work a multi scale investigation of important factors in the processability of AS and the properties of PLA/AS blends as new materials was presented. More specific contributions are listed below:

Investigation of the effect of DS of AS on the chain dynamics and molecular mobility at moderate temperature and ambient temperature conditions was completed. The concepts and techniques which were developed for synthetic polymers were employed to evaluate the chain dynamics of AS, a biopolymer, for the first time in the literature. Effect of temperature on hydrogen bonding and crystallization as the most influential parameters on the dynamic behavior is investigated.

Evaluation of the properties of the interphase (thickness and chain dynamics) of the PLA/AS blends as one the most determinant factors of blend properties was conducted. A combination of methods and techniques developed for synthetic polymer blends and nanocomposite were utilized to study the interphase of PLA/AS blends for the first time in the literature. In an attempt to better understand the nature of changes in interphase properties, physical interactions between components were also investigated.

Investigation of the isothermal and non-isothermal crystallization behavior of the PLA/AS blends. To the best our knowledge, the employment of the interphase properties in to explain isothermal and non-isothermal crystallization experiments on the PLA/AS blends was done for the first time in the literature. Lamellar crystalline structure of the blends was also investigated for better

understanding of the effect of interactions between PLA and AS on crystallization of the PLA/AS blends.

## 8.3. Recommendations

The results presented in this study lead to the following recommendations for future work. These recommendations are presented along two avenues, PLA/AS blend preparation and PLA/AS blend characterization.

### 8.3.1. Blend Preparation

#### 8.3.1.1. Blending Preformed AS Particles with PLA

Size distribution of the dispersed phase in a blend and differences of the size of the dispersed phase among the blends, add complexity to the investigation of the interface attribute to the final properties of the blends. Preforming AS particles and adding them to the PLA matrix would provide a means to obtain more uniform interface for all the blends which eventually would facilitate the investigation of the interface. Solvent/non-solvent method could be used to prepare AS particles. A small amount of a crosslinking agent could be used to make a loosely cross-linked structure and preserve the shape of the particle during the melt blending. The size of the particles could be controlled by changing the solvent/non-solvent ratio. The effect of the size of the particles on the interphase properties can be investigated as well.

#### 8.3.1.2. Investigation of the Effect of AS Concentration on Properties of PLA/AS Blends

The concentration of the AS dispersed phase in PLA/AS blends should lead to differences in morphology, interfacial characteristics and ultimately properties of the blend.

### 8.3.2. Blend Characterization

#### 8.3.2.1. Investigation of Interfacial Properties by Dielectric Spectroscopy

Dielectric spectroscopy can be used to investigate the chain dynamics in the interphase region. By direct measurement of the relaxation time of the chains in the interphase region, more comprehensive understanding of interfacial interactions is possible. However, making a good

sample and finding the appropriate experimental conditions (frequency of electric field oscillation and temperature) are challenges in using this technique.

#### 8.3.2.2. Study of Crystallization Using Cross Polarized Microscope Equipped With a Hot Plate

A cross polarized microscope provides the opportunity of direct measurement of crystal growth rate which can be used to provide more insights about the crystallization of PLA at the presence of AS. For instance, by investigation of crystal growth rate using Lauritzen–Hoffman theory, better understanding of interactions involved in conformational change of chain and chain folding during the crystallization can be achieved.

#### 8.3.2.3. Study of Transparency and Degradation Rate of PLA/AS Blends

Transparency, visual appearance and degradation rate of the PLA/AS blends are also very important factors in final applications that need to be investigated in the future.

# References


1. Mose, B.R. and S.M. Maranga, *A review on starch based nanocomposites for bioplastic materials.* Journal of Materials Science and Engineering B, 2011. **1**(2): p. 239-245.

2. Pimentel, T.P.F., et al., *Preparation and characterization of blends of recycled polystyrene with cassava starch.* Journal of Materials Science, 2007. **42**(17): p. 7530-7536.

3. Schlemmer, D., E. de Oliveira, and M. Araújo Sales, *Polystyrene/thermoplastic starch blends with different plasticizers: Preparation and thermal characterization.* Journal of Thermal Analysis and Calorimetry, 2007. **87**(3): p. 635-638.

4. Nasseri, R. and N. Mohammadi, *Starch-based nanocomposites: A comparative performance study of cellulose whiskers and starch nanoparticles.* Carbohydrate Polymers, 2014. **106**: p. 432-439.

5. Ferri, J.M., et al., *The effect of maleinized linseed oil (MLO) on mechanical performance of poly(lactic acid)-thermoplastic starch (PLA-TPS) blends.* Carbohydrate Polymers, 2016. **147**: p. 60-68.

6. Zuo, Y., et al., *Preparation and characterization of dry method esterified starch/polylactic acid composite materials.* International Journal of Biological Macromolecules, 2014. **64**: p. 174-180.

7. Wang, C., et al., *Effect of reaction conditions on grafting ratio and properties of starch nanocrystals-g-polystyrene.* Journal of applied polymer science, 2014. **131**(15): p. n/a-n/a.

8. Orford, P.D., et al., *Effect of water as a diluent on the glass transition behaviour of malto-oligosaccharides, amylose and amylopectin.* International journal of biological macromolecules, 1989. **11**(2): p. 91-96.

9. Ashogbon, A.O. and E.T. Akintayo, *Recent trend in the physical and chemical modification of starches from different botanical sources: A review.* Starch - Stärke, 2014. **66**(1-2): p. 41-57.

10. Fringant, C., J. Desbrières, and M. Rinaudo, *Physical properties of acetylated starch-based materials: Relation with their molecular characteristics.* Polymer, 1996. **37**(13): p. 2663-2673.

11. Auras, R., B. Harte, and S. Selke, *An Overview of Polylactides as Packaging Materials.* Macromolecular Bioscience, 2004. **4**(9): p. 835-864.

12. Garlotta, D., *A Literature Review of Poly(Lactic Acid).* Journal of Polymers and the Environment, 2001. **9**(2): p. 63-84.

13. Saeidlou, S., et al., *Poly(lactic acid) crystallization.* Progress in Polymer Science, 2012. **37**(12): p. 1657-1677.

14. Lim, L.T., R. Auras, and M. Rubino, *Processing technologies for poly(lactic acid).* Progress in Polymer Science, 2008. **33**(8): p. 820-852.

15. Kawai, T., et al., *Crystallization and Melting Behavior of Poly (l-lactic Acid).* Macromolecules, 2007. **40**(26): p. 9463-9469.

16. Le Corre, D., J. Bras, and A. Dufresne, *Starch nanoparticles: a review.* Biomacromolecules, 2010. **11**(5): p. 1139-1153.

17. Buléon, A., et al., *Starch granules: structure and biosynthesis.* International Journal of Biological Macromolecules, 1998. **23**(2): p. 85-112.

18. Pérez, S. and E. Bertoft, *The molecular structures of starch components and their contribution to the architecture of starch granules: A comprehensive review.* Starch - Stärke, 2010. **62**(8): p. 389-420.

19. Nasseri, R. and N. Mohammadi, *Starch-based nanocomposites: A comparative performance study of cellulose whiskers and starch nanoparticles.* Carbohydrate Polymers, 2014. **106**(0): p. 432-439.

20. Huneault, M.A. and H. Li, *Morphology and properties of compatibilized polylactide/thermoplastic starch blends.* Polymer, 2007. **48**(1): p. 270-280.

21. Li, H. and M.A. Huneault, *Comparison of sorbitol and glycerol as plasticizers for thermoplastic starch in TPS/PLA blends.* Journal of Applied Polymer Science, 2011. **119**(4): p. 2439-2448.

22. Zhang, Y., et al., *The Effect of Polymeric Chain Extenders on Physical Properties of Thermoplastic Starch and Polylactic Acid Blends.* Journal of Polymers and the Environment, 2012. **20**(2): p. 315-325.

23. Wang, N., et al., *Influence of formamide and water on the properties of thermoplastic starch/poly(lactic acid) blends.* Carbohydrate Polymers, 2008. **71**(1): p. 109-118.

24. Yokesahachart, C. and R. Yoksan, *Effect of amphiphilic molecules on characteristics and tensile properties of thermoplastic starch and its blends with poly(lactic acid).* Carbohydrate Polymers, 2011. **83**(1): p. 22-31.

25. Zhang, J.-F. and X. Sun, *Mechanical Properties of Poly(lactic acid)/Starch Composites Compatibilized by Maleic Anhydride.* Biomacromolecules, 2004. **5**(4): p. 1446-1451.

26. Xiong, Z., et al., *Preparation and characterization of poly(lactic acid)/starch composites toughened with epoxidized soybean oil.* Carbohydrate Polymers, 2013. **92**(1): p. 810-816.

27. Xiong, Z., et al., *The properties of poly(lactic acid)/starch blends with a functionalized plant oil: Tung oil anhydride.* Carbohydrate Polymers, 2013. **95**(1): p. 77-84.

28. Jariyasakoolroj, P. and S. Chirachanchai, *Silane modified starch for compatible reactive blend with poly(lactic acid).* Carbohydrate Polymers, 2014. **106**: p. 255-263.

29. Wokadala, O.C., N.M. Emmambux, and S.S. Ray, *Inducing PLA/starch compatibility through butyl-etherification of waxy and high amylose starch.* Carbohydrate Polymers, 2014. **112**: p. 216-224.

30. Li, S., et al., *Preparation and characterization of acorn starch/poly(lactic acid) composites modified with functionalized vegetable oil derivates.* Carbohydrate Polymers, 2016. **142**: p. 250-258.

31. Halal, S.L.M.E., et al., *Structure, morphology and functionality of acetylated and oxidised barley starches.* Food chemistry, 2015. **168**: p. 247-256.

32. Ačkar, Đ., et al., *Starch modification by organic acids and their derivatives: A Review.* Molecules, 2015. **20**(10): p. 19554-19570.

33. Dicke, R., *A straight way to regioselectively functionalized polysaccharide esters.* Cellulose, 2004. **11**(2): p. 255-263.

34. Farinha, J.P.S., O. Vorobyova, and M.A. Winnik, *An Energy Tranfer Study of the Interface Thickness in Blends of Poly(butyl methacrylate) and Poly(2-ethylhexyl methacrylate).* Macromolecules, 2000. **33**(16): p. 5863-5873.

35. Virgilio, N., et al., *High Contrast Imaging of Interphases in Ternary Polymer Blends Using Focused Ion Beam Preparation and Atomic Force Microscopy.* Macromolecules, 2005. **38**(6): p. 2368-2375.

36. Cheng, S., et al., *Interfacial Properties of Polymer Nanocomposites: Role of Chain Rigidity and Dynamic Heterogeneity Length Scale.* Macromolecules, 2017. **50**(6): p. 2397-2406.

37. Pukánszky, B., *Interfaces and interphases in multicomponent materials: past, present, future.* European Polymer Journal, 2005. **41**(4): p. 645-662.

38. Liang, Y.-Y., et al., *Role of surface chemical groups on carbon nanotubes in nucleation for polymer crystallization: Interfacial interaction and steric effect.* Polymer, 2013. **54**(23): p. 6479-6488.

39. Helfand, E. and Y. Tagami, *Theory of the Interface between Immiscible Polymers. II.* The Journal of chemical physics, 1972. **56**(7): p. 3592-3601.

40. Helfand, E. and Y. Tagami, *Theory of the Interface Between Immiscible Polymers.* The Journal of chemical physics, 1972. **57**(4): p. 1812-1813.

41. Helfand, E., *Theory of inhomogeneous polymers: Fundamentals of the Gaussian random-walk model.* The Journal of chemical physics, 1975. **62**(3): p. 999-1005.

42. Helfand, E. and A.M. Sapse, *Theory of unsymmetric polymer–polymer interfaces.* The Journal of chemical physics, 1975. **62**(4): p. 1327-1331.

43. Helfand, E., *Theory of inhomogeneous polymers: Lattice model for polymer–polymer interfaces.* The Journal of chemical physics, 1975. **63**(5): p. 2192-2198.

44. Yokoyama, H. and E.J. Kramer, *Mutual Diffusion of Asymmetric Block Copolymers with Homopolymers.* Macromolecules, 2000. **33**(5): p. 1871-1877.

45. Rharbi, Y. and M.A. Winnik, *Interface Thickness of a Styrene−Methyl Methacrylate Block Copolymer in the Lamella Phase by Direct Nonradiative Energy Transfer.* Macromolecules, 2001. **34**(15): p. 5238-5248.

46. Kawaguchi, D., et al., *Precise Analyses of Short-Time Relaxation at Asymmetric Polystyrene Interface in Terms of Molecular Weight by Time-Resolved Neutron Reflectivity Measurements.* Macromolecules, 2011. **44**(23): p. 9424-9433.

47. Schnell, R., M. Stamm, and C. Creton, *Direct Correlation between Interfacial Width and Adhesion in Glassy Polymers.* Macromolecules, 1998. **31**(7): p. 2284-2292.

48. Klein, J., *The Interdiffision of Polymers.* Science, 1990. **250**(4981): p. 640-646.

49. Zhang, H., K. Lamnawar, and A. Maazouz, *Rheological Modeling of the Mutual Diffusion and the Interphase Development for an Asymmetrical Bilayer Based on PMMA and PVDF Model Compatible Polymers.* Macromolecules, 2013. **46**(1): p. 276-299.

50. Perrin, P. and R.E. Prud'homme, *SAXS Measurements of Interfacial Thickness in Amorphous Polymer Blends Containing a Diblock Copolymer.* Macromolecules, 1994. **27**(7): p. 1852-1860.

51. Edwards, S.A., et al., *Probing the interface behaviour of injection molded thermoplastics by micro-thermal analysis and temperature-modulated differential scanning calorimetry.* Polymer, 2003. **44**(13): p. 3661-3670.

52. Roe, R.-J., *Methods of X-ray and neutron scattering in polymer science*. Vol. 739. 2000: Oxford University Press on Demand.

53. Donth, E., *The size of cooperatively rearranging regions at the glass transition.* Journal of Non-Crystalline Solids, 1982. **53**(3): p. 325-330.

54. Berruezo, M., et al., *Preparation and characterization of polystyrene/starch blends for packaging applications.* Journal of Plastic Film and Sheeting, 2014. **30**(2): p. 141-161.

55. Rahmat, A.R., et al., *Approaches to improve compatibility of starch filled polymer system: A review.* Materials Science and Engineering: C, 2009. **29**(8): p. 2370-2377.

56. Park, J.W., et al., *Biodegradable polymer blends of poly(L-lactic acid) and gelatinized starch.* Polymer Engineering & Science, 2000. **40**(12): p. 2539-2550.

57. Zhou, L., et al., *Toughening polylactide with polyether-block-amide and thermoplastic starch acetate: Influence of starch esterification degree.* Carbohydrate Polymers, 2015. **127**: p. 79-85.

58. Zeng, S., et al., *Preparation and properties of biodegradable blend containing poly (propylene carbonate) and starch acetate with different degrees of substitution.* Carbohydrate Polymers, 2011. **86**(3): p. 1260-1265.

59. Mahmood, T., M.A. Turner, and F.L. Stoddard, *Comparison of Methods for Colorimetric Amylose Determination in Cereal Grains.* Starch - Stärke, 2007. **59**(8): p. 357-365.

60. Shogren, R.L. and A. Biswas, *Acetylation of starch with vinyl acetate in imidazolium ionic liquids and characterization of acetate distribution.* Carbohydrate Polymers, 2010. **81**(1): p. 149-151.

61. Nara, S. and T. Komiya, *Studies on the Relationship Between Water-satured State and Crystallinity by the Diffraction Method for Moistened Potato Starch.* Starch - Stärke, 1983. **35**(12): p. 407-410.

62. Kozicki, W. and P. Kuang, *An alternative method for evaluation of intrinsic viscosity.* The Canadian Journal of Chemical Engineering, 1996. **74**(3): p. 429-432.

63. Salemis, P. and M. Rinaudo, *Molecular weight-viscosity relationship for amylopectin, a highly branched polymer.* Polymer Bulletin, 1984. **12**(4): p. 283-285.

64. Cowie, J.M.G., *Studies on amylose and its derivatives. Part I. Molecular size and configuration of amylose molecules in various solvents.* Die Makromolekulare Chemie, 1960. **42**(1): p. 230-247.

65. Guettler, B.E., C. Moresoli, and L.C. Simon, *Contact angle and surface energy analysis of soy materials subjected to potassium permanganate and autoclave treatment.* Industrial Crops and Products, 2013. **50**: p. 219-226.

66. Van Oss, C.J., *Interfacial forces in aqueous media*2006: CRC press.

67. Neumann, A.W., R. David, and Y. Zuo, *Applied surface thermodynamics*. Vol. 151. 2010: CRC Press.

68. Owens, D.K. and R.C. Wendt, *Estimation of the surface free energy of polymers.* Journal of applied polymer science, 1969. **13**(8): p. 1741-1747.

69. Craig, R.E., *Determination of the density of crystalline solids in the undergraduate laboratory.* Journal of Chemical Education, 1989. **66**(7): p. 599.

70. Chi, H., et al., *Effect of acetylation on the properties of corn starch.* Food Chemistry, 2008. **106**(3): p. 923-928.

71. Tupa, M., et al., *Simple organocatalytic route for the synthesis of starch esters.* Carbohydrate Polymers, 2013. **98**(1): p. 349-357.

72. Luo, Z.-G. and Y.-C. Shi, *Preparation of Acetylated Waxy, Normal, and High-Amylose Maize Starches with Intermediate Degrees of Substitution in Aqueous Solution and Their Properties.* Journal of Agricultural and Food Chemistry, 2012. **60**(37): p. 9468-9475.

73. Zhang, L., et al., *Study on the morphology, crystalline structure and thermal properties of yellow ginger starch acetates with different degrees of substitution.* Thermochimica Acta, 2009. **495**(1–2): p. 57-62.

74. Pu, H., et al., *An Oral Colon-Targeting Controlled Release System Based on Resistant Starch Acetate: Synthetization, Characterization, and Preparation of Film-Coating Pellets.* Journal of Agricultural and Food Chemistry, 2011. **59**(10): p. 5738-5745.

75. Rundle, R.E., J.F. Foster, and R.R. Baldwin, *On the Nature of the Starch—Iodine Complex1*. Journal of the American Chemical Society, 1944. **66**(12): p. 2116-2120.

76. Saenger, W., *The structure of the blue starch-iodine complex.* Naturwissenschaften. **71**(1): p. 31-36.

77. Teitelbaum, R.C., S.L. Ruby, and T.J. Marks, *On the structure of starch-iodine.* Journal of the American Chemical Society, 1978. **100**(10): p. 3215-3217.

78. Shogren, R.L., *Preparation, thermal properties, and extrusion of high-amylose starch acetates.* Carbohydrate Polymers, 1996. **29**(1): p. 57-62.

79. Wang, X., et al., *Study on the morphology, crystalline structure and thermal properties of yam starch acetates with different degrees of substitution.* Science in China Series B: Chemistry, 2008. **51**(9): p. 859-865.

80. Zhu, J.-f., G.-h. Zhang, and Z.-c. Lai, *Synthesis and characterization of maize starch acetates and its biodegradable film.* Polymer-Plastics Technology and Engineering, 2007. **46**(12): p. 1135-1141.

81. Holt, A.P., et al., *Dynamics at the Polymer/Nanoparticle Interface in Poly(2-vinylpyridine)/Silica Nanocomposites.* Macromolecules, 2014. **47**(5): p. 1837-1843.

82. Sperling, L.H., *Introduction to physical polymer science*2015: John Wiley & Sons.

83. Volkert, B., et al., *A comparison of different synthesis routes for starch acetates and the resulting mechanical properties.* Carbohydrate Polymers, 2010. **79**(3): p. 571-577.

84. Bello-Pérez, L.A., et al., *Effect of low and high acetylation degree in the morphological, physicochemical and structural characteristics of barley starch.* LWT - Food Science and Technology, 2010. **43**(9): p. 1434-1440.

85. Granza, A., et al., *Effects of acetylation and acetylation–hydroxypropylation (dual-modification) on the properties of starch from Carioca bean (Phaseolus vulgaris L.).* Journal of Thermal Analysis and Calorimetry, 2015. **119**(1): p. 769-777.

86. Tupa, M.V., et al., *Organocatalytic acetylation of starch: Effect of reaction conditions on DS and characterisation of esterified granules.* Food Chemistry, 2015. **170**: p. 295-302.

87. Liu, X., et al., *Kinetics and mechanism of thermal decomposition of cornstarches with different amylose/amylopectin ratios.* Starch - Stärke, 2010. **62**(3-4): p. 139-146.

88. Elomaa, M., et al., *Determination of the degree of substitution of acetylated starch by hydrolysis, 1H NMR and TGA/IR.* Carbohydrate Polymers, 2004. **57**(3): p. 261-267.

89. Marmur, A., *Soft contact: measurement and interpretation of contact angles.* Soft Matter, 2006. **2**(1): p. 12-17.

90. Xu, Y., et al., *Preparation and characterization of organic-soluble acetylated starch nanocrystals.* Carbohydrate Polymers, 2010. **80**(4): p. 1078-1084.

91. Biresaw, G. and C.J. Carriere, *Interfacial tension of poly(lactic acid)/polystyrene blends.* Journal of Polymer Science Part B: Polymer Physics, 2002. **40**(19): p. 2248-2258.

92. Sumita, M., et al., *Dispersion of fillers and the electrical conductivity of polymer blends filled with carbon black.* Polymer bulletin, 1991. **25**(2): p. 265-271.

93. Moynihan, C.T., et al., *Dependence of the glass transition temperature on heating and cooling rate.* The Journal of Physical Chemistry, 1974. **78**(26): p. 2673-2677.

94. Mohanty, A.K., M. Misra, and L.T. Drzal, *Natural fibers, biopolymers, and biocomposites*2005: CRC press.

95. Nasseri, R. and N. Mohammadi, *Modeling of starch retrogradation onset in its aqueous solution using thermoreversible gelation concept.* Carbohydrate Polymers, 2014. **99**: p. 325-330.

96. Van Soest, J.J.G. and N. Knooren, *Influence of glycerol and water content on the structure and properties of extruded starch plastic sheets during aging.* Journal of applied polymer science, 1997. **64**(7): p. 1411-1422.

97. Betancur, A.D., G.L. Chel, and H.E. Cañizares, *Acetylation and Characterization of Canavalia ensiformis Starch.* Journal of Agricultural and Food Chemistry, 1997. **45**(2): p. 378-382.

98. deAzevedo, E.R., et al., *Centerband-Only Detection of Exchange: Efficient Analysis of Dynamics in Solids by NMR.* Journal of the American Chemical Society, 1999. **121**(36): p. 8411-8412.

99. Karayiannis, N.C., V.G. Mavrantzas, and D.N. Theodorou, *Detailed Atomistic Simulation of the Segmental Dynamics and Barrier Properties of Amorphous Poly(ethylene terephthalate) and Poly(ethylene isophthalate).* Macromolecules, 2004. **37**(8): p. 2978-2995.

100. Choudhury, R.P., et al., *Chain Dynamics in Antiplasticized and Annealed Poly(ethylene terephthalate) Determined by Solid-State NMR and Correlated with Enhanced Barrier Properties.* Macromolecules, 2012. **45**(2): p. 879-887.

101. Schaefer, J., E.O. Stejskal, and R. Buchdahl, *Magic-Angle 13C NMR Analysis of Motion in Solid Glassy Polymers.* Macromolecules, 1977. **10**(2): p. 384-405.

102. Eyring, H., *Viscosity, Plasticity, and Diffusion as Examples of Absolute Reaction Rates.* The Journal of Chemical Physics, 1936. **4**(4): p. 283-291.

103. Boller, A., C. Schick, and B. Wunderlich, *Modulated differential scanning calorimetry in the glass transition region.* Thermochimica Acta, 1995. **266**: p. 97-111.

104. Wunderlich, B., et al., *Modulated differential scanning calorimetry in the glass transition region: II. The mathematical treatment of the kinetics of the glass transition.* Journal of Thermal Analysis and Calorimetry, 1996. **47**(4): p. 1013-1026.

105. Boller, A., I. Okazaki, and B. Wunderlich, *Modulated differential scanning calorimetry in the glass transition region. Part III. Evaluation of polystyrene and poly (ethylene tetrephthalate).* Thermochimica Acta, 1996. **284**(1): p. 1-19.

106. Okazaki, I. and B. Wunderlich, *Modulated differential scanning calorimetry in the glass transition region. V. Activation energies and relaxation times of poly(ethylene terephthalate)s.* Journal of Polymer Science Part B: Polymer Physics, 1996. **34**(17): p. 2941-2952.

107. Wunderlich, B. and I. Okazaki, *Modulated differential scanning calorimetry in the glass transition region.* Journal of thermal analysis, 1997. **49**(1): p. 57-70.

108. Thomas, L.C., et al., *Modulated differential scanning calorimetry in the glass transition region, IV. Pseudo-isothermal analysis of the polystyrene glass transition.* Thermochimica Acta, 1997. **291**(1): p. 85-94.

109. Montina, T., P. Wormald, and P. Hazendonk, *13C Solid-State NMR of the Mobile Phase of Poly(vinylidene fluoride).* Macromolecules, 2012. **45**(15): p. 6002-6007.

110. Choudhury, R.P., et al., *Chain dynamics in antiplasticized and annealed poly (ethylene terephthalate) determined by solid-state NMR and correlated with enhanced barrier properties.* Macromolecules, 2012. **45**(2): p. 879-887.

111. Schäler, K., et al., *Dynamics in Crystallites of Poly(ε-caprolactone) As Investigated by Solid-State NMR.* Macromolecules, 2013. **46**(19): p. 7818-7825.

112. Nambiar, R.R. and F.D. Blum, *Segmental Dynamics of Bulk Poly(vinyl acetate)-d3 by Solid-State 2H NMR: Effect of Small Molecule Plasticizer.* Macromolecules, 2008. **41**(24): p. 9837-9845.

113. Garbow, J.R., J. Goetz, and J. Asrar, *Polymers of Methyl-Substituted N-Phenylnorbornene-5,6-dicarboximide: Characterization of Structure and Dynamics.* Macromolecules, 1998. **31**(12): p. 3925-3930.

114. Calucci, L., et al., *Structure and Dynamics of Flour by Solid State NMR: Effects of Hydration and Wheat Aging.* Biomacromolecules, 2004. **5**(4): p. 1536-1544.

115. Tang, H. and B.P. Hills, *Use of 13C MAS NMR to Study Domain Structure and Dynamics of Polysaccharides in the Native Starch Granules.* Biomacromolecules, 2003. **4**(5): p. 1269-1276.

116. Sefcik, M.D., et al., *Analysis of the Room-Temperature Molecular Motions of Poly(ethylene terephthalate).* Macromolecules, 1980. **13**(5): p. 1132-1137.

117. Weyer, S., A. Hensel, and C. Schick, *Temperature Modulated CalorimetryPhase angle correction for TMDSC in the glass-transition region.* Thermochimica Acta, 1997. **304**: p. 267-275.

118. Slichter, C.P., *Principles of magnetic resonance*. Vol. 1. 2013: Springer Science & Business Media.

119. Vogel, H., *The law of the relation between the viscosity of liquids and the temperature.* Phys. Z, 1921. **22**: p. 645-646.

120. Fulcher, G.S., *ANALYSIS OF RECENT MEASUREMENTS OF THE VISCOSITY OF GLASSES.* Journal of the American Ceramic Society, 1925. **8**(6): p. 339-355.

121. Tammann, G. and W. Hesse, *Die Abhängigkeit der Viscosität von der Temperatur bie unterkühlten Flüssigkeiten.* Zeitschrift für anorganische und allgemeine Chemie, 1926. **156**(1): p. 245-257.

122. Angell, C.A., *Perspective on the glass transition.* Journal of Physics and Chemistry of Solids, 1988. **49**(8): p. 863-871.

123. Agapov, A.L., et al., *Effect of Polar Interactions on Polymer Dynamics.* Macromolecules, 2012. **45**(20): p. 8430-8437.

124. Delpouve, N., et al., *Structural Dependence of the Molecular Mobility in the Amorphous Fractions of Polylactide.* Macromolecules, 2014. **47**(15): p. 5186-5197.

125. Bouthegourd, E., et al., *Size of the cooperative rearranging regions vs. fragility in complex glassy systems: Influence of the structure and the molecular interactions.* Physica B: Condensed Matter, 2013. **425**: p. 83-89.

126. Angell, C.A., *Spectroscopy simulation and scattering, and the medium range order problem in glass.* Journal of Non-Crystalline Solids, 1985. **73**(1–3): p. 1-17.

127. Angell, C.A., *Formation of Glasses from Liquids and Biopolymers.* Science, 1995. **267**(5206): p. 1924-1935.

128. Böhmer, R., et al., *Nonexponential relaxations in strong and fragile glass formers.* The Journal of Chemical Physics, 1993. **99**(5): p. 4201-4209.

129. Rijal, B., L. Delbreilh, and A. Saiter, *Dynamic Heterogeneity and Cooperative Length Scale at Dynamic Glass Transition in Glass Forming Liquids.* Macromolecules, 2015. **48**(22): p. 8219-8231.

130. Evans, C.M., et al., *Fragility is a Key Parameter in Determining the Magnitude of Tg-Confinement Effects in Polymer Films.* Macromolecules, 2013. **46**(15): p. 6091-6103.

131. Kunal, K., et al., *Role of Chemical Structure in Fragility of Polymers: A Qualitative Picture.* Macromolecules, 2008. **41**(19): p. 7232-7238.

132. Grigoras, C.V. and A.G. Grigoras, *Nanoscale cooperativity on a series of statistical methacrylates copolymers with electron donor–acceptor pendant groups.* Journal of Thermal Analysis and Calorimetry, 2011. **103**(2): p. 661-668.

133. Nakanishi, M. and R. Nozaki, *Model of the cooperative rearranging region for polyhydric alcohols.* Physical Review E, 2011. **84**(1): p. 011503.

134. Arabeche, K., et al., *Study of the cooperativity at the glass transition temperature in PC/PMMA multilayered films: Influence of thickness reduction from macro- to nanoscale.* Polymer, 2012. **53**(6): p. 1355-1361.

135. Matsuoka, S. and X. Quan, *A model for intermolecular cooperativity in conformational relaxations near the glass transition.* Macromolecules, 1991. **24**(10): p. 2770-2779.

136. Adam, G. and J.H. Gibbs, *On the Temperature Dependence of Cooperative Relaxation Properties in Glass-Forming Liquids.* The Journal of Chemical Physics, 1965. **43**(1): p. 139-146.

137. Schmidtke, B., et al., *Temperature Dependence of the Segmental Relaxation Time of Polymers Revisited.* Macromolecules, 2015. **48**(9): p. 3005-3013.

138. Fringant, C., et al., *Preparation of mixed esters of starch or use of an external plasticizer: two different ways to change the properties of starch acetate films.* Carbohydrate Polymers, 1998. **35**(1): p. 97-106.

139. Schantz, S. and S.L. Maunu, *Temperature Dependence of Segmental Mobility in Poly(ethylene oxide) Complexed with Ba(ClO4)2: a Carbon-13 NMR Study.* Macromolecules, 1994. **27**(23): p. 6915-6921.

140. Koh, J.J., X. Zhang, and C. He, *Fully biodegradable Poly(lactic acid)/Starch blends: A review of toughening strategies.* International Journal of Biological Macromolecules, 2018. **109**: p. 99-113.

141. Vaidya, U.R. and M. Bhattacharya, *Properties of blends of starch and synthetic polymers containing anhydride groups.* Journal of Applied Polymer Science, 1994. **52**(5): p. 617-628.

142. Ke, T. and X.S. Sun, *Starch, Poly(lactic acid), and Poly(vinyl alcohol) Blends.* Journal of Polymers and the Environment, 2003. **11**(1): p. 7-14.

143. Sarazin, P., et al., *Binary and ternary blends of polylactide, polycaprolactone and thermoplastic starch.* Polymer, 2008. **49**(2): p. 599-609.

144. Kong, X., et al., *A Pseudo Equation-of-State Approach for the Estimation of Solubility Parameters of Polyethylene by Inverse Gas Chromatography.* Macromolecules, 2002. **35**(22): p. 8586-8590.

145. Ruzette, A.-V.G. and A.M. Mayes, *A Simple Free Energy Model for Weakly Interacting Polymer Blends.* Macromolecules, 2001. **34**(6): p. 1894-1907.

146. Agrawal, A., et al., *Constrained nonlinear optimization for solubility parameters of poly(lactic acid) and poly(glycolic acid)—validation and comparison.* Polymer, 2004. **45**(25): p. 8603-8612.

147. Cheng, B., et al., *Effects of stereo-regularity on the single-chain mechanics of polylactic acid and its implications on the physical properties of bulk materials.* Nanoscale, 2017. **9**(38): p. 14312-14316.

148. Nakanishi, Y., et al., *Conformation of amylose in dimethyl sulfoxide.* Macromolecules, 1993. **26**(16): p. 4220-4225.

149. Norisuye, T., *Viscosity Behavior and Conformation of Amylose in Various Solvents.* Polym J, 1994. **26**(11): p. 1303-1307.

150. Cheung, Y.W., et al., *Small-Angle Scattering Investigations of Poly(.epsilon.-caprolactone)/Polycarbonate Blends. 2. Small-Angle X-ray and Light Scattering Study of Semicrystalline/Semicrystalline and Semicrystalline/Amorphous Blend Morphologies.* Macromolecules, 1994. **27**(9): p. 2520-2528.

151. Vonk, C., *Investigation of non-ideal two-phase polymer structures by small-angle X-ray scattering.* Journal of Applied Crystallography, 1973. **6**(2): p. 81-86.

152. Ruland, W., *Small-angle scattering of two-phase systems: determination and significance of systematic deviations from Porod's law.* Journal of Applied Crystallography, 1971. **4**(1): p. 70-73.

153. Hanakata, P.Z., J.F. Douglas, and F.W. Starr, *Interfacial mobility scale determines the scale of collective motion and relaxation rate in polymer films.* Nature communications, 2014. **5**: p. 4163.

154. Stevenson, J.D. and P.G. Wolynes, *On the surface of glasses.* The Journal of chemical physics, 2008. **129**(23): p. 234514.

155. Higashida, N., et al., *Ellipsometric measurements of positive η parameters between dissimilar polymers and their temperature dependence.* Macromolecules, 1992. **25**(20): p. 5259-5262.

156. Sargsyan, A., et al., *The amount of immobilized polymer in PMMA SiO2 nanocomposites determined from calorimetric data.* European Polymer Journal, 2007. **43**(8): p. 3113-3127.

157. Katiyar, V. and H. Nanavati, *Ring-opening polymerization of L-lactide using N-heterocyclic molecules: mechanistic, kinetics and DFT studies.* Polymer Chemistry, 2010. **1**(9): p. 1491-1500.

158. Eklind, H., et al., *Characterization of the Interphase in PPO/PMMA Blends Compatibilized by P(S-g-EO).* Macromolecules, 1996. **29**(3): p. 984-992.

159. Espartero, J.L., et al., *NMR Analysis of Low Molecular Weight Poly(lactic acid)s.* Macromolecules, 1996. **29**(10): p. 3535-3539.

160. Battegazzore, D., J. Alongi, and A. Frache, *Poly (lactic acid)-based composites containing natural fillers: thermal, mechanical and barrier properties.* Journal of Polymers and the Environment, 2014. **22**(1): p. 88-98.

161. Iannace, S. and L. Nicolais, *Isothermal crystallization and chain mobility of poly(L-lactide).* Journal of Applied Polymer Science, 1997. **64**(5): p. 911-919.

162. Rogers, C. and J. Comyn, *Polymer permeability.* Elsevier, New York, 1985: p. 11-73.

163. Chow, W.S., Y.Y. Leu, and Z.A. Mohd Ishak, *Water Absorption of Poly(lactic acid) Nanocomposites: Effects of Nanofillers and Maleated Rubbers.* Polymer-Plastics Technology and Engineering, 2014. **53**(8): p. 858-863.

164. Jiang, X., et al., *Effects of hygrothermal aging on glass-fibre reinforced polymer laminates and adhesive of FRP composite bridge: Moisture diffusion characteristics.* Composites Part A: Applied Science and Manufacturing, 2014. **57**: p. 49-58.

165. Van Krevelen, D.W. and K. Te Nijenhuis, *Properties of polymers: their correlation with chemical structure; their numerical estimation and prediction from additive group contributions*2009: Elsevier.

166. Rubinstein, M. and R.H. Colby, *Polymer physics*2003: OUP Oxford.

167. Delaby, I., et al., *Droplet deformation in polymer blends during uniaxial elongational flow: Influence of viscosity ratio for large capillary numbers.* Journal of Rheology, 1994. **38**(6): p. 1705-1720.

168. Zhang, J., et al., *Disorder-to-Order Phase Transition and Multiple Melting Behavior of Poly(l-lactide) Investigated by Simultaneous Measurements of WAXD and DSC.* Macromolecules, 2008. **41**(4): p. 1352-1357.

169. Pukánszky, B. and E. Fekete, *Adhesion and Surface Modification*, in *Mineral Fillers in Thermoplastics I: Raw Materials and Processing*, J. Jancar, et al., Editors. 1999, Springer Berlin Heidelberg: Berlin, Heidelberg. p. 109-153.

170. Wittmann, J.C. and B. Lotz, *Epitaxial crystallization of polymers on organic and polymeric substrates.* Progress in Polymer Science, 1990. **15**(6): p. 909-948.

171. Sarikhani, K., et al., *Effect of well-dispersed surface-modified silica nanoparticles on crystallization behavior of poly (lactic acid) under compressed carbon dioxide.* Polymer, 2016. **98**: p. 100-109.

172. Ning, N., et al., *Realizing the enhancement of interfacial interaction in semicrystalline polymer/filler composites via interfacial crystallization.* Progress in Polymer Science, 2012. **37**(10): p. 1425-1455.

173. Choudalakis, G. and A.D. Gotsis, *Permeability of polymer/clay nanocomposites: A review.* European Polymer Journal, 2009. **45**(4): p. 967-984.

174. Comyn, J., *Polymer permeability*2012: Springer Science & Business Media.

175. Sperling, L.H., *Introduction to physical polymer science*2005: John Wiley & Sons.

176. Bussiere, P.O., et al., *Effect of ZnO nanofillers treated with triethoxy caprylylsilane on the isothermal and non-isothermal crystallization of poly(lactic acid).* Physical Chemistry Chemical Physics, 2012. **14**(35): p. 12301-12308.

177. Cai, J., et al., *Isothermal crystallization kinetics of thermoplastic starch/poly(lactic acid) composites.* Carbohydrate Polymers, 2011. **86**(2): p. 941-947.

178. Li, S., et al., *Parameters characterizing the kinetics of the nonisothermal crystallization of thermoplastic starch/poly(lactic acid) composites as determined by differential scanning calorimetry.* Journal of Applied Polymer Science, 2013. **129**(6): p. 3566-3573.

179. Solarski, S., M. Ferreira, and E. Devaux, *Characterization of the thermal properties of PLA fibers by modulated differential scanning calorimetry.* Polymer, 2005. **46**(25): p. 11187-11192.

180. Kim, M.S., J.C. Kim, and Y.H. Kim, *Effects of take-up speed on the structure and properties of melt-spun poly(L-lactic acid) fibers.* Polymers for Advanced Technologies, 2008. **19**(7): p. 748-755.

181. Wu, D., H. Xu, and M. Hakkarainen, *From starch to polylactide and nano-graphene oxide: fully starch derived high performance composites.* RSC Advances, 2016. **6**(59): p. 54336-54345.

182. Wokadala, O.C., et al., *Morphology, thermal properties and crystallization kinetics of ternary blends of the polylactide and starch biopolymers and nanoclay: The role of nanoclay hydrophobicity.* Polymer, 2015. **71**: p. 82-92.

183. Gumus, S., G. Ozkoc, and A. Aytac, *Plasticized and unplasticized PLA/organoclay nanocomposites: Short- and long-term thermal properties, morphology, and nonisothermal crystallization behavior.* Journal of Applied Polymer Science, 2012. **123**(5): p. 2837-2848.

184. Papageorgiou, G.Z., et al., *Crystallization kinetics and nucleation activity of filler in polypropylene/surface-treated SiO2 nanocomposites.* Thermochimica Acta, 2005. **427**(1): p. 117-128.

185. Wunderlich, B., *Macromolecular physics*. Vol. 2. 2012: Elsevier.

186. Jeziorny, A., *Parameters characterizing the kinetics of the non-isothermal crystallization of poly(ethylene terephthalate) determined by d.s.c.* Polymer, 1978. **19**(10): p. 1142-1144.

187. Durmus, A., et al., *Nonisothermal crystallization kinetics of poly(ethylene terephthalate)/clay nanocomposites prepared by melt processing.* Polymer Composites, 2010. **31**(6): p. 1056-1066.

188. Dobreva, A. and I. Gutzow, *Kinetics of Non-isothermal Overall Crystallization in Polymer Melts.* Crystal Research and Technology, 1991. **26**(7): p. 863-874.

189. Strobl, G.R. and M. Schneider, *Direct evaluation of the electron density correlation function of partially crystalline polymers.* Journal of Polymer Science: Polymer Physics Edition, 1980. **18**(6): p. 1343-1359.

190. Park, J.W. and S.S. Im, *Miscibility and morphology in blends of poly(l-lactic acid) and poly(vinyl acetate-co-vinyl alcohol).* Polymer, 2003. **44**(15): p. 4341-4354.

191. Merfeld, G.D., et al., *Interfacial thickness in bilayers of poly(phenylene oxide) and styrenic copolymers.* Journal of Polymer Science Part B: Polymer Physics, 1998. **36**(17): p. 3115-3125.

192. Song, M., et al., *Modulated differential scanning calorimetry: 8. Interface development between films of polyepichlorohydrin and poly(vinyl acetate).* Polymer, 1997. **38**(3): p. 503-507.

193. Zhang, H., K. Lamnawar, and A. Maazouz, *Rheological modeling of the mutual diffusion and the interphase development for an asymmetrical bilayer based on PMMA and PVDF model compatible polymers.* Macromolecules, 2012. **46**(1): p. 276-299.

# Appendix I

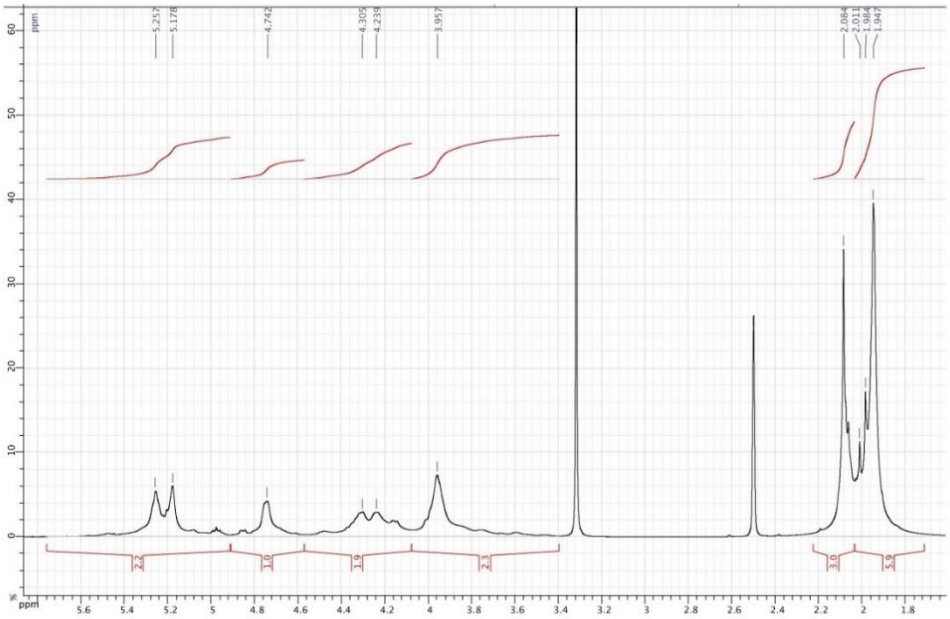

Figure I-1. $^{1}H$ NMR spectra of DS3.

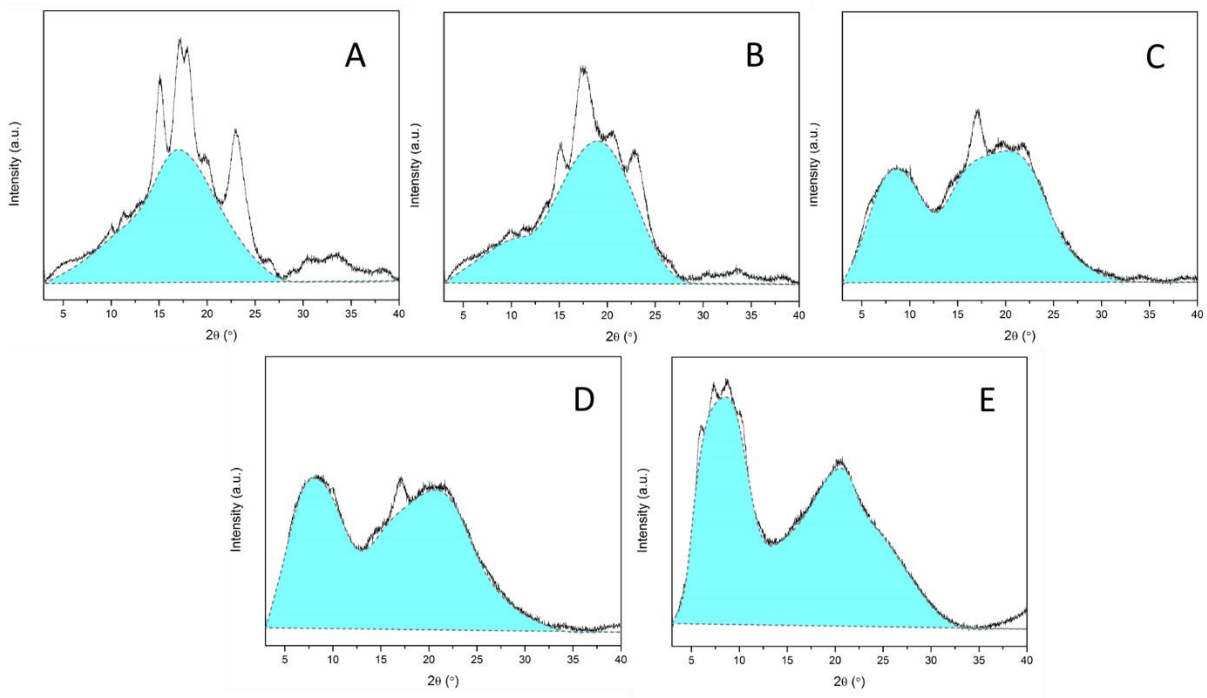


Figure 0I-2. Separation of the area under the diffractograms to crystalline and amorphous portions for acetylated starch (A) DS0, (B) DS0.5, (C) DS1.5, (D) DS2.5 and (E) DS3.

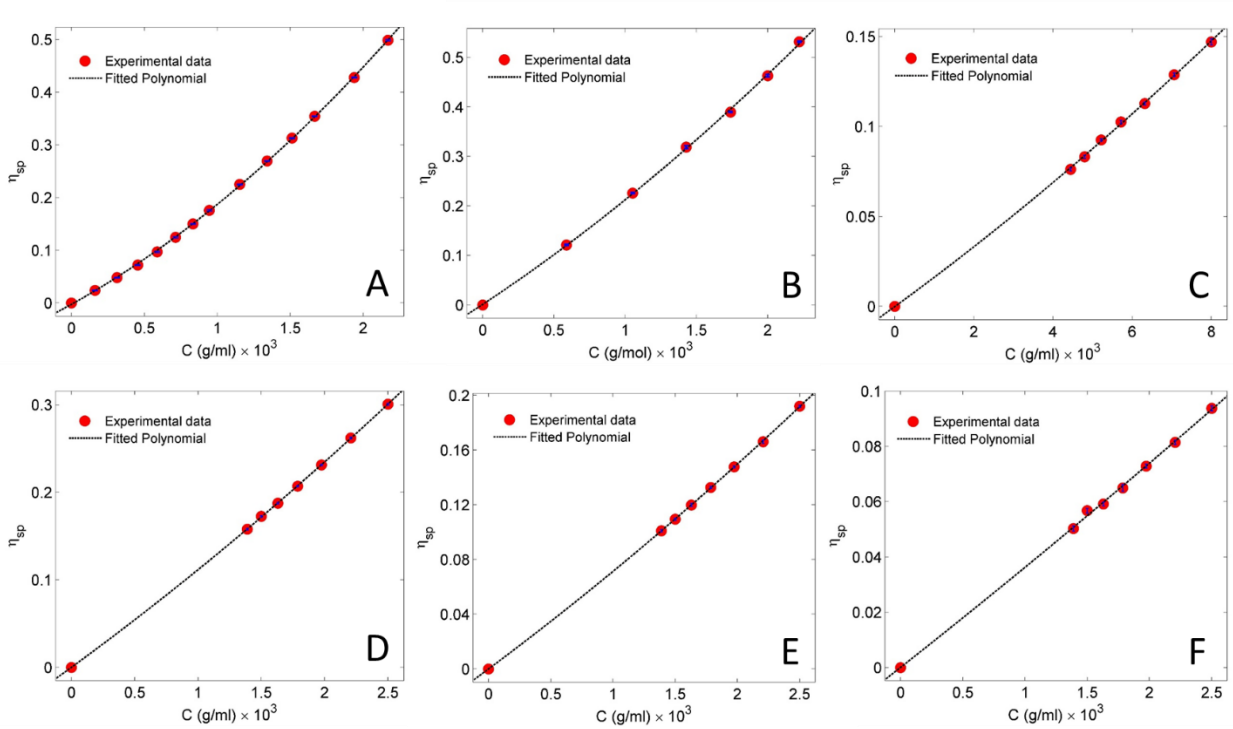


Figure I-3. $\eta_{sp}$ versus concentration of acetylated starch solutions: (A) DS0, (B) DS0 (unsaponified), (C) DS0.5, (D) DS1.5, (E) DS2.5 and (F) DS3. Dashed line is a 2nd order polynomial fitted on the experimental specific viscosities.

Table I-1. Representation of $\eta_{sp}$ versus concentration by 2nd order polynomial.

| degree of substitution | fitted polynomial | $R^2$ | SSE |
|---|---|---|---|
| **0** | $\eta_{sp} = [\eta]C + a_1C^2 + a_2$ | 0.9999 | $4.44\times10^{-5}$ |
| **0 (Unsaponified)** | $\eta_{sp} = [\eta]C + a_1C^2 + a_2$ | 0.9997 | $7.002\times10^{-5}$ |
| **0.5** | $\eta_{sp} = [\eta]C + a_1C^2 + a_2$ | 0.9997 | $3.85\times10^{-6}$ |
| **1.5** | $\eta_{sp} = [\eta]C + a_1C^2 + a_2$ | 1 | $1.13\times10^{-6}$ |
| **2.5** | $\eta_{sp} = [\eta]C + a_1C^2 + a_2$ | 1 | $7.68\times10^{-7}$ |
| **3** | $\eta_{sp} = [\eta]C + a_1C^2 + a_2$ | 0.9991 | $4.89\times10^{-6}$ |

Table I-2. Water mass loss and temperature of the maximum rate of mass loss for the second and third peak according to TGA measurements.

| **degree of substitution** | **water loss (%) (25-140°$C$)** | **temperature of the second peak of DTG (°$C$)** | **temperature of the third peak of DTG (°$C$)** |
|---|---|---|---|
| **0** | 8.5 | 313 | - |
| **0.5** | 5.3 | 290 | 367 |
| **1.5** | 6 | 274 | 367 |
| **2.5** | 5 | 279 | 370 |
| **3** | 2 | - | 367 |

Table I-3. Activation energy from fitting TGA data of the second and third peak of mass loss rate. Reported values represent 95% confidence intervals.

| **degree of Substitution** | **activation Energy at the temperature of the second peak of DTG (kJ/mol)** | | **activation Energy at the temperature of the third peak of DTG (kJ/mol)** | |
|---|---|---|---|---|
| **0** | 241±0.87 | SSE= $1.23\times10^{-4}$ $R^2$=0.999 | | - |
| **0.5** | 141±0.95 | SSE= $1.27\times10^{-4}$ $R^2$=0.999 | | - |
| **1.5** | 76.4±0.37 | SSE=$1.58\times10^{-5}$ $R^2$=0.999 | 141±0.58 | SSE=$6.25\times10^{-5}$ $R^2$=0.999 |
| **2.5** | 76.3±0.19 | SSE=$3.76\times10^{-6}$ $R^2$=0.999 | 197±1 | SSE=$1.88\times10^{-4}$ $R^2$=0.999 |
| **3** | | - | 287±1.12 | SSE=$2.56\times10^{-4}$ $R^2$=0.999 |

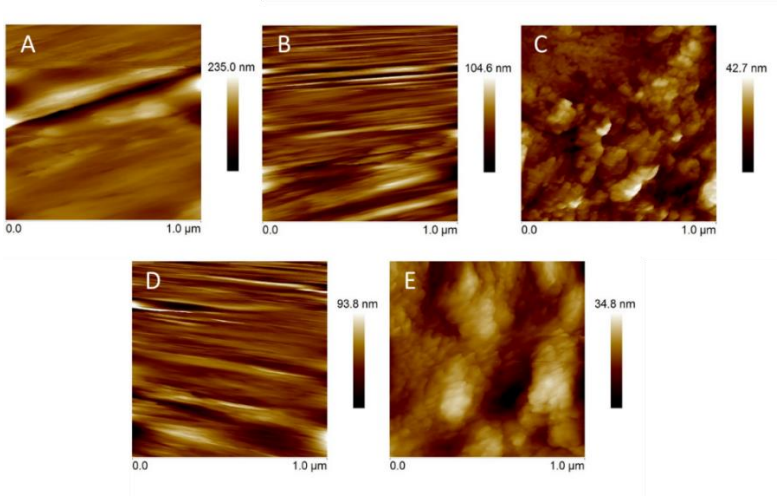


Figure I-4. AFM topographic images of acetylated starch pellets: (A) DS0, (B) DS0.5, (C) DS1.5, (D) DS2.5, and (E) DS3.

Table I-4. Arithmetic average roughness ($R_a$), root mean square roughness ($R_q$) and maximum height of peaks ($R_{MAX}$) of the surface of acetylated starch pellets.

| **degree of Substitution** | **$R_a$** (nm) | **$R_q$** (nm) | **$R_{MAX}$** (nm) |
|---|---|---|---|
| **0** | 15.5 | 24.7 | 306 |
| **0.5** | 10.2 | 13.5 | 125 |
| **1.5** | 4.17 | 5.51 | 42.8 |
| **2.5** | 8.49 | 11.8 | 166 |
| **3** | 3.88 | 4.92 | 33.3 |

Table I-5. Water and hexadecane contact angle and surface energy components of acetylated starch pellets. Reported values represent 95% confidence intervals. (n=3 for contact angels and for $\gamma^{Total}_{Nuemann}$; n=9 for $\gamma^{P}$, $\gamma^{D}$and $\gamma^{Total}$).

| **degree of Substitution** | **contact angle (°)** | | $\gamma^{P}$ (mJ/m$^2$) | $\gamma^{D}$ (mJ/m$^2$) | $\gamma^{Total}$ (mJ/m$^2$) | $\gamma^{Total}_{Nuemann}$ * (mJ/m$^2$) |
|---|---|---|---|---|---|---|
| | Water | Hexadecane | | | | |
| **0** | 41.27±6.87$^{a}$ | 15.2± 0.86$^{a}$ | 30.89±1.19$^{a}$ | 26.55±0.03$^{a}$ | 57.44±1.19$^{a}$ | 58.67±3.72$^{a}$ |
| **0.5** | 43.7±10.72$^{a}$ | 19± 8.48$^{a}$ | 29.66±1.94$^{a}$ | 25.99±0.33$^{b}$ | 55.66±1.92$^{a}$ | 57.32±5.97$^{a}$ |
| **1.5** | 60.13±3.48$^{b}$ | 20.5± 6.25$^{a}$ | 18.63±0.64$^{b}$ | 25.77±0.26$^{c}$ | 44.41±0.63$^{b}$ | 47.75±2.10$^{b}$ |
| **2.5** | 70.67±11.43$^{c}$ | 23.03± 6.22$^{b}$ | 12.28±1.84$^{c}$ | 25.34±0.30$^{d}$ | 37.61±1.83$^{c}$ | 41.29±7.07$^{c}$ |
| **3** | 79.47± 2.87$^{d}$ | 17.3± 4.73$^{a}$ | 7.18±0.36$^{d}$ | 26.26±0.17$^{a}$ | 33.44±0.37$^{d}$ | 35.81±1.79$^{d}$ |

* Total surface energy calculated using Nuemann's approach and water as the measuring liquid.

Values in the same column with different letter are significantly different based on multiple-comparison Bonferroni t-test at a significance level of α=0.1.

**Methodology for quantifying the apparent amylose content of starch samples**

The procedure for quantifying the apparent amylose content of starch samples is based on Mahmood *et al*'s cold NaOH-iodine method [59] with a few modifications. The calibration curve (Figure I-5) is prepared as follows. 5 mg mixtures of pure amylose (sigma, USA) and amylopectin (sigma, USA) are prepared with mass fraction of amylose varying from 0% to 40% in 10% increments. Each mixture is first suspended in 75 µL of 95% ethanol (Fisher Scientific, USA)-water solution and then 300 µL of 1M NaOH (Merck, Canada) solution is added. The mixture is vortexed until all the starch dissolves. Subsequent to solubilizing, 1 mL of water is added to the starch solution. A 200 µL sample is taken from the starch solution and neutralized with 1 mL of citric acid. 800 µL of iodine solution (0.2 g $I_2$ +2 g KI (Fisher Scientific, USA) +250 mL deionized water) are added to the neutralized starch solution. 10 mL of deionized water are then added to the solution. The absorbance is read at 620 nm against a reagent blank consisting of all the aforementioned reagents except amylose and amylopectin using a UV-vis spectrophotometer (Spectronic GENESYS 5, Thermo Scientific, Waltham, USA).

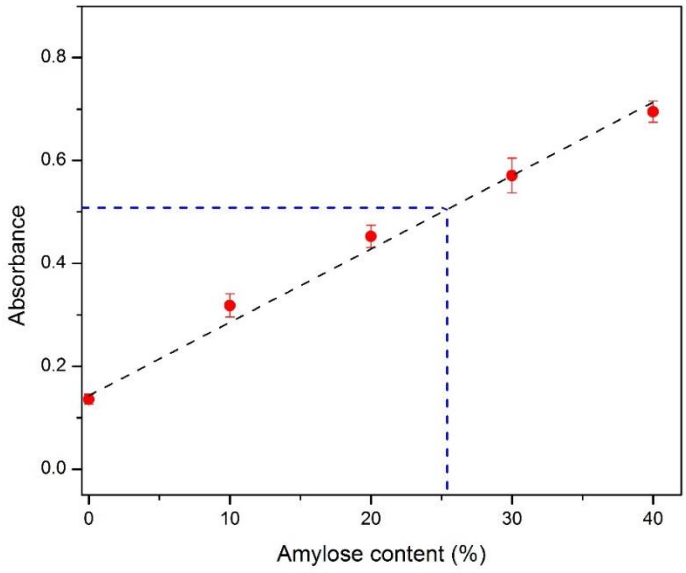


Figure I-5. Absorbance of amylose/amylopectin mixture solutions against amylose content. Calibration curve is acquired by fitting a line to experimental data (y = 0.0137x + 0.1603; $R^2$=0.9918 and SSE=0.0016). Error bars represent standard error (n=3). Dashed blue line determines measured absorbance and associated amylose content of starch sample.

In order to quantify the apparent amylose content, a 5 mg sample of starch is solubilized and stained as described above. Solution absorbance is measured at 620 nm against a reagent blank

consisting of all the aforementioned reagents except starch. The absorbance of starch solution was 0.52±0.05 and associated amylose content was 25.4±1.6.

**Correlation between absorbance and molecular weight of acetylated starches**

A 5 mg sample of acetylated starch with different DS, is solubilized and stained as described above. Solution absorbance is measured at 620 nm against a reagent blank consisting of all the aforementioned reagents except acetylated starch. Figure I-6 shows the comparison between trends in the absorbance of the acetylated starch samples and their molecular weight.

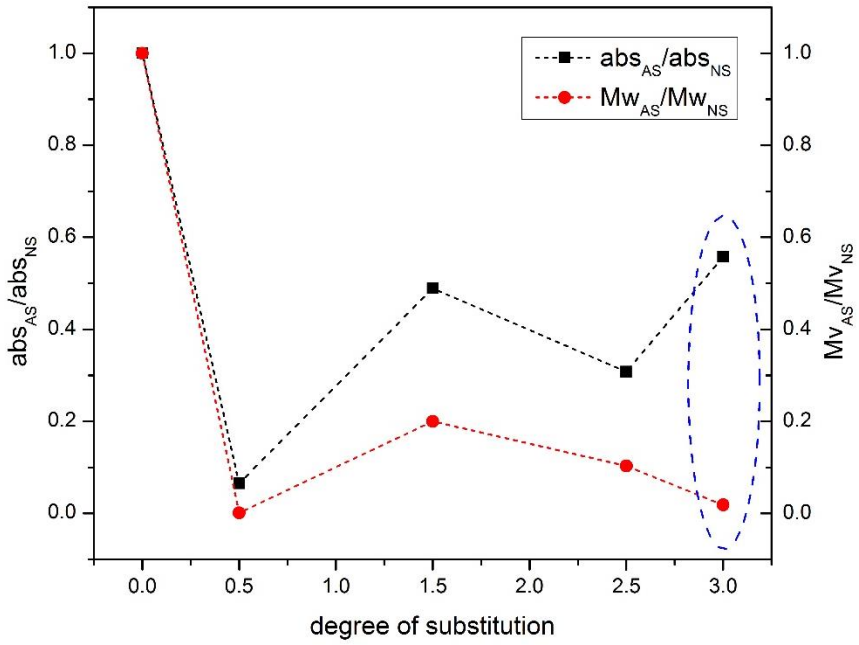


Figure I-6. Comparison between trends in the absorbance and molecular weight of acetylated starch samples. Absorbance and molecular weight values were normalized over the neat starch values.

# Appendix II

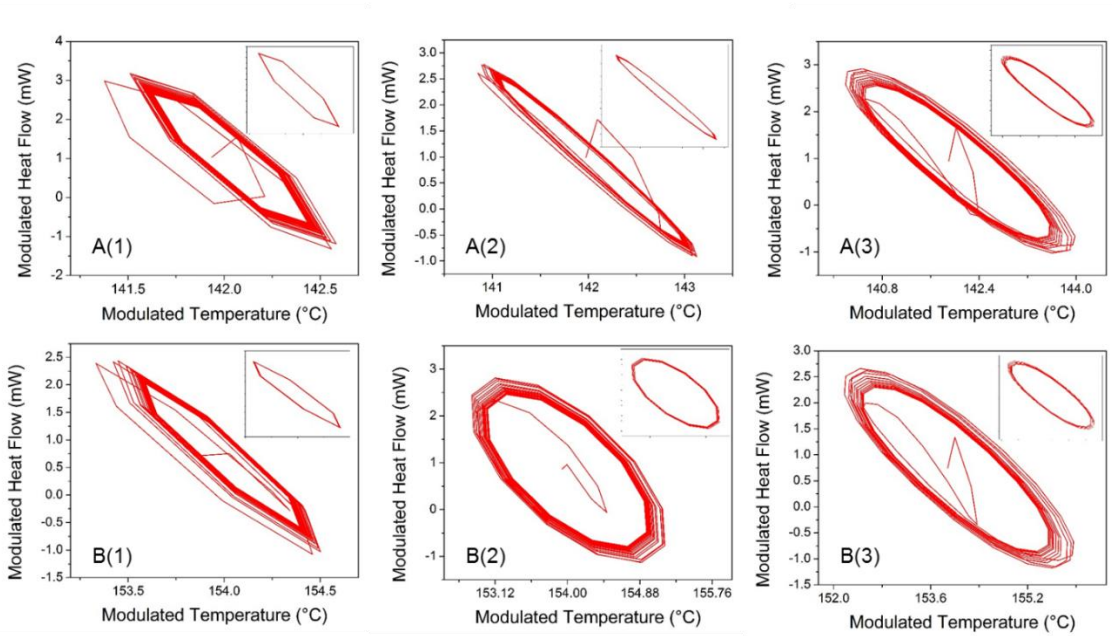


Figure II-1. Sample Lissajous plots of different degrees of substitution: (A) 1.5 and (B) 3. The modulation periods and amplitudes are: (1) 30s and 0.5°$C$, (2) 60s and 1°$C$ and (3) 90s and 1.5°$C$. Insets show the Lissajous plot of last 10 mins of data collection.

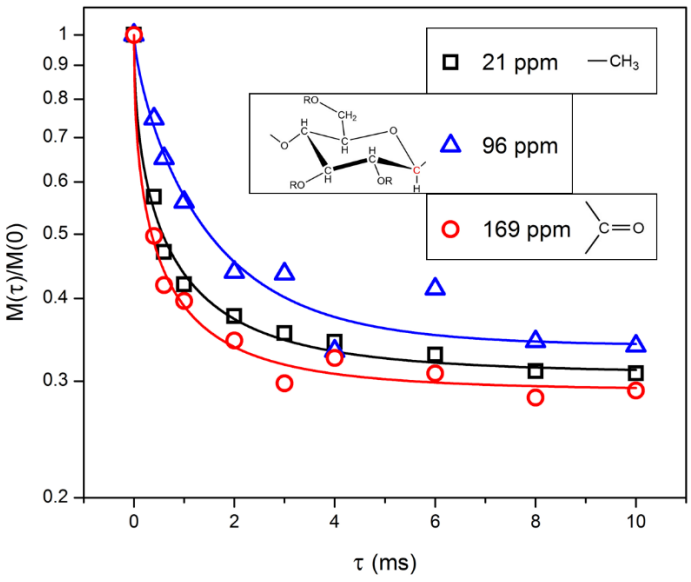


Figure II-2. Different demagnetization behavior of different carbons of DS3.

Table II-1. Spin-lattice relaxation time in the rotating frame for carbon,T_1ρ (C) (ms) and β, the nonexponentiality parameter for different carbons of DS3.

| **Carbon Chemical shift (ppm)** | $T_{1\rho}(C)$ **(ms)** | **β** |
|---|---|---|
| **21** | 0.34 ± 0.08 | 0.49 ± 0.10 |
| **96** | 0.93 ± 0.19 | 0.73 ± 0.20 |
| **169** | 0.23 ± 0.08 | 0.46 ± 0.11 |

# Appendix III

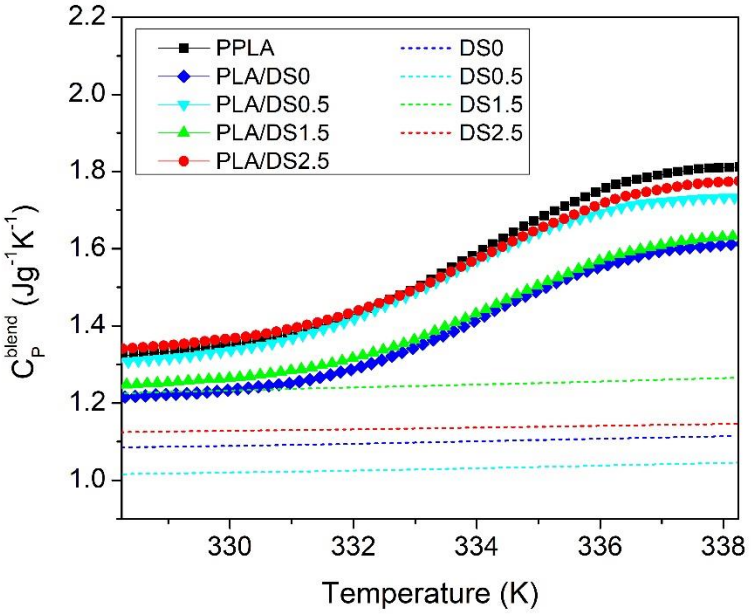


Figure III-1. The measured specific heat capacity curves for PLA/AS blens, prior to accounting for the AS contribution.

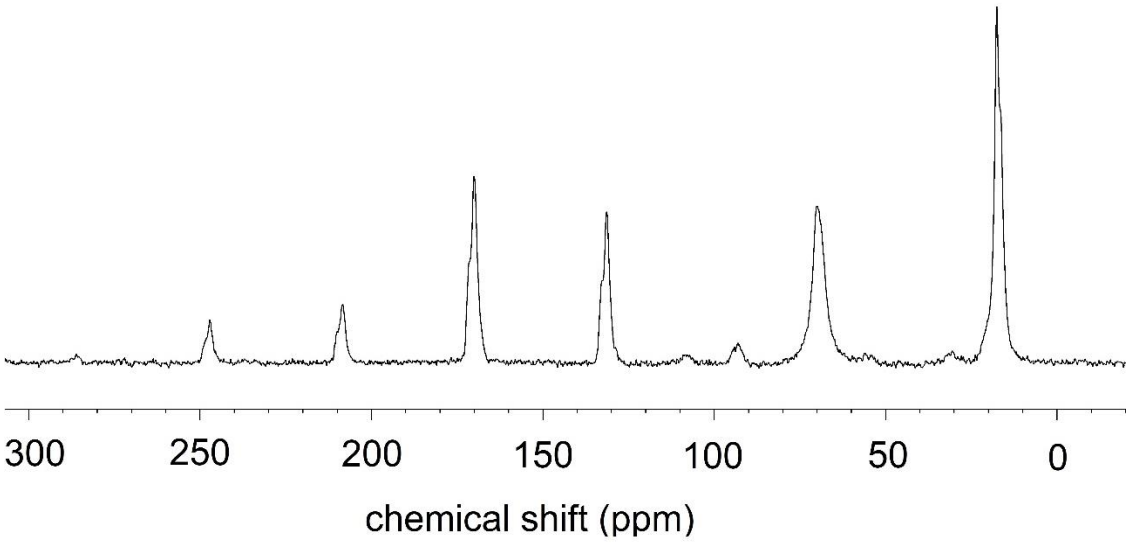


Figure III-2. $^{13}C$ CP/MAS spectra of quenched PLA/DS2.5 measured at 25°C.

Table III-1. Data for calculation of CRR length.

| Sample | $C_p(rubber)$ | $C_p(glass)$ | $\rho$ | $T_a$ | $\delta T$ | $\xi_a$ |
|---|---|---|---|---|---|---|
| **PLA/DS0** | 1.4638 | 1.0174 | 1.25 | 334.58 | 2.51 | 3.88 |
| **PLA/DS0.5** | 1.4868 | 1.0051 | 1.25 | 333.59 | 2.56 | 3.92 |
| **PLA/DS1.5** | 1.4495 | 1.0191 | 1.25 | 334.41 | 2.44 | 3.93 |
| **PLA/DS2.5** | 1.4967 | 1.0047 | 1.25 | 334.337 | 2.49 | 4.02 |

Table 0III-2. Examples of thickness of interphase in different polymer blends measured with different techniques.

| Polymer blend | Measurement method | Interphase thickness | reference |
|---|---|---|---|
| Poly(styrene)/poly(methyl methacrylate) | Small angle x-ray scattering | 1.8 nm | [50] |
| Poly(butyl methacrylate)/poly(2-ethylhexyl methacrylate) | Energy transfer method | 21 nm | [34] |
| Styrene-acrylonitrile (5% acrylonitrile)/poly(2,6-dimethyl-1,4-phenylene oxide) | Neutron refractivity | 1 nm as-cast<br>7.5 nm after 0.5hr annealing at 180°C | [191] |
| Poly(styrene)/poly(methyl methacrylate) | ellipsometry | 2.5 nm at 140°C | [155] |
| Polyepichlorohydrin/poly vinyl acetate (miscible blend) | Temperature modulated differential scanning calorimetry | 0.01-0.11 mm at 100°C by increasing the diffusion time from 200min-4600min | [192] |
| Poly(methyl methacrylate)/poly(vinylidene fluride) | Rheology | 50 $\mu$m after 2000s at 180°C | [193] |